Regulation of mammalian IRE1α:
Co-chaperones and their importance

Niko Amin-Wetzel

Christ's College

University of Cambridge

Date of submission: April 2018

This dissertation is submitted for the degree of Doctor of Philosophy

Preface

This dissertation is the result of my own work and includes nothing of which is the outcome of work done in collaboration except as declared in the Preface or specified in relevant figure legends and summarised in Appendix Table 5.

It is not substantially the same as any that I have submitted, or, is being concurrently submitted for a degree or diploma or other qualification at the University of Cambridge or any other University or similar institution except as declared in the Preface and specified in the text. I further state that no substantial part of my dissertation has already been submitted, or, is being concurrently submitted for any such degree, diploma or other qualification at the University of Cambridge or any other University or similar institution except as declared in the Preface and specified in the text.

It does not exceed the prescribed word limit for the relevant Degree Committee.

Part of this work has been presented in the following publication:

Amin-Wetzel, Niko, Reuben A. Saunders, Maarten J. Kamphuis, Claudia Rato, Steffen Preissler, Heather P. Harding, and David Ron. 2017. *A J-Protein Co-Chaperone Recruits BiP to Monomerize IRE1 and Repress the Unfolded Protein Response.* Cell. doi:10.1016/j.cell.2017.10.040.

Summary

When unfolded proteins accumulate in the endoplasmic reticulum (ER), the unfolded protein response (UPR) increases ER protein folding capacity to restore protein folding homeostasis. Unfolded proteins activate UPR signalling across the ER membrane to the nucleus by promoting oligomerisation of IRE1, a conserved transmembrane ER stress receptor. Despite significant research, the mechanism of coupling ER stress to IRE1 oligomerisation and activation has remained contested.

There are two proposed mechanisms by which IRE1 may sense accumulating unfolded proteins. In the direct binding mechanism, unfolded proteins are able to bind directly to IRE1 to drive its oligomerisation. In the chaperone inhibition mechanism, unfolded proteins compete for the repressive BiP bound to IRE1 leaving IRE1 free to oligomerise. Currently, these two mechanisms respectively lack compelling *in vivo* and *in vitro* evidence required to assess their validity.

The work presented here first describes *in vivo* experiments that identify a role of the ER co-chaperone ERdj4 as an IRE1 repressor that promotes a complex between the luminal Hsp70 BiP and the luminal stress-sensing domain of IRE1α (IRE1^{LD}). This is then built on by a series of *in vitro* experiments showing that ERdj4 catalyses formation of a repressive BiP-IRE1^{LD} complex and that this complex can be disrupted by the presence of competing unfolded protein substrates to restore IRE1^{LD} to its default, dimeric, and active state. The identification of ERdj4 and the *in vitro* reconstitution of chaperone inhibition establish BiP and its J-domain co-chaperones as key regulators of the UPR.

This thesis also utilises the power of Cas9-CRISPR technology to introduce specific mutations into the endogenous IRE1α locus and to screen for de-repressing IRE1α mutations. Via this methodology, two predicted unstructured regions of IRE1 are found to be important for IRE1 repression. Finally, this thesis challenges recent *in vitro* findings concerning the direct binding mechanism.

Acknowledgments

Scientific progress is rarely achieved in isolation and my PhD has certainly been no different. I would like to take the opportunity to acknowledge those who have helped me on my journey.

I could not have asked for a better PhD supervisor than David. His patience, guidance and energy has been a constant throughout my time in the lab and even if I were to complete another five PhDs with him, I doubt I would come close to exhausting all that he could teach me. The double-edged sword of his daily presence in the lab is something I am indeed thankful for.

Thank you to all the members of the Ron lab for providing such a fun environment to work and particularly: Maarten and Claudia for performing the ERdj knock out screen and identifying ERdj4 as a co-chaperone of interest in IRE1 regulation. Nozomu for developing the ΔLD15 system. Heather for creating the original T17 cell line. Reuben for developing the BLI and FRET assays, sharing my enthusiasm for ERdj4 and his friendship. Steffen for being an excellent unofficial mentor to me in the Ron lab and bestowing me with much sage advice throughout the years.

My thanks also to the friends I have made here in Cambridge who helped me maintain the elusive work-life balance and their contributions to my board game collection.

My parents have always been there for me to support and push me at all the right points in my life to allow me to achieve my full potential and for this I cannot thank them enough.

Last but by no means least, I would like to thank Heewon, who has joined me on countless weekend jaunts to the lab to split cells or to finish a western blot. By now she is equally competent with a pipette and knows my project inside and out. She has been there for me at every step and always found a way to cheer me up when things weren't going so well.

I hope that I will be able to pay forward all the kindness and support I have received throughout the years and that the next stage of my life is equally enjoyable as my PhD has been.

Table of Contents

Abbreviations

2DG	2-Deoxyglucose
CD	Cytosolic Domain
CHO	Chinese Hamster Ovary
CLD	Core Luminal Domain
CPY	Carboxypeptidase
ER	Endoplasmic Reticulum
ERdj	ER-localised J-protein
FACS	Fluorescence Activated Cell Sorting
FRET	Föster Resonance Energy Transfer
HDR	Homology Directed Repair
IB	Immunoblot
IP	Immunoprecipitation
IRE1	Inositol Requiring Enzyme 1
LD	Luminal Domain
MPZ	Myelin Protein Zero
NBD	Nucleotide Binding Domain
NEF	Nucleotide Exchange Factors
OG	Oregon Green fluorophore
SBD	Substrate Binding Domain
SP	Signal Peptide

TAM	Tetramethylrhodamine fluorophore
Tg	Thapsigargin
Tm	Tunicamycin
TM	Transmembrane
UPR	Unfolded Protein Response
WT	Wildtype
XBP1us	Unspliced XBP1
XBP1s	Spliced XBP1

Chapter 1

Introduction

The unfolded protein response

The endoplasmic reticulum (ER) is the central hub for the synthesis of secretory and transmembrane proteins. Following co-translational insertion into the ER lumen, the nascent polypeptides fold into their specific tertiary structure. A large proportion of these proteins require aid in order to fold correctly, this is provided in the form of chaperone proteins. Under basal conditions, the influx of proteins, referred to as the folding load, is balanced against the folding capacity of the ER. Perturbations to this balance decrease the efficiency of protein folding and can lead to accumulation of unfolded (taken in this thesis to include misfolded) proteins, decreased cell function, and cell death. This is referred to as ER stress (taken in this thesis to refer to protein stress and distinct from lipid stress). Physiological perturbations to the balance can come from fluctuations in protein synthesis, e.g. during physiological upregulation of antibody or insulin production and secretion, or from exposure to harsh environmental conditions, e.g. high temperature. Experimentally various small molecules are used to induce the UPR: Thapsigargin (Tg) depletes ER calcium by inhibiting the replenishing SERCA calcium pumps (Sagara et al., 1991; Wong et al., 1993). Tunicamycin (Tm) inhibits the ER glycosylation machinery which is required for the correct folding of many proteins (Takatsuk et al., 1975). Dithiothreitol (DTT) perturbs the redox environment of the ER and reduces disulfides, which are required for the stability of many proteins (Okamura et al., 2000).

In eukaryotes, the folding load against capacity balance is constantly monitored and maintained by signalling pathways whose response to increasing levels of unfolded proteins is called the unfolded protein response (UPR) (Cox et al., 1997; Kozutsumi et al., 1988). The mammalian UPR consists of three signalling branches, each headed by a separate signal transducer located in the ER membrane, which monitors the state of the ER lumen (Figure 1.01). These three transducers are IRE1, PERK and ATF6, each of which output specific transcriptional programmes through the respective transcription factors of their signalling pathway: XBP1, ATF4 and ATF6-N. These transcription factors upregulate the genes necessary for ER synthesis and also increase expression of chaperones (Harding et al., 2003;

Sriburi et al., 2004; A. Lee et al., 2005). In addition to these transcriptional outputs, IRE1 and PERK reduce the protein folding load by degrading ER-protein encoding mRNAs and inhibiting global translation respectively. This dual pronged attack on decreasing folding load and increasing folding capacity aims to restore balance and protein folding homeostasis (reviewed in Walter and Ron, 2011).

A good deal is known about the effector functions of the UPR transducers, the physiological significance of ER stress, and the response to it (reviewed in Wang and Kaufman, 2016). However, the molecular mechanism(s) by which the UPR branches monitor the balance of folding load and capacity of the ER remains poorly understood. Studies to understand the sensing mechanism have largely focused on the most conserved of the signal transducers, namely IRE1, which is conserved in all eukaryotes.

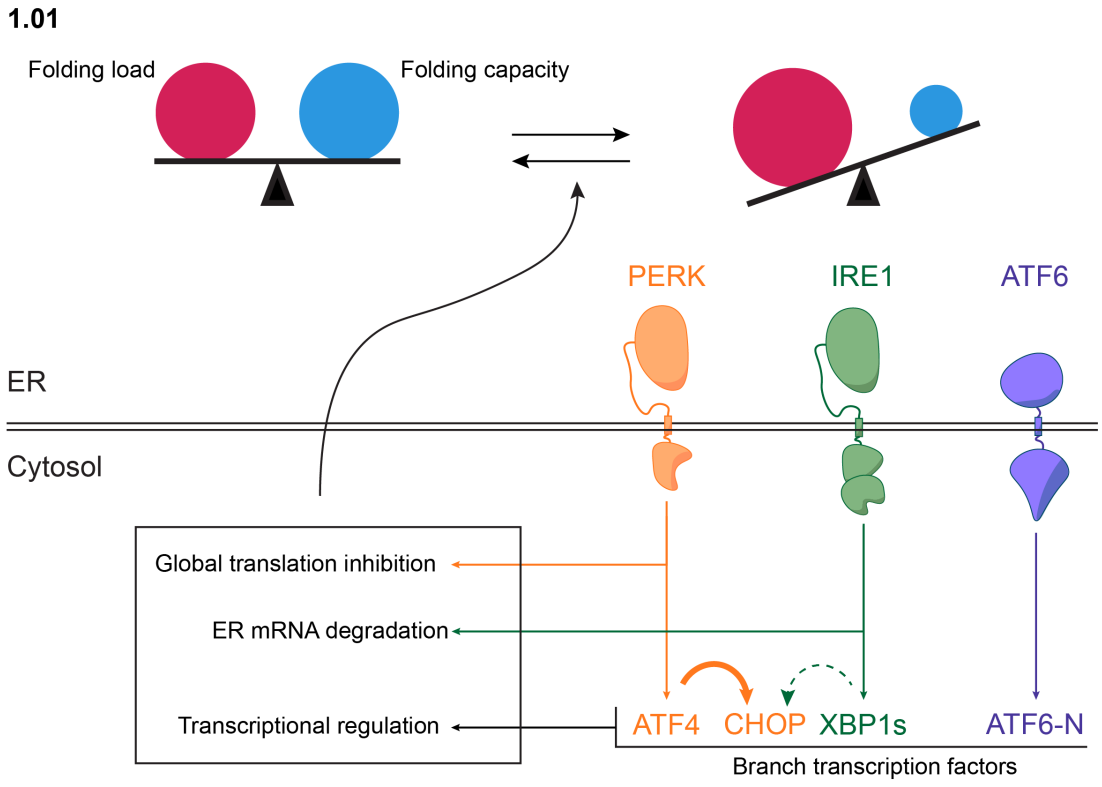

Figure 1.01 An outline of the UPR in which the balance between the folding load and capacity of the ER is monitored by signalling pathways, which act to restore perturbations to the balance through a variety of regulatory gene expression events.

IRE1 and its regulation

The majority of the mechanistic insight into IRE1 regulation has been obtained from studies on yIRE1 and mammalian IRE1 isoforms. This is in part due to the historical context of IRE1's discovery and part due to the potential relevance of IRE1 in human disease. In this thesis, where important, the distinction between yIRE1, and the mammalian isoforms, IRE1α, and IRE1β will be made.

An overview of IRE1

A series of genetic screens were responsible for the discovery and characterisation of yIRE1. yIRE1 first came to light as a protein kinase necessary for growth on low inositol media and was proposed to be an essential component in regulating inositol synthesis (it was also the first yeast transmembrane kinase identified) (Nikawa and Yamashita 1992).

IRE1 heads the sole UPR branch in yeast and consequently was found to be essential for the response and survival of yeast to stress (Cox et al., 1993; Mori et al., 1993). Its discovery in mammals was somewhat hampered by the low sequence homology of yIRE1 with the mammalian counterparts but it was found that mammals harboured two isoforms of IRE1, IRE1α and IRE1β. IRE1α is ubiquitously expressed in all tissues whilst expression of IRE1β is limited to the gut epithelium (X. Z. Wang et al., 1998; Tirasophon et al., 1998). The IRE1 cytosolic domain was seen to have sequence homology to the mammalian, oligomerisation-activated RNaseL endoribonuclease/kinase protein and lead to the discovery that yIRE1 was directly involved in the cytosolic non-conventional splicing mechanism that had been identified as a critical step in activating the UPR-essential Hac1 transcription factor in yeast (J S Cox and Walter 1996; Sidrauski and Walter 1997). The mammalian Hac1 orthologue is XBP1 which is similarly spliced by IRE1α/β to promote *XBP1* translation and the conserved *XBP1*-dependent gene expression program (Figure 1.02) (Yoshida et al., 2001; Calfon et al., 2002). IRE1 cleaves cytosolic unspliced XBP1 mRNA (XBP1us) at two conserved stem-loop sites and the two terminal fragments are then ligated by the tRNA ligase RTCB to form spliced XBP1 mRNA (XBP1s) (Lu et al., 2014; Jurkin et al., 2014).

This splicing event removes a translational STOP codon from the intron and places the second exon in frame with the first allowing the functional XBP1 transcription factor to be translated.

The primary output of IRE1 activity is generating the active XBP1 (as seen by the similarity in phenotype between IRE1 and XBP1 knockout animals) (Calfon et al., 2002; Iwawaki et al., 2010). However, activated IRE1 is also reported to activate the JNK signalling cascade via its cytosolic kinase domain and degrade ER localised mRNAs via its cytosolic endoribonuclease domain to reduce the synthesis of new ER protein (Urano et al., 2000; Hollien and Weissman 2006).

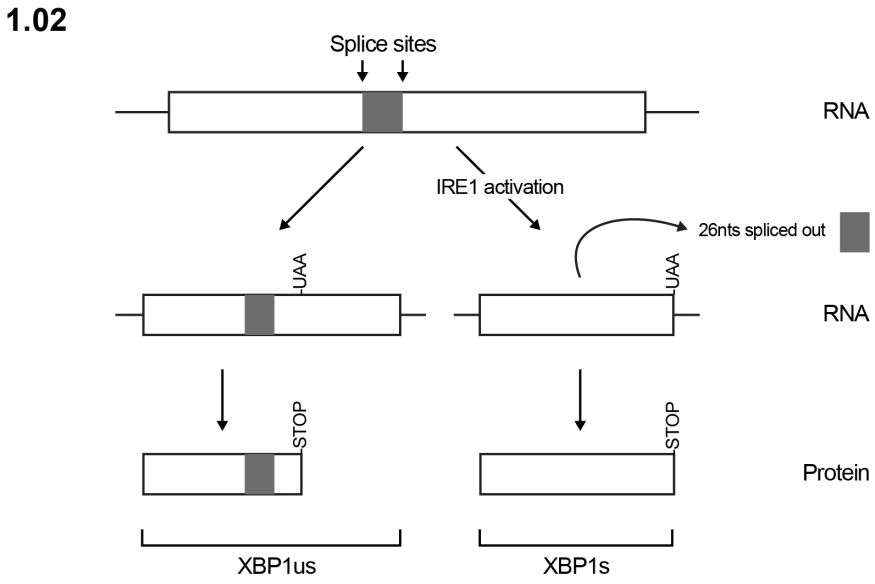

Figure 1.02 A schematic of the cytosolic splicing of XBP1us mRNA as catalysed by IRE1. The XBP1us mRNA contains an intron, which is excised by active IRE1, allowing the exons to be ligated to form the full coding sequence for the functional XBP1 transcription factor. In the absence of splicing, the intron causes a STOP codon in the exon to be in-frame and read during translation resulting in a non-functional XBP1.

As part of its activation mechanism in response to stress, IRE1 undergoes luminal domain (LD)-dimerisation-dependent trans-autophosphorylation on cytosolic serine residues (i.e. the kinase of one monomer phosphorylates the other monomer) (Shamu and Walter 1996). These cytosolic activation events of IRE1 are conserved and well understood, however this is not the case for the luminal events of IRE1. There are two main mechanisms by which IRE1 is thought to sense increasing levels of unfolded proteins: the chaperone inhibition and direct binding mechanisms. In the chaperone inhibition mechanism, IRE1 is held inactive by the principal component of the ER folding machinery, the BiP chaperone protein (Kar2 in yeast). During stress, accumulating unfolded proteins titrate BiP away from IRE1 in order to chaperone their folding leaving IRE1 free to dimerise and activate (Figure 1.03). The mechanism of direct binding, on the other, hand has IRE1's default state to be monomeric and association with unfolded proteins ligands is required to stabilise the active form. In the literature, description of the direct binding mechanism also tends to focus on the idea that the fully active form of IRE1 is an oligomeric structure rather than a mere dimer (Figure 1.04). It is important to note that these two mechanisms are not mutually exclusive and models of IRE1 regulation have been proposed featuring both of them.

Before examining the data supporting these models, the IRE1 protein will be described in more detail.

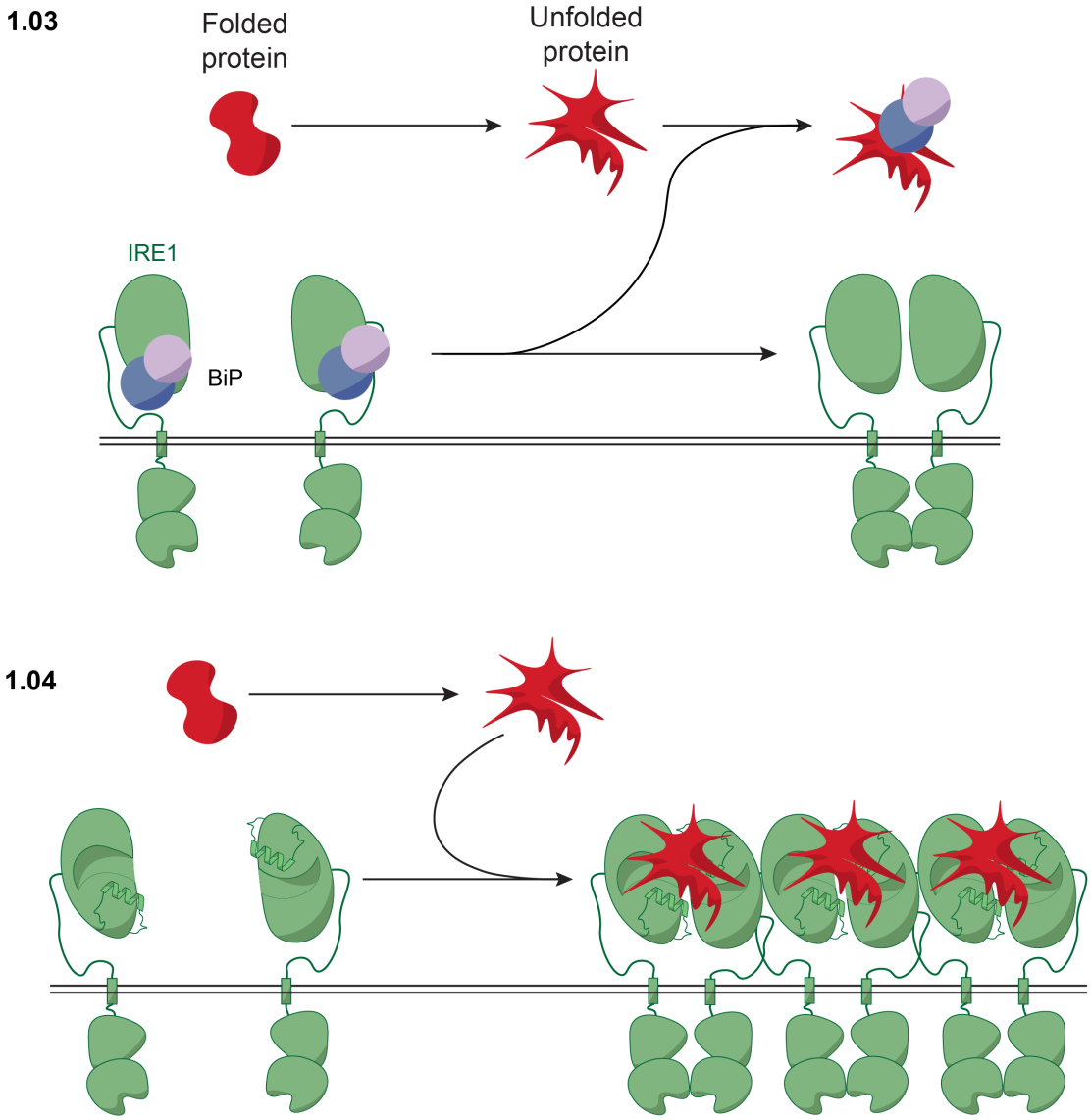

Figure 1.03 A cartoon of the chaperone-mediated regulation of IRE1. Under basal conditions, IRE1 is held inactive by the ER chaperone BiP. During stress, BiP is titrated away from IRE1 by accumulating unfolded proteins. This leaves IRE1 free to dimerise and activate.

Figure 1.04 A cartoon of IRE1 regulation via direct binding of unfolded proteins. Under basal conditions, IRE1 remains inactive. During stress, accumulating unfolded proteins bind to IRE1 and drive its oligomerisation and activation.

The structure of IRE1

Crystal structures of the yIRE1 and IRE1α LDs exist (Credle et al., 2005; Zhou et al., 2006). Despite the lack of sequence homology, the LD structures show a very similar core architecture (Figures 1.05-1.06[1]). This structured region of IRE1 is referred to as the core luminal domain (CLD)[2].

The IRE1α CLD domain is tethered to the transmembrane helix by a shorter stretch of amino acids referred to as the tail (See figure 1.05+1.07 for an overview of the IRE1α domain layout). It is predicted that this tail is largely unstructured as, unlike the CLD, it is accessible to protease during limited proteolysis experiments (Liu et al., 2003). Additionally this is supported by the yIRE1 CLD forming larger and more consistent crystals as compared to the full yIRE1 LD (Credle et al., 2005). The CLD is sufficient and necessary for IRE1α to dimerise both *in vivo* and *in vitro* and is therefore crucial to IRE1 function (Liu et al., 2003; Zhou et al., 2006). Previously the boundaries of the CLD had been unintentionally mapped through a tiling deletion screen, which identified regions of yIRE1 required for its response to stress. The results from this screen split yIRE1 into five regions where regions II and IV are needed for response to stress and make up the CLD (See Figure 1.07 bottom for yIRE1 layout) (Kimata et al., 2004).

The yIRE1 crystal structure revealed two IRE1 dimer interfaces, interface 1 and 2 (Figure 1.06+1.08), that, when mutated, impaired the ability of IRE1 to respond to stress (D Oikawa et al., 2005; Credle et al., 2005; Aragón et al., 2009). These interfaces are arranged such that yIRE1 could theoretically form oligomers. In contrast to yIRE1, the IRE1α LD crystal structure (Figure 1.05) showed only one of the two dimer interfaces (interface 1) mutation of which

---

[1] The 2HZ6 and 2BE1 crystal structures have been further refined to assign more of the electron density present to the protein sequence and therefore differ from the files in the protein database. Richard Mifsud of Randy Read's group carried out the refinement.

[2] The IRE1 CLD is defined by Zhou et al 2006 as consisting of residues 19-390, however, the IRE1α CLD crystal structure lacks assigned electron density for residues 370-390, suggesting that these residues are not so structured.

impairs dimerisation, auto-phosphorylation, and XBP1 splicing in response to stress (Zhou et al., 2006).

Multiple crystal structures of the IRE1 CD also exist and there is again a high structural similarity between the yIRE1 and IRE1α domains which supports the conserved aspects seen for IRE1 activity (reviewed in (K. P. K. Lee et al., 2008; Korennykh et al., 2011; Korennykh and Walter 2012).

1.05

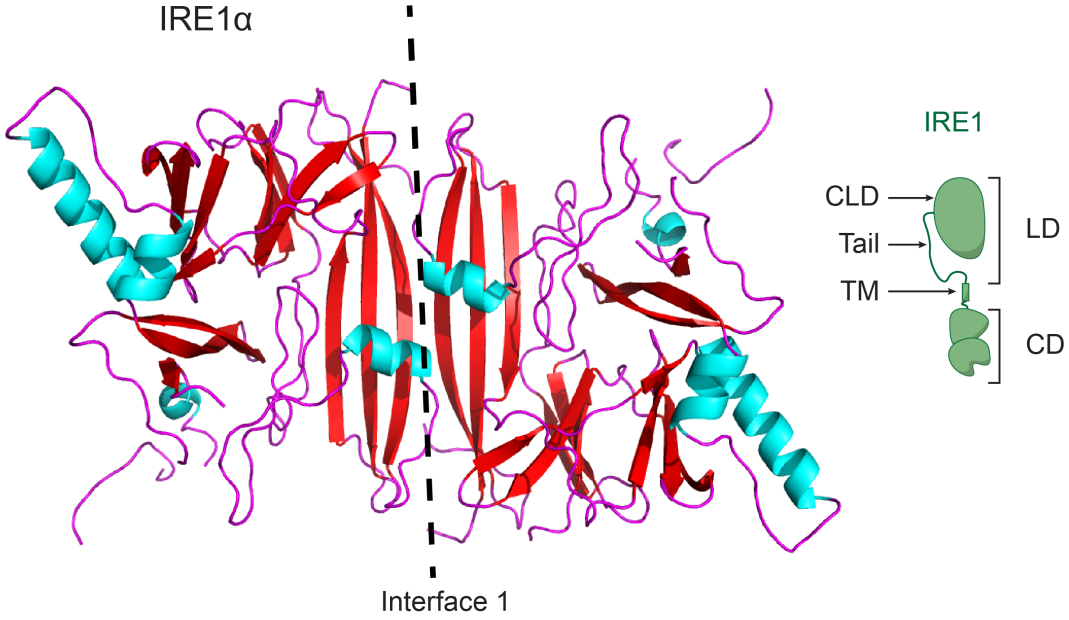

1.06

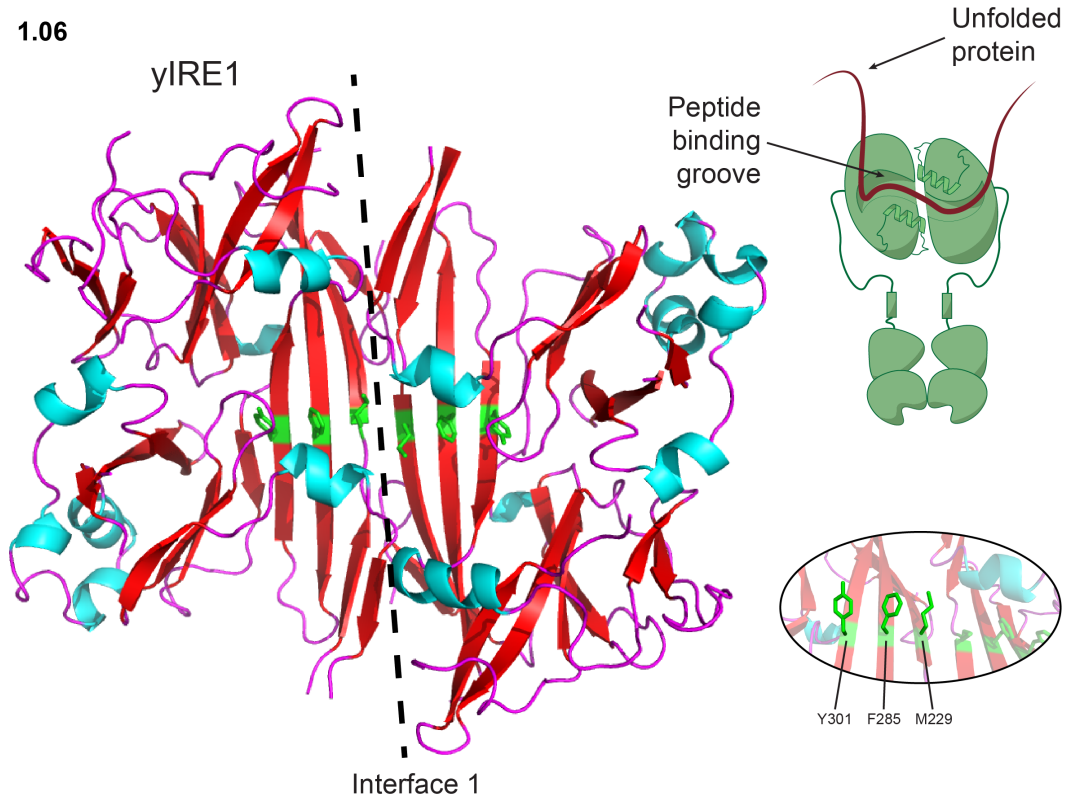

1.07

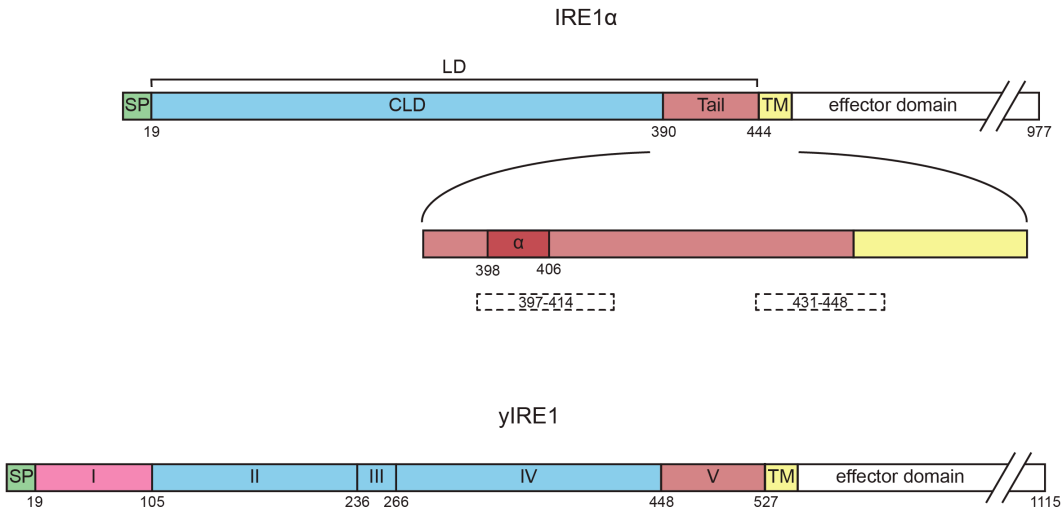

Figure 1.05 The crystal structure of the human IRE1α core luminal domain (Zhou et al., 2006 PDB: 2HZ6 further refined). The dashed line indicates the dimerisation interface 1. The cartoon (right) outlines the domain layout of IRE1: LD – Luminal domain, CLD – Core luminal domain, TM – Transmembrane domain, CD – Cytosolic domain.

Figure 1.06 View of interface 1 (indicated by the black dashed line) of the crystal structure of the yIRE1 core luminal domain (Credle et al., 2005 PDB: 2BE1 further refined). The dashed line indicates the dimerisation interface 1. The cartoon (top right) depicts how an extended unfolded protein is thought to occupy the proposed peptide binding groove which is flanked by helices in both in the crystal structure and the cartoon. Bottom right shows a view of the three hydrophobic sidechains at the base of the peptide binding groove. These residues are also coloured green in the full crystal structure (left).

Figure 1.07 The annotated domain/region layout of IRE1α (top) and yIRE1 (bottom). Blue – the core structured luminal domain (CLD), Red – the predicted unstructured IRE1 tail region, Green – the ER targeting signal peptide (SP), Yellow – the transmembrane domain (TM), Pink – region I unique to yIRE1. Dark red – the predicted IRE1α α-helix. Dashed boxes indicate regions of amphipathicity. Numbers indicate the amino acid residue numbers of the luminal domain element boundaries and the length of the luminal domain elements are scaled according to number of residues.

1.08

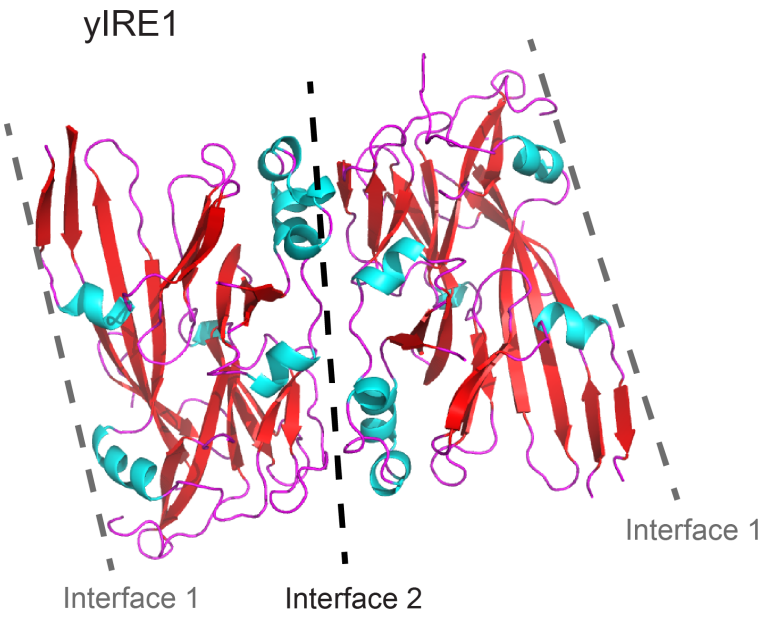

Figure 1.08 View of interface 2 (indicated by the back dashed line) of the crystal structure of the yIRE1 luminal domain (Credle et al., 2005 PDB: 2BE1 further refined). Interface 1 is indicated by the grey dashed lines.

Direct binding of IRE1 to unfolded proteins

The direct binding mechanism for IRE1 regulation was first proposed by Shamu & Walter 1996, however, it was only upon solving of the crystal yIRE1 LD crystal structure that this hypothesis was addressed experimentally. Scrutiny of the yIRE1 LD crystal structure (Figure 1.06) revealed an apparent MHC-I-like peptide-binding groove spanning interface 1 (Credle et al., 2005). This led to the hypothesis that unfolded proteins could engage and drive IRE1 dimerisation and activation through this site.

This model predicts that the ER proteome has a high abundance of peptides of sufficient affinity for IRE1 to drive its activation when they become exposed during stress. ER-localised proteins are through this model proposed to have a range of peptide sequences that become exposed during stress to drive IRE1 activation. Given the sensitivity of IRE1 to stress such peptide sequences would need to be abundant in the ER proteome.

Experimentally, this mode of IRE1 regulation has been explored in both yeast and mammals.

The β sheet base of the yIRE1 peptide-binding groove features exposed methionine, phenylalanine, and tyrosine amino acid side chains (M229, F285, Y301 : MFY - Figure 1.06) which, when mutated to alanine (individually or combined), decrease the ability of IRE1 to signal in response to stress (Credle et al., 2005). This is consistent with these residues providing a hydrophobic pocket to bind unfolded proteins (which have exposed hydrophobic regions). The crystal structure of IRE1α features a similar peptide-binding groove structure with the residues equivalent to MFY being K121, Y161, and Y179 (Zhou et al., 2006). The likelihood of hydrophobic peptides engaging with this groove is already decreased given that it seems unlikely that K121 would be able to interact with hydrophobic peptides. Unfortunately, it has not yet been possible to generate a stable IRE1α peptide-binding groove mutant[3], which

[3] Purified Y161A IRE1α is prone to precipitation and is seen to have a lower melting temperature, suggesting the overall protein structure is compromised (unpublished data and personal correspondence with Elif Karagoz). Similar

has made it difficult to assess the direct binding model via similar mutational analyses as those used for yIRE1.

If yIRE1 is able to bind unfolded proteins, then it might exhibit chaperone properties (so-called holdase activity) and, indeed, presence of yIRE1 in citrate synthase or luciferase aggregation assays inhibits aggregation in a manner dependent on MFY (Kimata et al., 2007; Daisuke Oikawa et al., 2009; Daisuke Oikawa et al., 2012). Furthermore, expression of mutant carboxypeptidase (CPY), a model unfolded protein, activates the yeast UPR and can be seen to interact with yIRE1 in a manner dependent on MFY (and to some extent the integrity of both dimerisation interfaces) (Promlek et al., 2011; Gardner and Walter 2011).

To assess the peptide sequence binding preferences of IRE1, peptide arrays derived from UPR inducing proteins have been used (Gardner and Walter 2011; Karagöz et al., 2017). These have identified a general preference of IRE1 for basic and hydrophobic amino acids, which is distinct from the binding preferences of BiP or Kar2 (Flynn et al., 1991; Blond-Elguindi et al., 1993). Incubation with high affinity peptide binding partners shifts IRE1 to higher order oligomers (dependent on MFY) and while interface 2 mutants remain able to bind these peptides, they no longer shift to higher molecular weight species (Gardner and Walter 2011; Karagöz et al., 2017). It is thought that peptide binding induces conformational changes in IRE1, allowing it to oligomerise.

The idea that unfolded proteins engage IRE1 is further built on by the possibility that region I of yIRE1 may tie in with the peptide-binding groove. It is proposed that a *cis*-interaction of region I and the peptide-binding groove maintains yIRE1 in a monomeric state until a sufficiently high affinity peptide competes for binding the groove (Mathuranyanon et al., 2015).

It is surprising that despite considerable effort no luminally localised peptide that binds IRE1 with high affinity has been identified. One can assume that

---

indications of compromised protein structure for Y161A and Y179A are seen *in vivo* (Kono et al., 2017 and unpublished data).

either the occurrences of such peptides are rare or that the measure of affinity *in vitro* has little bearing on the ability of such sequences to activate IRE1 *in vivo*. In either case the physiological relvance of the *in vitro* experiments supporting the direct binding model is questionable.

IRE1 oligomerisation in response to stress

Dimerisation is accepted as the minimal event necessary for IRE1 signalling, however, further oligomerisation may be important for full IRE1 activity and it is often investigated in the context of the direct binding model (though oligomerisation may also be required in the chaperone inhibition mechanism). Data regarding IRE1 oligomerisation predominantly comes from microscopy studies of cells expressing tagged IRE1 variants which reveal stress induced IRE1 clusters (Aragón et al., 2009; Li et al., 2010).

In yeast, IRE1 clustering is dependent on the integrity of both CD and LD dimer interfaces (though CD activity is not required), and correlates with increased interaction of yIRE1 molecules as assessed by CoIP (Kimata et al., 2007; Aragón et al., 2009; Promlek et al., 2011; Ishiwata-Kimata et al., 2013; van Anken et al., 2014; Halbleib et al., 2017). Disappearance of these clusters correlates with attenuation of yIRE1/IRE1α activity following an initial stress insult (Kimata et al., 2007; Li et al., 2010; Pincus et al., 2010).

It is interesting to note that Hac1 RNA also forms clusters in response to stress dependent on the presence of a clustering-competent IRE1 (Aragón et al., 2009; van Anken et al., 2014).

Tagged IRE1α is found to form stress induced clusters (Li et al., 2010; Daisuke Oikawa et al., 2012; Kitai et al., 2013; Sundaram et al., 2017). *In vitro* IRE1α LD can form higher order oligomers (Chuan Yin Liu et al., 2002) and endogenous IRE1α obtained from cells exposed to stress exists in higher molecular weight structures than in the absence of stress (Bertolotti et al., 2000). Though the IRE1α crystal structure shows only interface 1, crosslinking and subsequent mass spectrometry analysis has been used to propose the existence of a second interface analogous to the yIRE1 interface 2. When the residues involved in this hypothetical interface 2 are mutated IRE1α is unable to splice XBP1 or form oligomers in response to stress (Karagöz et al., 2017).

The idea that yIRE1 LD oligomerisation is important for its activation well matches similar *in vitro* observations for yIRE1 CD (Korennykh et al., 2009; Li et al., 2010, Lee et al 2008). This oligomerisation is captured crystalographically by the Walter group, however, it is absent from the crystal structure solved by the Sicheri group (K. P. K. Lee et al., 2008).

A caveat of IRE1 clustering is that it (and also IRE1 activity) is very sensitive to expression levels. For example, whilst a de-repressed yIRE1 mutant lacking regions I and V forms clusters under basal conditions, lowering the expression level removes this phenotype (Kimata et al., 2007; Daisuke Oikawa et al., 2009; Mathuranyanon et al., 2015). Similarly, cluster formation of IRE1α is very dependent on expression levels of the protein (and also to the magnitude of stress induced) (Sundaram et al., 2017). Furthermore, the geometry of the various IRE1 LD and CD interaction interfaces induces a membrane distorting helical structure to IRE1 oligomers, which may disfavour their formation at endogenous expression levels (Credle et al., 2005; Kimata et al., 2007). I am unaware of published experiments showing stress induced IRE1 cluster formation at endogenous levels of IRE1 expression and until this is achieved, there will always be doubt as to the physiological relevance of clusters.

Chaperone-mediated inhibition of IRE1

The UPR field is in agreement that IRE1 (and PERK) exists in complex with BiP, which is disrupted in response to a wide range of ER stressors (including Tm, Tg, DTT and inositol depletion) (Okamura et al., 2000; Bertolotti et al., 2000; Liu et al., 2003; Kimata et al., 2003; Kimata et al., 2004; Oikawa et al., 2007; Oikawa et al., 2009; Ishiwata-Kimata et al., 2013; Rubio et al., 2011; Carrara et al., 2015b; Oikawa et al., 2012). Importantly, this correlation extends to the endogenous BiP:IREα complex, which decreases in abundance during stress and increases during recovery (Bertolotti et al., 2000).

The contested issue is whether BiP dissociation actually drives IRE1 activation. One of the more compelling experiments for chaperone-mediated inhibition of IRE1 is that, during moderate UPR activation, the yIRE1 still bound to Kar2 is under-phosphorylated relative to the unbound yIRE1

(Okamura et al., 2000). However, essential follow-up experiments to probe this in more detail have not been reported.

Attempts have been made to characterise the Kar2 binding site on yIRE1 and these have all generally identified that the integrity of region V is essential for the formation of the stress-sensitive Kar2:yIRE1 complex (Kimata et al., 2004; Daisuke Oikawa et al., 2007; Pincus et al., 2010; Ishiwata-Kimata et al., 2013). However, a reproducible de-regulation of IRE1 activity is not seen in the various yIRE1 region V mutants and only subtle effects on yIRE1 dimerisation are observed (Ishiwata-Kimata et al., 2013). Furthermore in all cases the region V yIRE1 mutants still increase their activity in response to stress. For IRE1α however, region V (i.e. the tail) seems to play a more prominent role for repression and also, as seen for yIRE1, facilitates the association with BiP (Daisuke Oikawa et al., 2009).

As well as studies exploring IRE1 regulation through manipulations of IRE1 itself, some studies instead focus on BiP to probe the mechanism of chaperone inhibition. Over-expression and depletion of luminal Kar2 reveal a correlation between BiP/Kar2 levels and suppression of UPR branch signalling in response to stress (Hardwick et al., 1990; Dorner et al., 1992; Okamura et al., 2000; Bertolotti et al., 2000). It has also been found that temperature-sensitive mutants of Kar2 that remain bound to yIRE1 during stress prevent UPR signalling, whilst expression of those that are unable to bind yIRE1 result in constitutive UPR signalling (Kimata et al., 2003). These Kar2 mutants also display similar binding patterns with substrate, suggesting the Kar2:IRE1 interaction is a canonical chaperone substrate interaction (Kimata et al., 2003). This is further supported by BiP SBD alone being sufficient to bind IRE1α and that a mutant BiP unable to make high-affinity interactions with substrate is associated with less IRE1 compared to WT BiP (Liu et al., 2003). However, the nature of the IRE1/PERK interaction with BiP remains somewhat contested and has been characterised as a non-canonical interaction by some (Todd-Corlett et al., 2007; Sou et al., 2012; Carrara et al., 2015b; Kopp et al., 2018).

Unfortunately, because BiP plays a central and varied role in maintaining ER proteostasis multiple conclusions can be drawn from *in vivo* experiments,

which mutate or otherwise alter BiP. For example depletion or overexpression of BiP is likely to increase or decrease basal levels of unfolded proteins respectively and could through this indirectly affect IRE1 activity. Therefore these *in vivo* studies perturbing BiP do not contribute to the understanding of IRE1's regulation.

The response of IRE1 to lipid stress

IRE1 is also seen to respond to perturbations in ER membrane lipid composition during lipid stress (Volmer et al., 2013; Robblee et al., 2016; Halbleib et al., 2017; N. Kono et al., 2017).

yIRE1 is proposed to respond to such stress by virtue of an amphipathic helix (residues 526-542) partially overlapping with the TM, which partially deforms the membrane. During lipid stress, changes in membrane composition favour the gathering of IRE1 molecules to minimise the otherwise increased deformation of the membrane (Halbleib et al., 2017). Despite this proposed alternate mode of yIRE1 regulation, lipid stress still correlates with Kar2 release from yIRE1, though unlike in the response to protein stress, interface 2 is not required for yIRE1 activity (Ishiwata-Kimata et al., 2013). Whilst an analogous TM proximal amphipathic helix exists in IRE1α (Figure 1.07 top), mutational analysis reveals that amphipathicity is dispensable for sensing lipid stress and instead generic, physical properties of the TM are sufficient for response to changes in the ER membrane lipid composition (N. Kono et al., 2017). Neither yIRE1 nor IRE1α form clusters in response to lipid stress showing that IRE1 activity is not dependent on oligomerisation (Promlek et al., 2011; Kitai et al., 2013). This point still stands even if membrane properties during lipid stress are responsible for hindering oligomerisation rather than because of differences in the IRE1 activation mechanism (Kitai et al., 2013; Cohen et al., 2017).

The distinct responses of IRE1 to protein and lipid stress also indicate that the ER state is similarly distinct in these conditions. In yeast, it can be seen that, despite a similar level of yIRE1 activation, Kar2 incorporates into larger complexes during protein stress compared to lipid stress reflecting differences in the state of proteostasis (Promlek et al., 2011). In mammalian cells, loss of

Mdt-15 (a fatty acid synthesis transcription factor) activates IRE1 and PERK, and alters the ER membrane lipid composition but does not change the state of proteostasis (Hou et al., 2014).

Given that BiP dissociation from IRE1 is seen in response to both lipid and protein stress it suggests that it, unlike cluster formation, plays an essential role in IRE1 regulation.

Regulation of the PERK and ATF6 UPR branches

The UPR signal transducer PERK has similarities with IRE1 and an understanding of PERK regulation may give insight into the regulation of IRE1.

Despite having low sequence homology the structural homology of IRE1α LD and PERK LD is striking (Compare Figure 1.05 and Figure 1.09). Interface 1 is present in the PERK crystal structure (in addition to a novel one absent from IRE1 crystal structures) (Zhou et al., 2006; Carrara et al., 2015a). Unlike yIRE1, structurally PERK tetramers are seen to be ring like structures rather than filaments and are important for activation of PERK in response to stress (Carrara et al., 2015a). *In vitro* PERK LD forms oligomers with a (monomer-dimer) Kd of 0.53 μM (Zhou et al., 2006; M. Carrara et al., 2015). *In vivo* PERK is normally monomeric and, during stress, has been seen to redistribute into oligomers (even more so than IRE1α) which are enriched for the active phosphorylated PERK form (PERK-P) (Bertolotti et al., 2000).

The conservation of interface 1 between the evolutionarily distant yIRE1, IRE1α, and PERK proteins strongly supports that it is not formed through a crystal packing artefact and has an important physiological relevance to these proteins.

Like with IRE1α, an endogenous BiP:PERK complex can be detected, whose abundance decreases in response to stress and is destabilised by ATP. This complex is also seen to reform post-stress in a manner that correlates well with deactivation of PERK-P by dephosphorylation (Bertolotti et al., 2000). Furthermore deletions in the equivalent to region V (Figure 1.07) of PERK decrease the abundance of BiP:PERK complexes and correlate with increased basal auto-phosphorylation of PERK (Ma et al., 2002).

Domain swap experiments with IRE1 and the finding that artificial dimerisation of PERK LD with an antibody results in CD activation suggests that activation of PERK CD is achieved simply by inducing dimerisation (C Y Liu et al., 2000; Bertolotti et al., 2000). From this it could be extrapolated that the same holds true for IRE1 CD and that dimerisation is sufficient for activation, rather than by propagation of a conformational change from the LD via the TM, as seen for other dimeric signal transducers, e.g. the insulin receptor (and other tyrosine kinase receptors) (L. Ye et al., 2017).

The activation mechanism of the ATF6 branch is quite different from the IRE1/PERK branches. During stress the ATF6 type II membrane protein traffics to the Golgi apparatus where site-1 and site-2 proteases cleave the N-terminal CD to liberate the ATF6-N transcription factor in a mechanism similar to regulation of SREBP (sterol regulatory element-binding proteins) (Haze et al., 1999; J. Ye et al., 2000). Despite this very different activation mechanism, a regulatory role for BiP may still prevail as ATF6 is seen to exist in a chaperone-substrate complex with BiP that dissociates in response to stress (J. Shen et al., 2005).

1.09

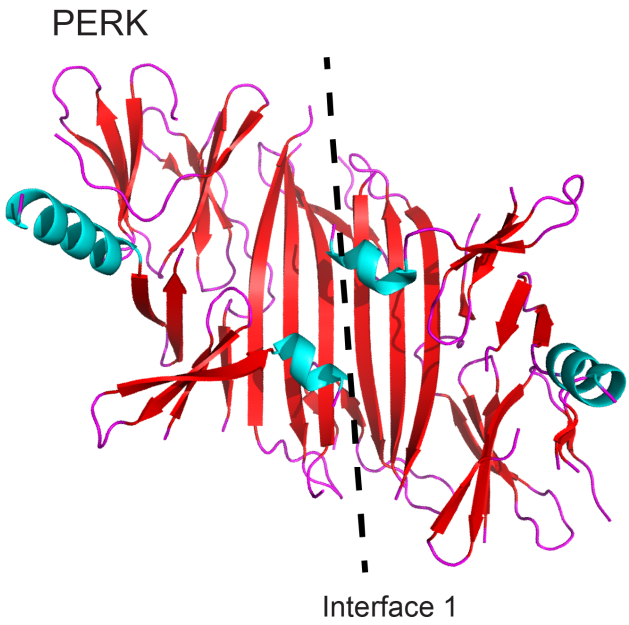

Figure 1.09 The crystal structure of the human PERK luminal domain (Carrara et al., 2015a PDB: 4YZS). The black dashed line indicates the dimer interface, which is structurally related to interface 1 of IRE1.

The inverse correlation between BiP association and stress for all three mammalian UPR branches points towards an evolutionarily conserved mechanism which relies on the specialised chaperone activity of BiP to monitor the levels of unfolded proteins in the ER.

However, to investigate chaperone inhibition, both experimental design and the interpretation of data from them needs to be informed by a clearer understanding of BiP activity and how this is regulated.

Hsp70s and regulation of chaperone activity

BiP is a member of the Hsp70 protein chaperone family. This family spans all kingdoms of life and was initially discovered through their involvement in the bacterial heat shock response in which they play a crucial role in preventing the aggregation of accumulating misfolded proteins.

Though mammalian cells express 17 different Hsp70s, BiP is the sole Hsp70 of the ER and is also the most abundant member of the ER's chaperone constituents (Ghaemmaghami et al., 2003; Daugaard et al., 2007). Hsp70 number varies considerably between eukaryotes with as few as 7 in *Schizosaccharomyces Pombe* or up to 26 in *Orya Sativa*, however BiP (or its homologues) remains the sole Hsp70 of the ER across eukaryotes (Craig and Marszalek 2017). BiP is involved in all facets of proteostasis: in assisting co-translational translocation of the nascent peptide, chaperoning the folding of nascent and misfolded proteins, and targeting terminally misfolded proteins for degradation (reviewed in Gething 1999; Dudek et al., 2009; Wang et al., 2017). Under basal conditions, BiP is present at high concentrations in the ER and is strongly transcriptionally upregulated during the UPR (Kozutsumi et al., 1988; Chang et al., 1989).

Like other Hsp70s, the BiP protein is comprised of a substrate-binding domain (SBD) and a nucleotide-binding domain (NBD) (Figure 1.10, see also the related structure of DnaK-ATP PDB:4B9Q Kityk et al., 2012). The SBD comprises of a core β-sheet base and an α-helical lid between which BiP substrates are bound. The NBD is an ATPase whose nucleotide state couples to large conformational changes of the SBD through contacts mediated by the

conserved linker region connecting the two domains. In the ATP-bound state the SBD exists in the “open” form where the lid makes extensive contacts with the NBD rather than covering the SBD β-sheet base (Figure 1.10 top BiP:ATP). In this conformation BiP has high k_{on} and k_{off} rates for substrates, resulting in an overall low affinity of binding. Hydrolysis of ATP to ADP switches the SBD to the high-affinity “closed” state with low k_{on} and k_{off} rates (Figure 1.10 bottom). Nucleotide exchange of ADP for ATP is required to switch BiP back to the “open” form and complete the chaperone cycle (Swain et al., 2007; Bertelsen et al., 2009; Kityk et al., 2012; M. P. Mayer 2013).

The intrinsic ATPase and nucleotide exchange activities of BiP (and of Hsp70s in general) are low and co-chaperones are required to drive these activities in a regulated manner for BiP to function as an efficient chaperone (Figure 1.11) (Liberek et al., 1991).

Nucleotide exchange of BiP is regulated by nucleotide exchange factors (NEFs) and the mammalian ER has two, Sil1 and Grp170 (reviewed in Behnke et al., 2015), and these are important for stimulating the release of BiP from substrates.

On the other side of the BiP chaperone cycle (Figure 1.11), is the hydrolysis of ATP, which is stimulated by ER-localised J-domain proteins (ERdjs). The eight ERdj variants in mammalian cells have in common a conserved J-domain (Figure 1.12), which is responsible for interacting with and stimulating BiP’s ATPase activity (reviewed in Kampinga and Craig, 2010; Mayer, 2013).

All J-domains share the histidine-proline-aspartate (HPD) motif which, from structural analyses, is seen to extend into the ATPase site of the NBD in order to stimulate ATP hydrolysis (Kityk et al., 2017). The point mutation of the histidine of the HPD motif to glutamine (HPD -> QPD) is a highly effective way to inactivate the ability of a J-domain to stimulate Hsp70 ATPase activity without compromising the fold of the rest of the protein (Kassenbrock and Kelly 1989; Wall et al., 1994; Wei and Hendershot 1995; M. Mayer et al., 2003).

1.10

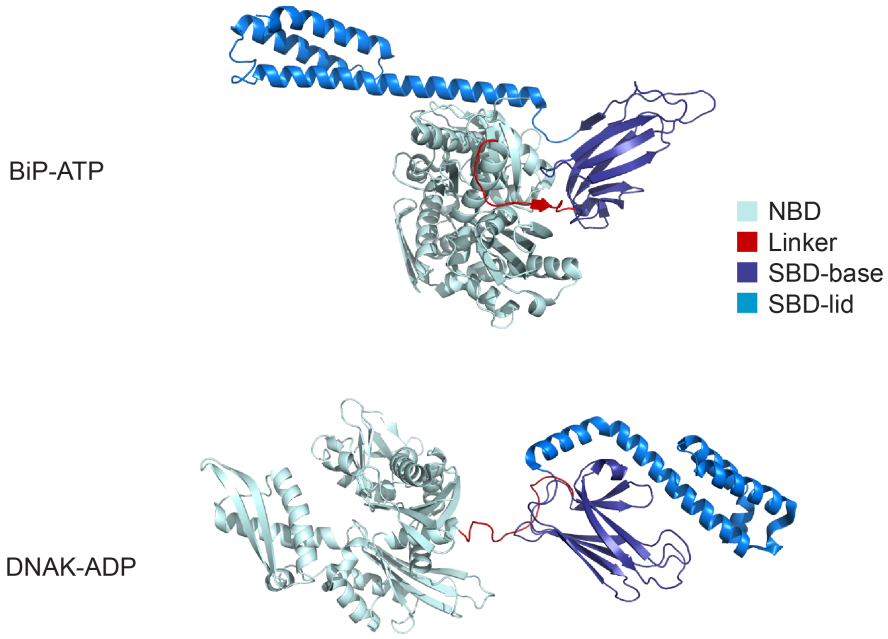

1.11

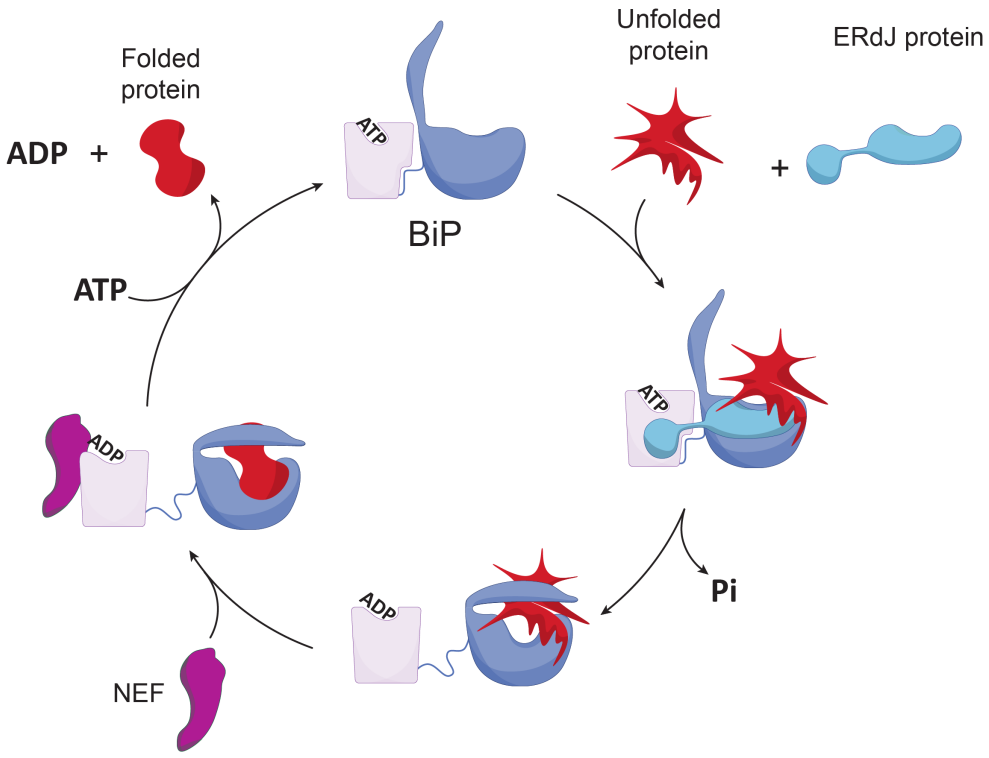

Figure 1.10 Top: Crystal structure of the BiP-ATP complex (PDB: 5E84). Bottom: NMR structure of the DnaK-ADP complex (PDB: 2KHO). Red – inter-domain linker, Light blue – NBD, Blue – α-helical lid of SBD, Dark blue – core of SBD

Figure 1.11 Cartoon of the BiP chaperone cycle (adapted from Preissler et al., 2015a). Light pink – BiP nucleotide binding domain, Dark blue – BiP substrate binding domain, Purple – nucleotide exchange factor (NEF), Light blue – ER localised J protein (ERdj).

Whilst stimulation of ATP hydrolysis by BiP is crucial for efficient chaperone activity, it is equally important that it occurs in the context of substrate. ERdj proteins ensure this is the case by binding to BiP substrate through additional protein domains (which differ significantly between the different ERdjs).

This means that when BiP-ATP makes transient low-affinity interactions with its substrates, ERdj proteins are optimally positioned to stimulate ATP hydrolysis and switch BiP to its low k_{off}, ADP-bound state coincident with substrate occupation of the SBD. The resultant binding of BiP to substrate is said to be an ultra-affinity interaction where the binding affinity is higher than the equilibrium values observed for either BiP:ATP or BiP:ADP. Such non-equilibrium ATP hydrolysis-dependent conformational cycles lie at the heart of the ability of Hsp70s to function as efficient chaperones (reviewed in Misselwitz et al., 1998; Kampinga and Craig 2010; De Los Rios and Barducci 2014).

Insight into the importance of J-domain proteins in directing Hsp70 activity came from study of the now archetypal bacterial DnaK-DnaJ pair. The DnaK Hsp70 holds the heat shock transcription factor (HSF) inactive via a canonical chaperone-substrate interaction. During heat stress, misfolded proteins begin to accumulate and DnaK is titrated away from HSF allowing it to activate the cell's heat shock transcriptional programme (Abravaya et al., 1992; Tomoyasu et al., 1998). The formation of the DnaK:HSF complex is catalysed by the J-domain containing DnaJ, which independently binds HSF and stimulates the ATP hydrolysis by DnaK during its low-affinity association with HSF to switch it to a high-affinity interaction (Gamer et al., 1996).

1.12

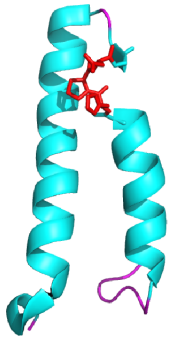

ERdj5 J domain

Figure 1.12 Crystal structure of the J-domain of ERdj5 (PDB: 5AYK). Note in Red the conserved histidine, proline, aspartate (HPD) motif.

This well understood system in bacteria sets a precedent for the ability of a chaperone/co-chaperone pair to regulate the activity of a signalling protein and how competition for the chaperone during stress can be an effective activator.

Goal

There are two proposed mechanisms by which IRE1 activates in response to protein stress. One suggests that the direct binding of unfolded proteins to the IRE1 LD induces the activating dimerisation and oligomerisation of IRE1. The alternative hypothesis holds that the UPR is organised along principles similar to its cytosolic counterpart, the heat shock response, in which IRE1 is held inactive by BiP, which is titrated away during stress.

The correlation between BiP dissociation from and activation of IRE1 is undisputed. However, although there is a clear evolutionary precedent for the chaperone inhibition model, attributing more than correlation to the dissociation event during the UPR is not possible with the current published data. Progress in this regard has been hampered by the inability of BiP to be mutated without compromising the ER proteostasis environment and the absence of an *in vitro* system reconstituting the *in vivo* observations. Until either of these hindrances is addressed it will be difficult to build an argument of causation for the BiP dissociation event.

On the other hand, the direct binding model is primarily supported by *in vitro* data, which centres on the ability of peptides that bind the groove of IRE1 to drive it into oligomeric structures. *In vivo* work building on the knowledge of these peptides has, however, not been forthcoming and therefore the physiological relevance of the *in vitro* observations remains ambiguous and decreases the credibility of this model.

With the advent of new gene-editing technologies and insights from the Hsp70 regulation field, this PhD aimed to investigate aspects of IRE1 regulation mechanisms. This thesis will outline the *in vivo* data supporting the role of ERdj4 facilitating a repressive BiP:IRE1 complex before describing the *in vitro* reconstitution of this system. Following this, mutational analyses probing IRE1 regulation and experiments directly assessing the binding of IRE1-activating peptides to the IRE1 peptide-binding groove will be described. Finally, these results will be discussed in context of the literature and used to suggest a current model for regulation of IRE1.

Chapters 2 - 5

Results

Chapter 2: *In vivo* evidence for IRE1α regulation by ERdj4

The CHO dual UPR-reporter cell line

Mammals have three independent signalling pathway branches constituting the UPR. This is convenient for studying the regulation of IRE1 as changes in its activity can be assessed against the other branches to reveal specific branch effects of interest, rather than effects on global ER proteostasis. With this in mind, a dual UPR-reporter Chinese hamster ovary (CHO) cell line was created. A pre-existing CHO cell line (X. Z. Wang et al., 1998) stably expressing a CHOP::GFP reporter, primarily under the control of PERK activity (Figure 1.01), was transduced with a retrovirus encoding an XBP1s::Turquoise reporter (a modified version of the XBP1s::Venus reporter from Iwawaki et al., 2004) which was integrated into the genome. The XBP1::Turquoise reporter (Figure 2.01) contains an out-of-frame Turquoise CDS which, upon splicing by active IRE1, is moved in frame allowing the Turquoise fluorescent protein to be correctly translated. The resultant dual UPR-reporter cell line readily responds to various ER stressors (Figure 2.01). Several rounds of selection were required to isolate a clone (S21) that stably expressed both reporters and is now a useful tool for *in vivo* studies on the UPR (Sekine et al., 2016; N. Kono et al., 2017). The S21 clone was used to generate all cell lines elaborated in this thesis and in experiments is referred to as WT. This dual UPR-reporter cell line is a useful tool for capturing the significant heterogeneity of proteostasis in stressed or transfected cell populations by the high-throughput technique of flow cytometry. As will be seen, having a fluorescence-based read-out of UPR phenotypes also greatly facilitates genome editing of UPR components.

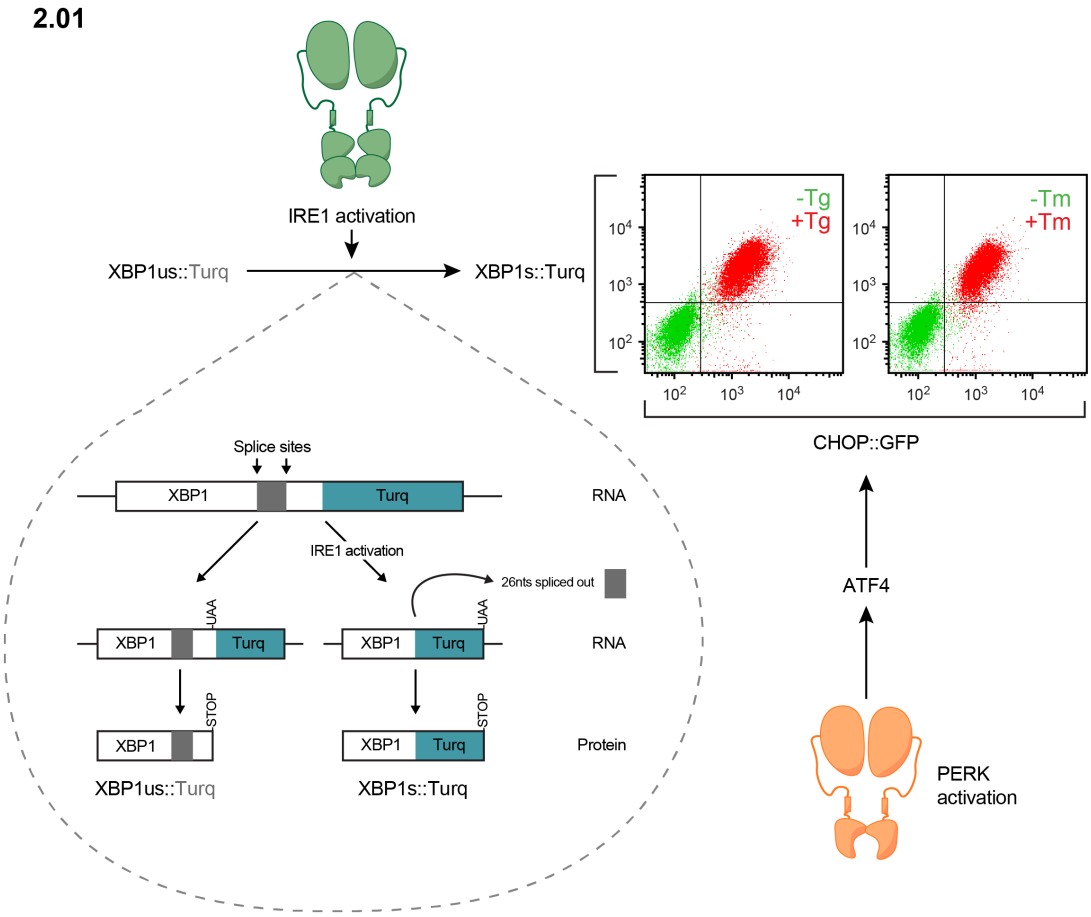

Figure 2.01 A schematic depicting the stably expressed XBP1s::Turquoise fluorescent gene reporter used to give a read-out on endogenous IRE1 activity. The unspliced mRNA contains a STOP codon upstream of the out-of-frame Turquoise fluorescent protein open reading frame (ORF). When the 26 nucleotide intron is removed by the active IRE1, the Turquoise ORF is no longer out of frame nor has a STOP codon preceding it. The resultant translated product is a fusion protein of the XBP1 and Turquoise protein (also see figure 1.02 for an overview of endogenous XBP1 regulatory splicing by IRE1). Shown also are dual channel flow cytometry plots of the XBP1s::Turquoise and CHOP::GFP gene reporters of 10,000 WT cells per condition treated as indicated.

ERdj4 selectively represses IRE1α signalling in mammalian cells

As described in the introduction, BiP is recruited to its substrates by ERdj co-chaperones. Given that *in vivo* evidence suggests the proposed repressive BiP:IRE1 complex forms through a canonical chaperone-substrate interaction it was hypothesised that ERdj proteins may catalyse the formation of this complex. Therefore, to examine the potential role of ERdjs in recruiting BiP to IRE1 to repress signalling, CRISPR-Cas9 genome editing was used to systematically inactivate the genes encoding the eight known ERdjs in S21 cells, defined by their ER targeting signal peptide and luminal J-domain (Table 2.01). Clones harbouring frame-shift insertion/deletion mutations in the respective ERdjs were isolated and levels of IRE1 and PERK activity under non-stress conditions assessed by flow cytometry (Figure 2.02).

It was seen that deletion of ERdj2 (Sec63) strongly activated both reporters, consistent with a role for this co-chaperone in supporting ER proteostasis or in repression of both IRE1 and PERK. In contrast, deletion of ERdj4 preferentially activated the XBP1::Turquoise reporter. The minor activation of

Name in thesis	Other name/s
ERdj1	Mjt1 and Dnajc1
ERdj2	Sec63
ERdj3	HEDJ and Dnajb11
ERdj4	MDG-1 and Dnajb9
ERdj5	JPDI and Dnajc10
ERdj6	p58IPK and Dnajc3
ERdj7	Dnajc25
ERdj8	Dnajc16

Table 2.01 A glossary of the different mammalian ERdjs and their alternate names.

CHOP::GFP observed in the ΔERdj4 cells was completely suppressed by treatment with the selective IRE1 inhibitor 4μ8c (Figure 2.03), indicating that it arose not from PERK activity but rather from IRE1's downstream contribution to *CHOP* induction (Figure 1.01) (X. Z. Wang et al., 1998). Together these observations suggest that, unlike ΔERdj2, activation of the IRE1 branch by ΔERdj4 is unlikely to reflect solely compromised ER protein folding.

2.02

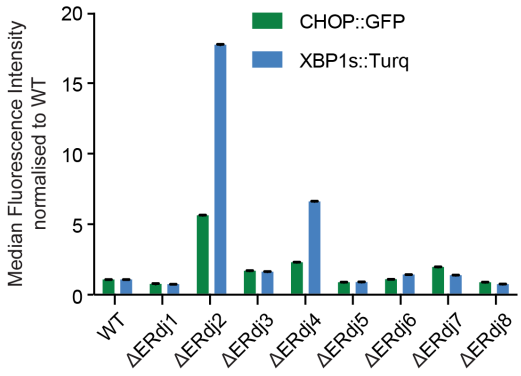

2.03

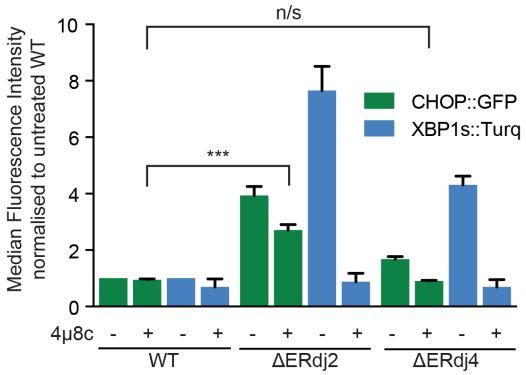

Figure 2.02 XBP1s::Turquoise and CHOP::GFP reporter activity in CHO cells with the indicated ER-localised J-protein (ERdj) deleted. Shown is the median fluorescence (± SEM) from 20,000 cells, normalised to wildtype (WT). Data for figures generated by Maarten Kamphuis and Claudia Rato.

Figure 2.03 XBP1s::Turquoise and CHOP::GFP activity in CHO cells untreated or treated with the IRE1 inhibitor 4μ8C, which blocks IRE1-dependent CHOP activation. Fluorescence normalised to WT. (Mean of medians ± SD, n=3, ***p = 0.0005, repeated measurements one-way ANOVA, Dunnett's multiple corrections test). Data for figures generated by Maarten Kamphuis and Claudia Rato.

ERdj4 is a small 25.5 kDa soluble protein with an N-terminal J-domain and a poorly defined C-terminal region involved in protein binding, referred to here as the targeting domain (Figure 2.04). To assess whether both the J- and targeting domains of ERdj4 were involved in IRE1 repression different ERdj4 mutants were created and transfected into the *ΔERdj4* cells and the XBP1s::Turquoise reporter measured by flow cytometry (Figure 2.05-2.07)

2.04

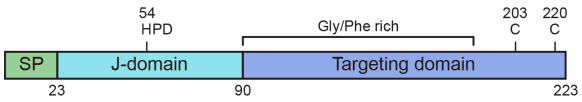

2.05

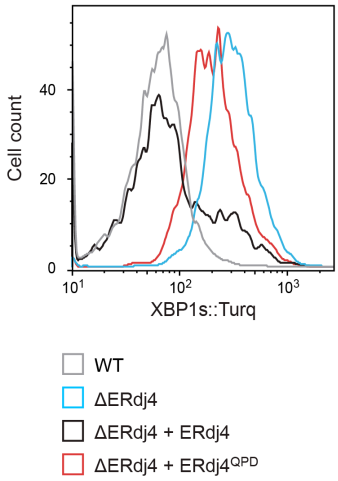

2.06

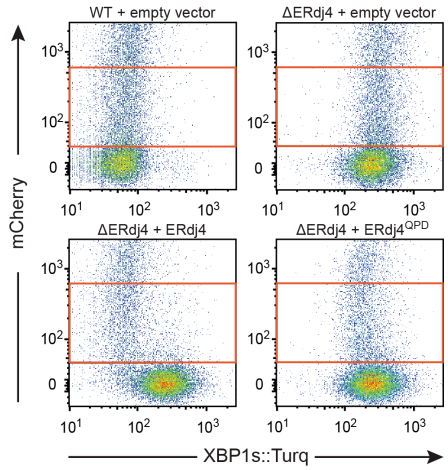

Figure 2.04 A schematic of the domain layout of ERdj4. Green – Signal peptide (SP), Light blue – the ERdj4 J-domain, Dark blue – the ERdj4 targeting domain. Numbers indicate the amino acid residue numbers of the domain element boundaries and the length of the domain elements are scaled according to number of residues. The location of the conserved J-domain HPD motif and targeting-domain cysteine residues are indicated.

Figure 2.05 XBP1s::Turquoise signals from cells transfected with empty plasmid or with mCherry marked plasmid encoding ERdj4 with a wildtype or inactive J domain (ERdj4^{QPD}). Transfected cells gated for moderate mCherry expression levels as shown in figure 2.06.

Figure 2.06 Dual channel flow cytometry plots of the XBP1s::Turquoise reporter and mCherry (a transfection marker) in wildtype and ΔERdj4 cells transiently transfected with a mCherry-tagged plasmid encoding no ERdj4 (“empty”), wildtype ERdj4 and mutant ERdj4^{QPD}. The red rectangle delineates the gate used to select cells expressing moderate levels of mCherry-tagged plasmid for the histogram shown in figure 2.05.

Wildtype ERdj4 was able to attenuate IRE1 activity in ΔERdj4 cells, but the H54Q mutant ERdj4 (ERdj4^{QPD}) that lacks J-domain activity, was largely inert (Figure 2.05-2.06). Expression of an ER-localised truncated ERdj4 fused to mCherry (containing the J-domain, but lacking the targeting domain), failed to attenuate IRE1 activity in ΔERdj4 cells and instead further activated both the IRE1 and PERK reporters (Figure 2.07). This feature was absent from the QPD J-domain mutant and is consistent with the idea that deregulated J-domain activity would perturb protein-folding homeostasis in the ER. These data show that the integrity of both J- and targeting domains is required for IRE1 repression by ERdj4.

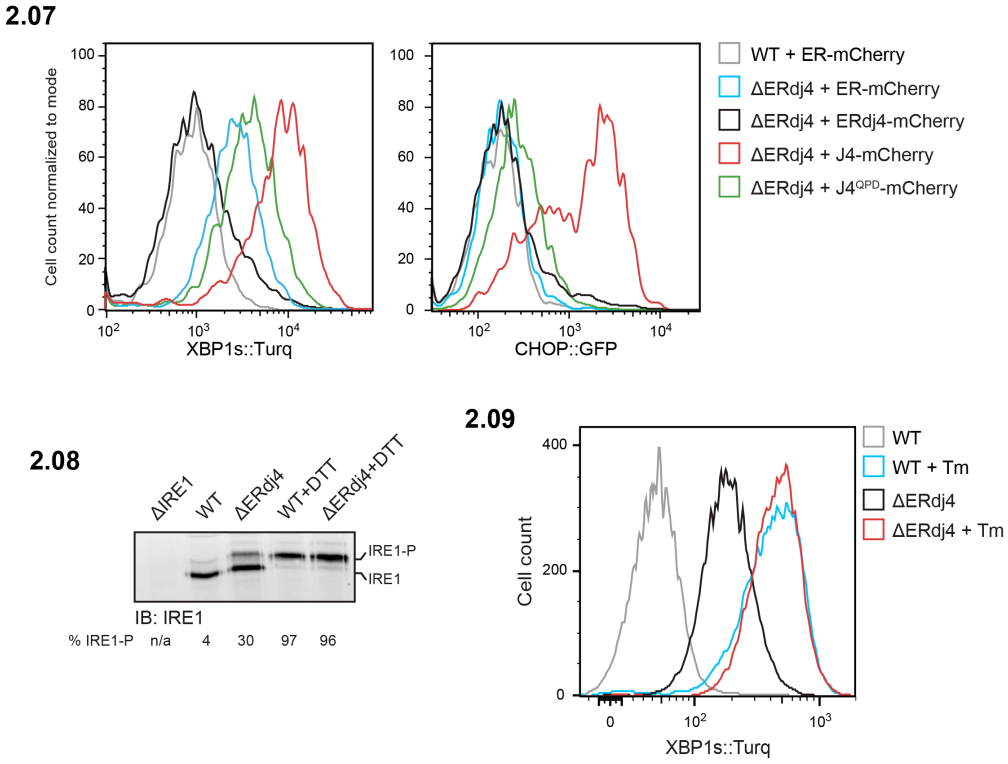

Figure 2.07 XBP1s::Turquoise and CHOP::GFP signals from cells transfected with ER-localised mCherry (ER-mCherry, a control) or mCherry tagged full-length ERdj4 (ERdj4-mCherry), mCherry tagged ERdj4 isolated J-domain (1-90) (J4-mCherry; WT and QPD). Transfected cells were gated for moderate mCherry expression as in figure 2.05.

Figure 2.08 Immunoblot of immunoprecipitated endogenous IRE1α after Phos-tag SDS-PAGE. Where indicated, cells were treated with dithiothreitol (DTT). Fraction of active (phosphorylated) IRE1-P from this representative blot is noted.

Figure 2.09 XBP1s::Turquoise signals from wildtype or ΔERdj4 cells. Where indicated, cells were treated with tunicamycin (Tm).

De-repression of IRE1, as seen by the elevated XBP1s::Turquoise, should be accompanied by increased levels of the active phosphorylated IRE1α under basal conditions. Indeed phosphorylation of endogenous IRE1α in the absence of stress was consistently higher in ΔERdj4 CHO cells compared to the WT parental cells (Figure 2.08). Interestingly the IRE1 in *ΔERdj4* cells still responded to ER stress as seen when measuring IRE1α phosphorylation (Figure 2.08) or levels of XBP1s::Turquoise (Figure 2.09). This indicates that other mechanisms of IRE1α regulation persist in the absence of ERdj4.

The chaperone inhibition model states that IRE1 repression correlates with the abundance of a BiP:IRE1^{LD} complex. In keeping with this is was found that the amount of BiP recovered in complex with endogenous IRE1α from ΔERdj4 cells was reduced by half, relative to the wild-type cells (Figure 2.10).

In the absence of one of its repressors it would be expected that IRE1α activity would be sensitised to ER stress. However, treatment of WT and *ΔERdj4* cells with a titration of Tm revealed that, though XBP1s::Turquoise levels were consistently higher in *ΔERdj4* cells, the IRE1 response to Tm was not sensitised by the absence of ERdj4. This can be seen by the EC_{50} values and the normalised XBP1s::Turquoise plot (Figure 2.11). This could be explained by adaptive transcriptional changes of the cell to keep the sensitivity of IRE1 in an optimum window required for efficient proteostasis.

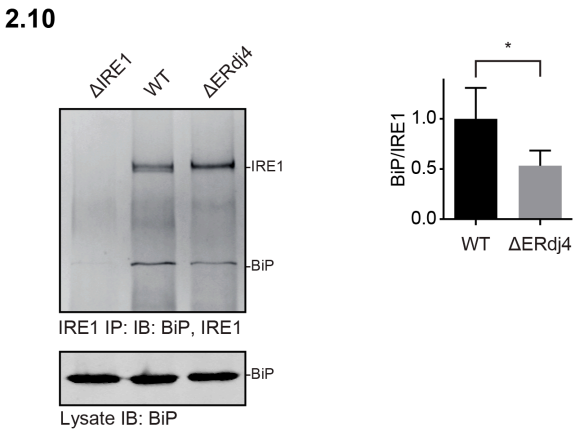

Figure 2.10 Representative immunoblot of endogenous IRE1α and associated BiP recovered from the indicated cell lines by immunoprecipitation of IRE1α. Ratio of BiP to IRE1 signal in 6 independent experiments. Mean ± SD, *p = 0.0118 parametric ratio paired Student's t test).

A similar finding is seen in the bacterial heat shock response where lowering levels of DnaK and DnaJ causes elevated HSP levels under basal conditions but the system remains equally sensitive to heat shock (Tomoyasu et al., 1998). An altered response to heat stress only becomes apparent during the recovery period in which HSP levels remain elevated rather than decreasing in the presence of correct levels of DnaK and DnaJ (Tomoyasu et al., 1998).

This is particularly interesting when bearing in mind the many yIRE1 region V experiments that do not detect a role of Kar2 binding in yIRE1 regulation as assessed by yIRE1 activation but do see delayed attenuation (Pincus et al., 2010; Ishiwata-Kimata et al., 2013; Mathuranyanon et al., 2015). It may well turn out that, as in the bacterial system, homeostasis obscures the role of Hsp70 regulation during induction of signal transducers.

The homeostatic nature of the system is also evident from the negative feedback loop of IRE1 activation resulting in ERdj4 upregulation, which is able to deactivate IRE1. Other feedback mechanisms likely exist to dampen the system and it would be interesting to assess the affects loss of ERdj4 has on attenuation of IRE1 activity during stress.

2.11

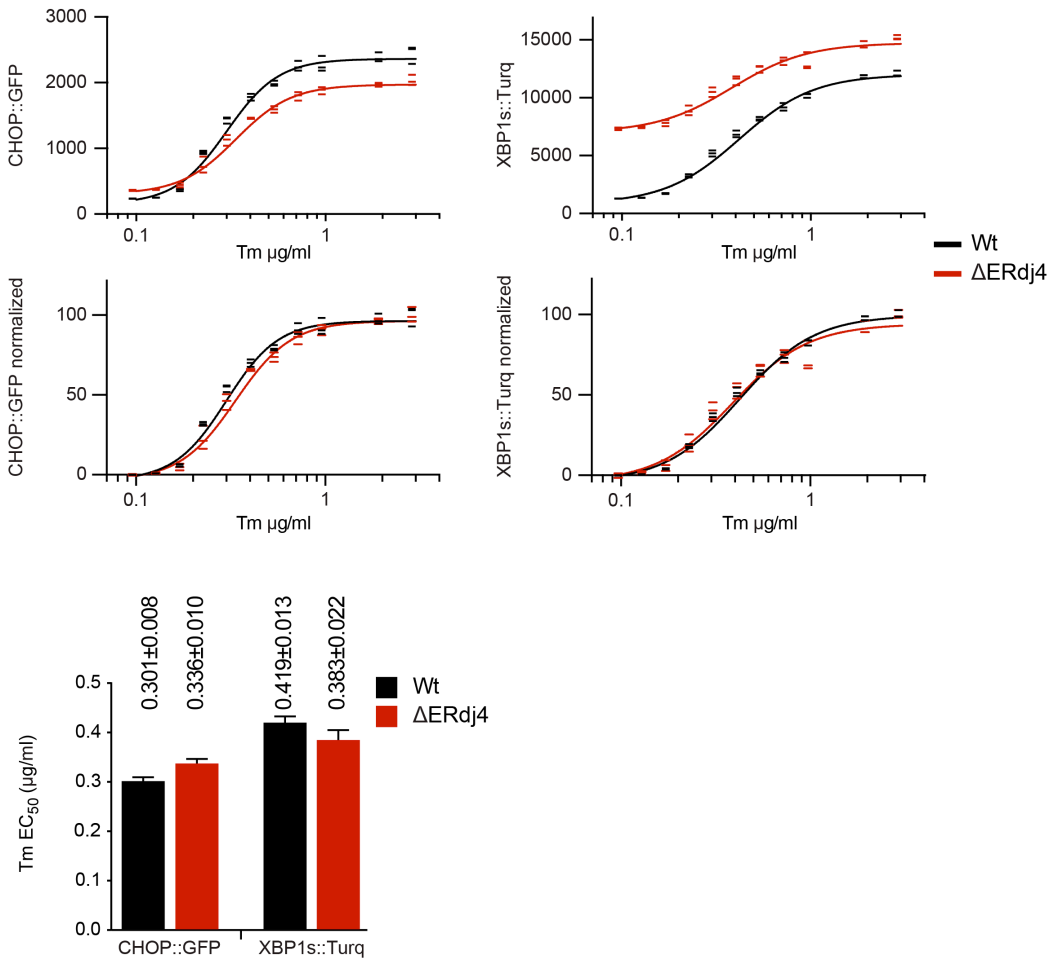

Figure 2.11 Plot of tunicamycin (Tm) concentration-dependent changes in XBP1s::Turquoise and CHOP::GFP reporter gene activity in wildtype and ΔERdj4 cells. Shown are the median fluorescence values (raw or normalised to the untreated sample as indicated) obtained from 10,000 cells in experimental triplicates and the fit to sigmoidal does-response curve. The bar chart shows the Tunicamycin EC_{50} values for CHOP::GFP and XBP1s::Turquoise reporters in the indicated cell lines.

ERdj4 promotes association of BiP with the structured core region of the IRE1α luminal domain in cells

To probe further ERdj4's role in BiP recruitment to IRE1^{LD}, the cytosolic effector domain of hIRE1α was replaced with glutathione S-transferase (GST), yielding a convenient sensor, comprised of IRE1α's luminal and transmembrane domain (TM) fused to cytosolic GST and uncoupled from downstream signalling (Figure 2.12). IRE1^{LD}-GST recovered by glutathione affinity chromatography from ΔERdj4 cells was associated with some BiP. However, in ΔERdj4 cells, co-transfection of IRE1^{LD}-GST with wildtype ERdj4 increased the recovery of BiP by 2.5-fold compared with co-transfection of ERdj4^{QPD} (Figure 2.13). The specificity of ERdj4's effect on IRE1 was assessed using the UPR relevant PERK and ERdj6 proteins. ERdj4 co-expression did not increase the recovery of BiP in complex with the luminal domain of PERK (Figure 2.14). Similarly, ERdj6, another UPR-induced ERdj protein (Yan et al., 2002), did not increase recovery of BiP in complex with IRE1^{LD}-GST (Figure 2.15). ERdj4 thus has a specific capacity to promote a BiP:IRE1^{LD} complex *in vivo*.

As described in the introduction, the tail of IRE1α (and the analogous region V

2.12

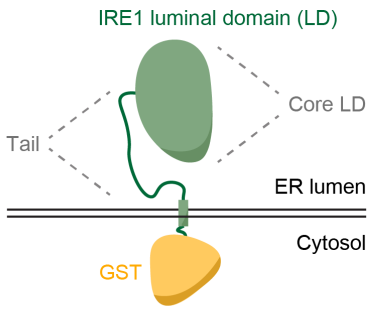

2.13

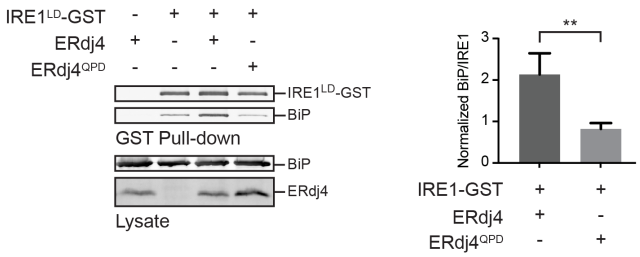

Figure 2.12 Schema of the IRE1^{LD}-GST protein containing the entire human IRE1α luminal and transmembrane domains (residues 19-486) fused to glutathione S-transferase (GST).

Figure 2.13 Representative immunoblots of IRE1^{LD}-GST and endogenous BiP, recovered by glutathione affinity chromatography or in lysate of transfected ΔERdj4 cells. The bar chart shows the ratio of BiP to IRE1^{LD}-GST signal from 4 experiments. Mean ± SD. **p = 0.0048, parametric ratio paired Student's t test).

of yIRE1) has been shown to be important for BiP binding and involved in the repression of IRE1α. The tail may therefore be required for ERdj4-mediated formation of the repressive BiP:IRE1^{LD}-GST complex. However, in Δ*ERdj4* cells ERdj4 was still able to increase BiP recovery with IRE1^{CLD}-GST (Figure 2.16), indicating its ability to act on the CLD alone. The potential role played by the IRE1α tail therefore remains unclear.

BiP has been reported to associate with IRE1^{LD} in a nucleotide-independent manner via its NBD rather than, more conventionally, by its SBD (Carrara et al., 2015b; Kopp et al., 2018). However, addition of ATP destabilised both the BiP:IRE1^{LD}-GST and the endogenous BiP:IRE1 complexes showing that *in vivo* the BiP:IRE1 complex is sensitive to nucleotide (Figure 2.17-2.18). Together, these findings indicate that BiP engages the IRE1^{CLD} as a canonical Hsp70 substrate, an event that is promoted by ERdj4.

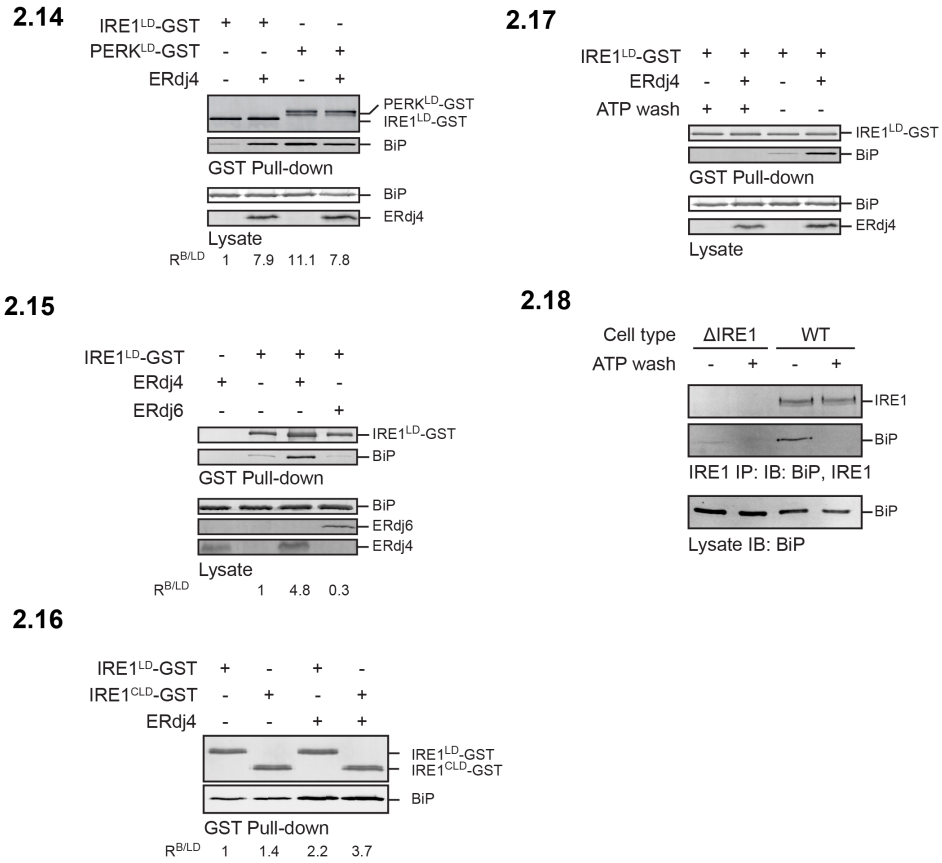

Figure 2.14 As in figure 2.13; compares IRE1^{LD}-GST to PERK^{LD}-GST. R(B/LD) notes the ratio of the BiP signal to the GST from the representative experiment shown.

Figure 2.15 As in figure 2.13; compares ERdj4 to ERdj6.

Figure 2.16 As in figure 2.13; compares IRE1^{LD}-GST to IRE1^{CLD}-GST.

Figure 2.17 As in figure 2.13; prior to elution with sample buffer, the indicated glutathione sepharose beads were incubated for 5 minutes with 3 mM ATP at room temperature.

Figure 2.18 Immunoblot of endogenous IRE1α and BiP recovered from CHO cells of the indicated genotype by immunoprecipitation of IRE1α. Prior to elution with sample buffer the indicated protein-A sepharose beads were incubated with ATP (as in figure 2.17). The bottom panel shows the input of BiP in the two samples.

Estimating the monomer-dimer equilibrium of endogenous IRE1α (Creating the endogenous Q105C IRE1α)

To determine whether the ERdj4-promoted BiP:IRE1^{LD}-GST complex influenced the IRE1^{LD} monomer-dimer transition that would initiate the UPR, a method to measure stress-relevant IRE1^{LD} dimerisation in cells was established. The crystal structure of dimeric human IRE1^{LD} reveals a polar interaction between the Q105 side chains of opposing protomers (Figure 2.19). It was hypothesised that presence of a cysteine at position 105 might permit the formation of detectable, stress-inducible, disulfide-linked IRE1 dimers. To assess the validity of this hypothesis, the Q105C mutation was introduced into the endogenous IRE1α locus in the dual UPR-reporter cell line. This was achieved in a two-step process in which, first, an appropriate guide sequence was used to target Cas9 endonuclease to introduce a double strand break (DSB) in the IRE1α genomic locus adjacent to the Q105 encoding sequence. In the absence of an appropriate DNA repair sequence, the cell repairs this DSB with error-prone non-homologous end joining DNA repair machinery. Such DNA repair can result in mutations, including frame shift mutations, which effectively knock out the expression of a gene. Fluorescence activated cell sorting (FACS) was used to isolate an IRE1α knock out clone (ΔIRE1) and the gene locus sequenced to verify the presence of a knock out mutation. The ΔIRE1 cell line provided a convenient background for the second step of creating an endogenous Q105C mutation (Figure 2.20).

2.19

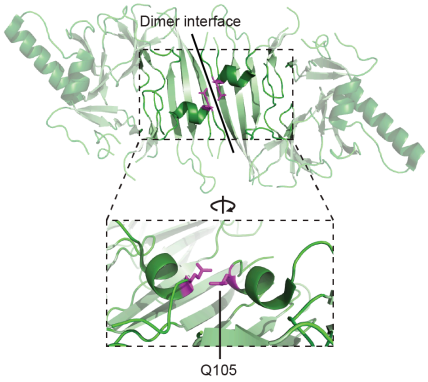

Figure 2.19 Crystal structure of human IRE1^{LD} (PDB 2HZ6) highlighting Q105 (purple) at the dimer interface.

A guide-directed Cas9 was again used to introduce a new DSB close to the Q105 encoding sequence in the ΔIRE1 cells. This time, a DNA repair sequence encoding either IRE1^{WT} or IRE1^{Q105C} was provided to the cells, allowing homology directed recombination (HDR) repair of the locus using the DNA repair sequence as a template[4]. Treatment of these cells with an ER stressor revealed the sub-population that had correctly repaired their IRE1α. 2-deoxyglucose (2DG) was used in these experiments because it is a reversible glycosylation inhibitor and a milder ER stressor when compared to Tm that increases the viability of cells during FACS and more clearly reveals differences in the WT and Q105C IRE1 activities.

FACS was used to collect repaired clones (Figure 2.21) and a mixed population for analysis (Figure 2.22). It was found that IRE1^{Q105C} CHO cells retained the ability to mount a UPR (Figure 2.20-2.22). IRE1^{Q105C} is expressed at a lower level than wild-type IRE1, possibly because it is less stable in cells. This decreased expression level likely accounts for the attenuated induction of the IRE1 branch of the UPR in IRE1^{Q105C} cells (Figure 2.20-2.22). Despite its lower level of expression, ER stress induction by Tg-mediated luminal calcium depletion resulted in the formation of a disulfide in the IRE1^{Q105C} mutant cells (Figure 2.23), reflecting the close proximity of the cysteines in the activated dimer and providing a readout for stress-relevant IRE1^{LD} dimer formation *in vivo*. Importantly, activation of IRE1^{Q105C} is not dependent on disulfide formation for activation, as seen by the ability of the ER stressor DTT to stimulate IRE1^{Q105C} phosphorylation (Figure 2.24) whilst simultaneously disrupting the oxidising environment required for disulfide bond formation in the ER (Figure 2.23). IRE1^{Q105C} activation therefore likely occurs in a similar manner as IRE1^{WT}. Evidence of the ability of IRE1^{Q105C} to form Q105C-Q105C disulfide bonds, comes from the clear disulfide species seen when a modified IRE1^{LD}-GST (with the Q105C mutation) is co-expressed with FLAG tagged full length IRE1^{Q105C} (Figure 2.25-2.26).

---

[4]The Q105C repair template introduced an additional C109S mutation to avoid potential C105-C109 disulfide bond formation.

2.21

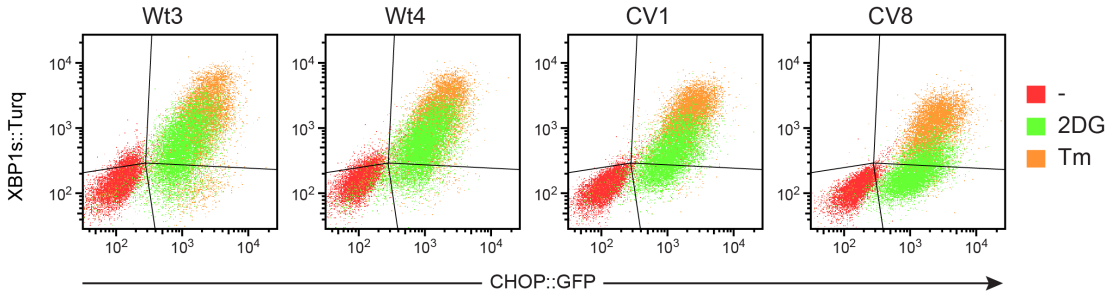

2.22

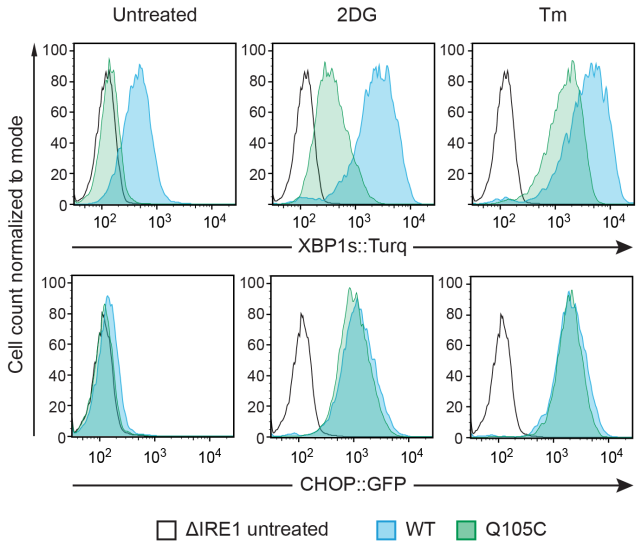

Figure 2.21 Dual channel flow cytometry plots of the XBP1s::Turquoise and CHOP::GFP gene reporter signals from representative clones obtained from ΔIRE1 cells challenged with Wt or Q105C repair templates. 10,000 events were collected per condition.

Figure 2.22 Histogram of XBP1s::Turquoise and CHOP::GFP signals obtained by flow cytometry analysis of the indicated cell lines untreated or exposed overnight to 2-deoxyglucose (2DG, 4mM), or tunicamycin (Tm, 2.5 µg/ml).

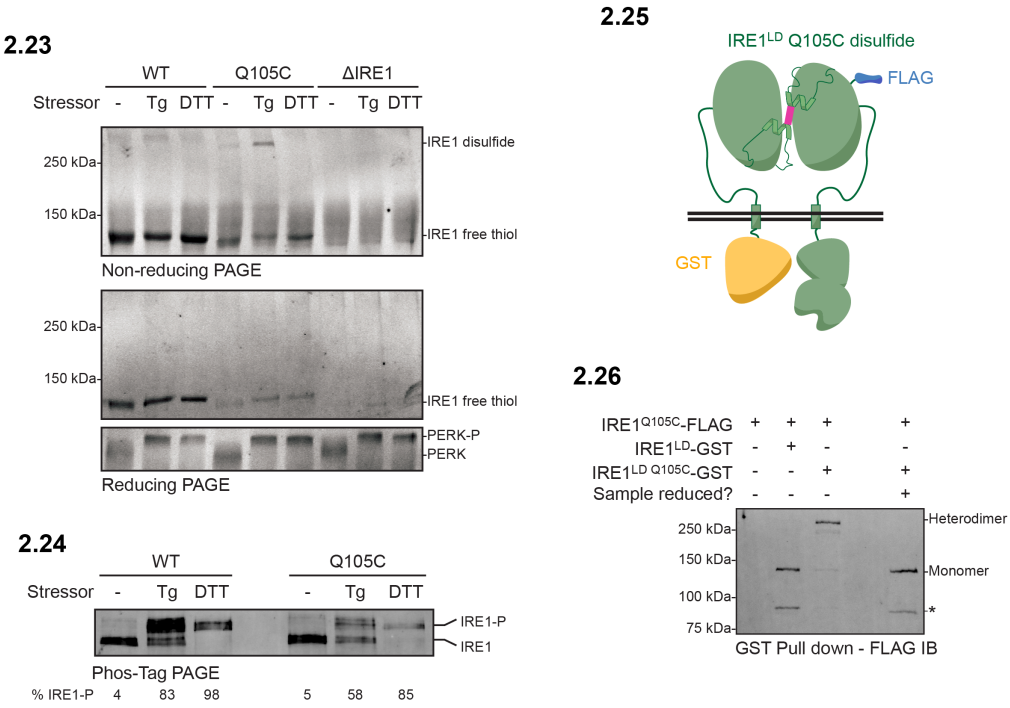

Figure 2.23 Representative immunoblot of endogenous IRE1α and PERK recovered from the indicated cell lines by immunoprecipitation of IRE1α or PERK and resolved by reducing and non-reducing SDS-PAGE. ER stress was induced by thapsigargin (Tg) or DTT. Data for figure generated by Heather Harding

Figure 2.24 Reducing Phos-Tag SDS-PAGE of endogenous IRE1α recovered from wildtype or IRE1^{Q105C} cells treated in the indicated manner. Fraction of active (phosphorylated) IRE1-P from this representative blot is noted.

Figure 2.25 IRE1$^{LD\ Q105C}$-GST and IRE1^{Q105C}-FLAG with Q105C-Q105C disulfide indicated.

Figure 2.26 Immunoblot of FLAG-IRE1^{Q105C} recovered by glutathione affinity chromatography from transfected WT CHO cells. Samples were reduced with DTT or left oxidised to preserve disulfide species. Star indicates degraded FLAG-IRE1^{Q105C} species.

ERdj4 opposes IRE1α luminal domain dimerisation in cells

The ability of ERdj4 to catalyse formation of the repressive BiP:IRE1 complex should be accompanied by a decrease in IRE1 dimerisation. To this end $IRE1^{LD\ Q105C}$-GST was used to gauge the effect of ERdj4 on the monomer-dimer ratio (Figure 2.27). Unlike endogenous $IRE1^{Q105C}$ (Figure 2.23), exogenously expressed $IRE1^{LD\ Q105C}$-GST is abundant and spontaneously forms disulfide-linked $IRE1^{LD\ Q105C}$-GST dimers. When co-transfected, wild-type ERdj4 decreased by 2.5-fold the fraction of disulfide-linked, dimeric $IRE1^{LD\ Q105C}$-GST. $ERdj4^{QPD}$ had no effect on the monomer-dimer ratio highlighting the importance of the J-domain activity (Figure 2.27). Immunoprecipitation of endogenous BiP from cells transfected with $IRE1^{LD\ Q105C}$-GST and ERdj4 variants again reveals the ability of ERdj4 to increase the abundance of a nucleotide-sensitive BiP:IRE1 complex in a manner that is dependent on a functional J-domain (Figure 2.28). Interestingly, ERdj4 increases the association of BiP with both $IRE1^{LD\ Q105C}$-GST free thiol IRE1 and disulfide linked $IRE1^{LD\ Q105C}$-GST species at a ratio that reflects the distribution of the $IRE1^{LD\ Q105C}$ species in the cells. This suggests that both ERjd4 and BiP are able to bind IRE1 monomers and dimers and may provide clues to their respective binding sites as discussed later.

2.27

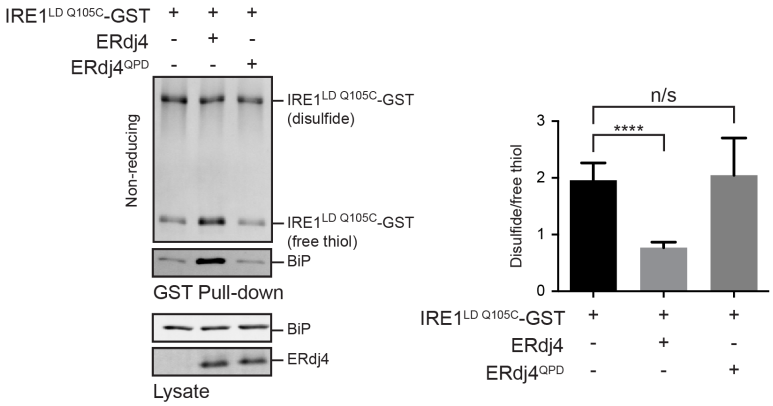

2.28

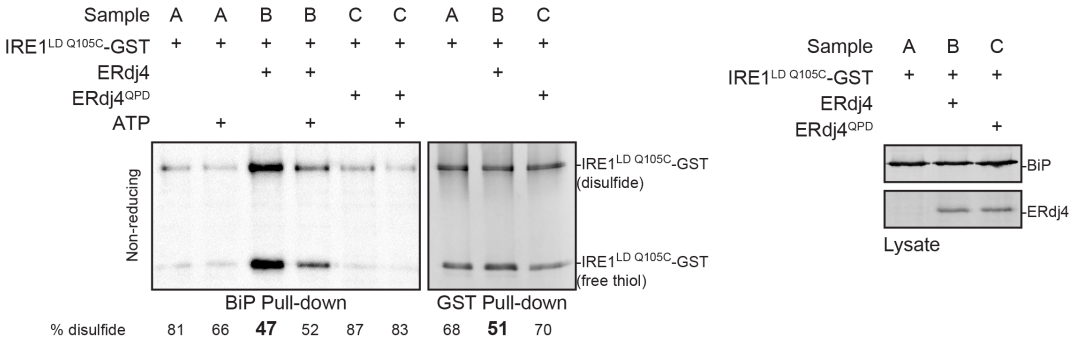

Figure 2.27 Representative immunoblot of IRE1$^{LD\ Q105C}$-GST and BiP recovered from ΔERdj4 cells transfected with indicated constructs and resolved by non-reducing SDS-PAGE. The bar chart shows the ratio of disulfide-bound IRE1$^{LD\ Q105C}$-GST dimer to free thiol in indicated samples. Quantified in 6 independent experiments (mean ± SD, n=6, ****p <0.0001, unpaired Student's t test with Welch's correction).

Figure 2.28 Immunoblots of IRE1$^{LD\ Q105C}$-GST recovered by glutathione affinity chromatography or BiP immunoprecipitation and resolved on a non-reducing SDS-PAGE. Immunoblots of endogenous BiP and expressed ERdj4 variants in lysate of transfected ΔERdj4 cells are also shown. The percentage of IRE1$^{LD\ Q105C}$-GST disulfide linked dimers is noted. Prior to elution with sample buffer, the indicated protein-A sepharose beads were incubated for 5 minutes with 3 mM ATP at room temperature.

Chapter 2 summary

The data described here point towards an important role for ERdj4 *in vivo* in repressing IRE1α activity. The previously reported inverse correlation between IRE1 activation and levels of the BiP:IRE1 complex holds true in the *ΔERdj4* cells and is consistent with a role for ERdj4 acting as a co-chaperone to load BiP onto IRE1 in canonical chaperone-substrate event. The nature of the BiP:IRE1 complex is supported by the sensitivity it exhibits to incubation with ATP.

Use of IRE1^{Q105C} allowed the effect of ERdj4 on stress-relevant IRE1 dimerisation to be monitored and revealed that the repression of activity correlated with monomerisation. It is noteworthy that the presence of this disulfide in the IRE1 dimer would likely occlude the peptide-binding groove making it difficult to reconcile the direct binding model with the data presented here.

Chapter 3: *In vitro* evidence for IRE1α regulation by ERdj4

To investigate the role of ERdj4 directly promoting a repressive BiP:IRE1 complex it was attempted to reconstitute the system *in vitro.*

Purifying a functional ERdj4

Whilst both IRE1α and BiP had previously been successfully purified from bacteria (Zhou et al., 2006; Carrara et al., 2015b; Preissler et al., 2015a), ERdj4 has not, and obtaining a purified functional form of the protein proved to be challenging (see Table 3.01 for an overview of the various constructs trialled). Despite being an ER resident protein, ERdj4 is neither glycosylated nor known to be otherwise post-translationally modified, and a standard bacterial expression system was therefore chosen for purification. The initial ERdj4 constructs, with and without N-terminal solubilising domains, all suffered from poor solubility and formed aggregates during the expression and purification (Table 3.01 1764, 1763, 1762).

The targeting domain of ERdj4 is not known to be structured and therefore may be prone to aggregation outside of the native ER environment. ERdj4 with a C-terminal MBP solubilising domain was expressed (GST-ERdj4-MBP) and purified, yielding an abundant and soluble protein. Despite this success, GST-ERdj4-MBP was very poor at loading BiP onto IRE1, despite displaying J-domain activity (as assessed by experiments detailed later). Several attempts were made to remove either solubilising domain post-purification of GST-ERdj4-MBP in case they inhibited the ability of ERdj4 to engage with IRE1. However, these attempts resulted in precipitation of the protein.

ERdj4 possess two cysteines at its far C-terminus which, when expressed in the ER, may be involved in an intra-molecular disulfide bond (Figure 2.04). To facilitate the formation of such a potential disulfide, a different bacterial expression strain (Origami BDE3) was chosen with an oxidising cytosol to permit disulfide formation. Use of a purification strategy aimed at preserving disulfide bonds was successful in generating a soluble ERdj4 protein (His-Sumo-ERdj4^{ox}) able to load BiP onto IRE1, suggesting that a structure stabilising disulfide forms in ERdj4. The purified His-Sumo-ERdj4^{ox} contained multiple contaminating C-terminal truncations and so the MBP solubilising

domain was added to protect the C-terminus from degradation. His-Sumo-ERdj4-MBP^{ox} was however significantly less active than His-Sumo-Erdj4^{ox}. Given the potential importance of the targeting domain in facilitating interactions with IRE1, a longer flexible linker (LL) was included to separate ERdj4 and MBP, thereby reducing steric hindrance. The resultant His-Sumo-ERdj4-LL-MBP^{ox} protein was similarly active as His-Sumo-ERdj4^{ox} but did not have the contaminating truncated species.

From this, it seems that the ERdj4 protein has a structurally important disulfide and requires an unhindered targeting domain to make productive interactions with substrate.

Lab #	ERdj4 residues 24-223		Bacterial strain	Soluble?	Functional?
	N- tag	C- tag			
1764	None	None	Standard	No	n/a
1763	GST	None	Standard	No	n/a
1762	His-Sumo	None	Standard	No	n/a
1772	GST	MBP (SL)	Standard	Yes	Very low
2012	His-Sumo	None	Origami	Yes	High
2104	His-Sumo	MBP (SL)	Origami	Yes	Low
2108	His-Sumo	MBP (LL)	Origami	Yes	High

Table 3.01 An outline of the various ERdj4 constructs trialled to generate a purified ERdj4 from bacteria. SL-short linker, LL-long linker.

ERdj4 promotes association of BiP with the structured core region of the IRE1α luminal domain *in vitro*

The successfully purified constituents were used to investigate ERdj4 mediated formation of the BiP:IRE1 complex and the importance of this as a regulatory event (Figure 3.01). An IRE1^{LD} lacking endogenous cysteines was chemically labelled with biotin on its C-terminus (IRE1^{LD}-bio) via a D443C mutation. Formation of a BiP:IRE1^{LD}-bio complex was assessed by recovery on immobilised streptavidin (Figure 3.02). It was found that BiP and IRE1^{LD} formed a complex only in the presence of ERdj4[5] and ATP (Figure 3.03, lanes 2, 4, 9). Like its *in vivo* counterpart (Figure 2.17-2.18), the isolated BiP:IRE1^{LD} complex thus formed was sensitive to disruption by incubation with ATP (Figure 3.03, upper panel. The residual BiP eluted with SDS, lower panel, reflects incompleteness of the preceding ATP elution, as demonstrated in figure 3.04 where a further decrease in BiP signal can be seen going from lanes 1 and 2 to lanes 3 and 4 respectively with further ATP elutions). The ERdj4^{QPD} mutation and mutations in BiP that interfered with its ATPase activity (BiP^{T229A} McCarty & Walker 1991) or substrate binding ability (BiP^{V461F} Laufen et al., 1999) greatly enfeebled complex formation (Figure 3.03, lanes 5, 7, 8). Association of BiP's isolated NBD with the IRE1^{LD} was not observed (Figure 3.05), pointing away from the non-canonical BiP:IRE1 interaction previously suggested by Carrara et al., 2015b and Kopp et al., 2018.

Together the data from figures 3.04 and 3.05 suggest instead that the BiP:IRE1 complex is a canonical chaperone-substrate interaction and therefore requires the functional integrity of BiP's SBD and NBD as well as the presence of ATP and the functional ERdj4 co-chaperone.

[5] The 37 kDa His-Sumo-ERdj4^{ox} was used for these assays rather than the 77 kDa His-Sumo-ERdj4-LL-MBP^{ox} to allow the ERdj4 protein to be distinguished from the 71 kDa BiP protein.

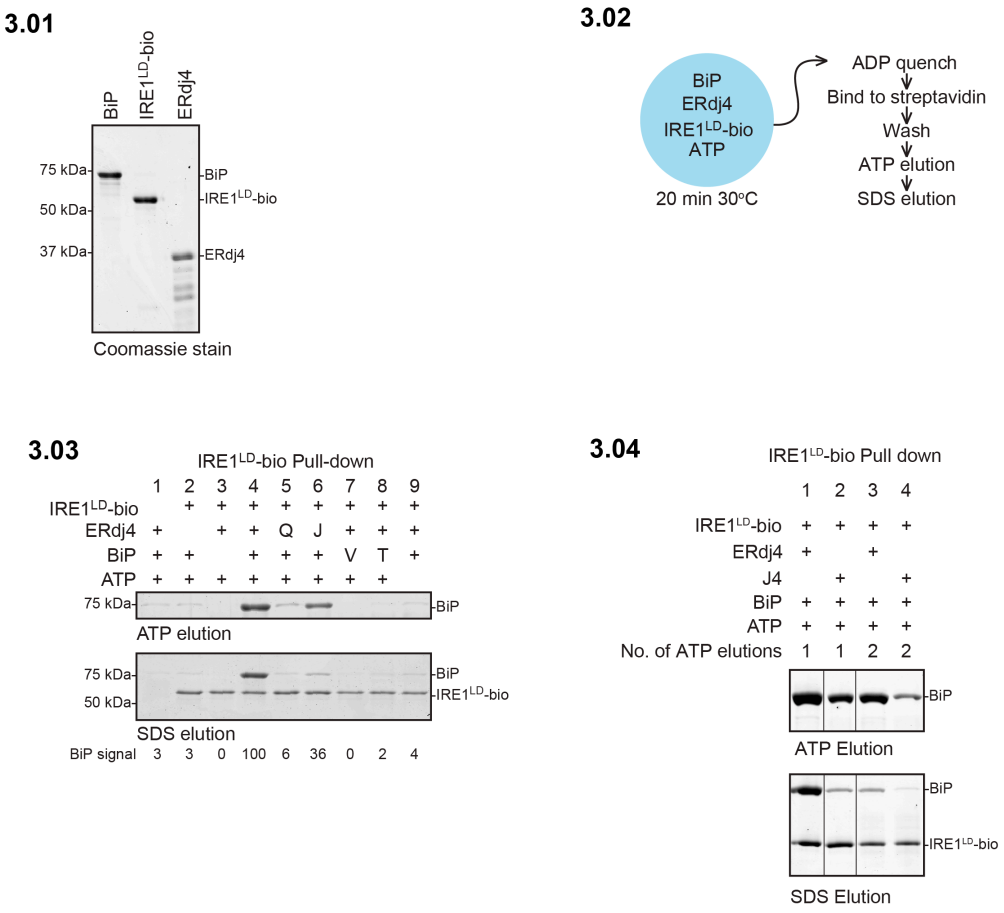

Figure 3.01 Coomassie stain of purified BiP, IRE1^{LD}-bio, and ERdj4 after SDS-PAGE.

Figure 3.02 Schema of the experiment shown in figure 3.03.

Figure 3.03 Coomassie-stained SDS-PAGE gel of biotinylated IRE1^{LD}-bio and BiP recovered on a streptavidin matrix from reactions constituted as indicated. Concentrations used were 5 µM IRE1^{LD}-bio, 8 µM ERdj4, 30 µM BiP, and 2 mM ATP. Q = ERdj4^{QPD}, T = BiP^{T229A}, V = BiP^{V461F}, J = isolated J-domain of ERdj4. Proteins were eluted sequentially with ATP (ATP elution) and SDS sample buffer (SDS elution).

Figure 3.04 Coomassie-stained SDS-PAGE gel of biotinylated IRE1^{LD}-bio and BiP recovered on a streptavidin matrix from reactions constituted as indicated. Lanes 1 and 2 show protein recovered as outlined figure 3.02. The streptavidin matrix of samples for lanes 3 and 4 went through one additional ATP elution step prior to elution in sample buffer and the proteins eluted in the second ATP elution step resolved on the gel.

The isolated J-domain of ERdj4 retained some ability to promote a BiP:IRE1^{LD} complex (Figure 3.03, lane 6), but was reproducibly weaker than full-length ERdj4, attesting to the importance of the C-terminal targeting domain of ERdj4 *in vitro* in directing it to load BiP onto IRE1 as also seen *in vivo*.

To gauge the stoichiometry of the BiP:IRE1 complex size exclusion chromatography analysis was carried out in which the elution of an Oregon Green labeled IRE1 (IRE1^{LD}-OG) was monitored alone and in complex with BiP (as catalysed by ERdj4). As shown the complex elutes as high molecular weight species that exceeds the predicted size of a single BiP molecule bound to IRE1^{LD}-OG (Figure 3.06). It is therefore likely that multiple BiP molecules engage the IRE1^{LD} via multiple binding sites or as BiP oligomers. An indication of stoichiometry can also be gleaned from the Coomassie stained gels, which also suggest more than one BiP molecule associates with IRE1^{LD}-bio (Figure 3.03).

As shown *in vivo,* ERdj4 is able to act on the core IRE1^{CLD} alone. The same held true for the *in vitro* system as, in the presence of ATP, ERdj4 could recruit BiP to IRE1^{CLD}-bio, indicating that the IRE1^{LD} tail region is not essential for ERdj4-dependent complex formation between IRE1 and BiP (Figure 3.07).

To determine whether ERdj4 and BiP interfere with IRE1^{LD} dimerisation *in vitro*, a non-biotinylated, Tetramethylrhodamine (TAM)-labelled fluorescent IRE1^{LD} probe was produced (IRE1^{LD}-TAM) and the effect measured of BiP, ERdj4 and ATP on recovery of IRE1^{LD}-TAM in complex with IRE1^{LD}-bio (Figure 3.08). Consistent with the high affinity of IRE1^{LD} protomers for each other, IRE1^{LD}-TAM formed a stable complex with IRE1^{LD}-bio that was readily recovered on immobilised streptavidin. However, introduction of wildtype BiP, wildtype ERdj4, and ATP interfered with the IRE1^{LD} dimer whilst forming a BiP:IRE1^{LD}-bio complex (Figure 3.09). The defect in the isolated J-domain of ERdj4 in loading BiP is better revealed here (lane 10) as it shows the total BiP bound to IRE1 through a single sample buffer elution rather than the separated ATP and sample buffer elutions.

To explore the importance of NEF in completing the BiP cycle in the ERdj4-IRE1 system the mammalian ER localised NEF GRP170 was included in reaction mixtures. It was seen that the presence of GRP170 significantly

increased the amount of BiP recovered with IRE1^{LD}-bio and further attenuated recovery of IRE1^{LD}-TAM (Figure 3.10). This showcases the importance of both NEF and ERdj co-chaperones in enhancing the efficiency of BiP's activity.

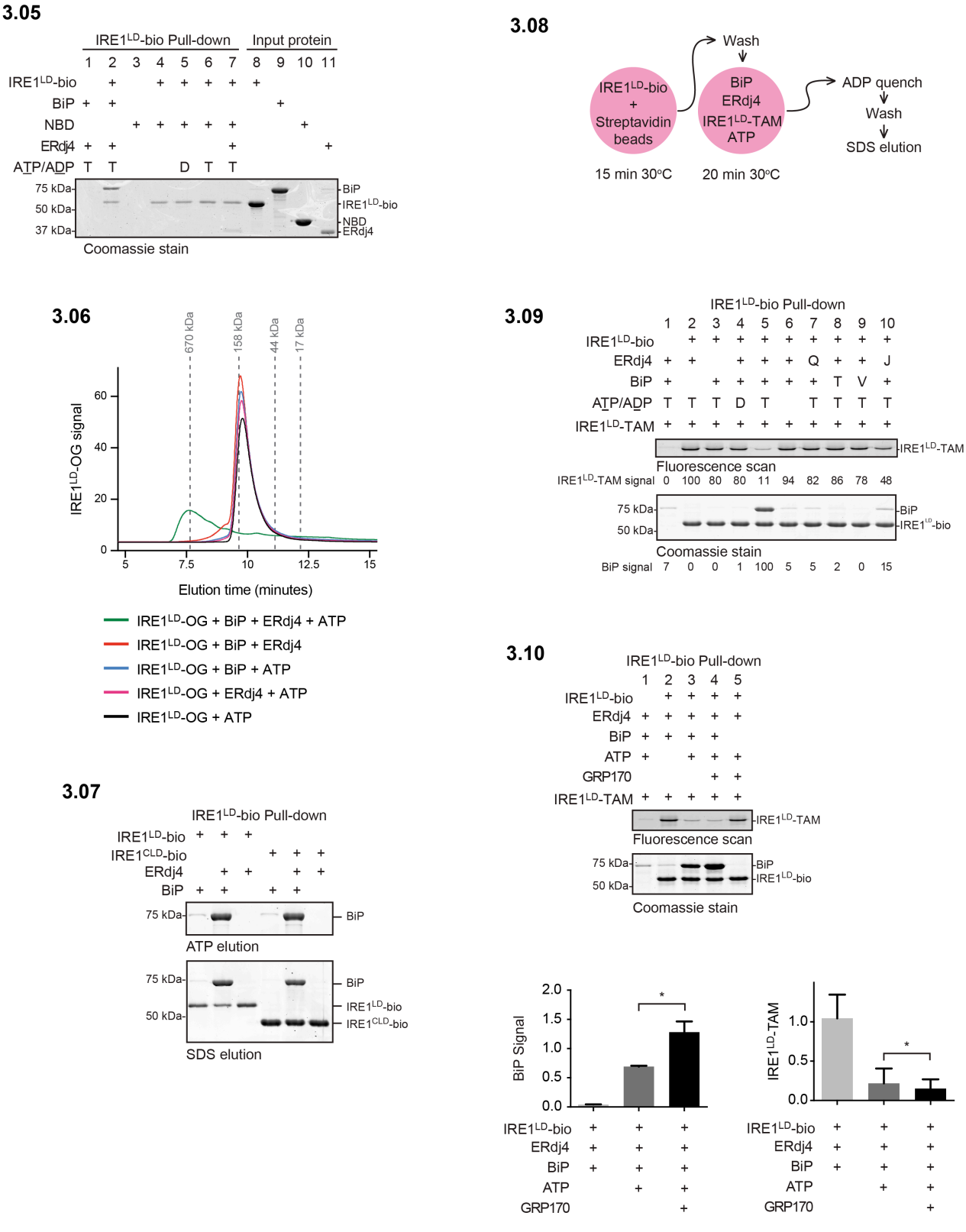

Figure 3.05 Coomassie-stained SDS-PAGE gel of biotinylated IRE1^{LD}-bio and BiP recovered on a streptavidin matrix from reactions constituted as in figure 3.02-3.03, with BiP or the nucleotide-binding domain of BiP (NBD) as indicated. Data for figure generated by Reuben Saunders.

Figure 3.06 Fluorescence trace (Ex: 496 nm Em: 524 nm) of IRE1^{LD}-OG elution from a Sec3 size-exclusion chromatography column. Reaction mixtures of the indicated composition were incubated at 30°C for 20 minutes and clarified at 21,000 g for 5 mins. Concentrations used: 0.7 μM IRE1^{LD}-OG, 5 μM ERdj4, 40 μM BiP, 2 mM ATP.

Figure 3.07 As in figure 3.02-3.03, with IRE1^{CLD}.

Figure 3.08 Schema of the experiment shown in figure 3.09.

Figure 3.09 Sequential fluorescence scan and Coomassie-stain of the same SDS-PAGE gel of proteins recovered on immobilised streptavidin from reactions assembled from the indicated components. The IRE1^{LD}-bio-loaded beads were allowed to associate with fluorescently labelled IRE1^{LD}-TAM, whose recovery in the pull-down reports on the integrity of the IRE1^{LD} dimer. Concentrations used were 0.5 μM IRE1^{LD}-TAM, 8 μM ERdj4, 30 μM BiP, and 2 mM ATP. Q=ERdj4^{QPD}, T=BiP^{T229A}, V=BiP^{V461F}, J=isolated J-domain of ERdj4.

Figure 3.10 As in figure 3.08-3.09, with 1 μM GRP170. Quantification of the effect of GRP170 on BiP association with IRE1^{LD}-bio bar chart displays mean ± SD, n = 3, *p = 0.0223 by Student's paired ratio t test. Quantification of the effect of GRP170 on IRE1^{LD}-TAM association with IRE1^{LD}-bio bar chart displays mean ± SD, n = 3, *p = 0.0293 by Student's paired ratio t test.

ERdj4 opposes IRE1α luminal domain dimerisation *in vitro*

Bio-layer interferometry (BLI) was used to dissect ERdj4-mediated BiP recruitment to $IRE1^{LD}$. BLI has some similarities to the well-known surface plasmon resonance technique in that the reflection of an incident wavelength of light is sensitive to the chemical environment around the reflective surface. This sensitivity to chemical environment can be used to monitor protein binding events in real-time.

Using BLI robust binding between immobilised $IRE1^{LD}$-bio on the BLI sensor and ERdj4 in solution could be detected that was not dependent on the functional integrity of the J domain or the presence of other factors (Figure 3.11). The isolated J-domain of ERdj4 was not seen to interact with the $IRE1^{LD}$-bio sensor, implicating the C-terminal domain of ERdj4 in the binding event. This observation explains the defect in the J-domain alone in forming a BiP:$IRE1^{LD}$ complex, as it has no domain guiding its activity. The ERdj4:$IRE1^{LD}$-bio complex had a very low k_{off} rate that was also exhibited by the inverse $IRE1^{LD}$:ERdj4-bio complex (Figure 3.12). In the absence of ATP, the binary complex of $IRE1^{LD}$-bio and ERdj4 interacted minimally with BiP. Nor did the binary complex interact with mutants of BiP (BiP^{T229A} and BiP^{V461F}), even in the presence of ATP. However, immersing the sensor loaded with the ERdj4:$IRE1^{LD}$-bio complex into a solution of BiP and ATP gave rise to a highly reproducible, transient, positive BLI signal, followed by its decline towards the baseline signal of the $IRE1^{LD}$-bio-loaded BLI sensor (observed before formation of the ERdj4:$IRE1^{LD}$-bio complex; Figure 3.11. green trace). The kinetics of this biphasic swing in the BLI signal were increased both by the amount of ERdj4 bound to the $IRE1^{LD}$-bio-loaded BLI sensor and by the concentration of BiP (data not shown). This biphasic swing suggested that the loading of BiP onto IRE1 was displacing the very same ERdj4 that catalysed the event.

To assess this the protein content of the BLI sensor preceding and following its immersion into the solution containing BiP and ATP was analysed and this revealed the presence of ERdj4 in the former steady state and its absence from the latter (Figure 3.13). These observations are consistent with ERdj4's ability to promote formation of a complex between BiP and $IRE1^{LD}$ through

directed ATP hydrolysis, and to maintain this complex by facilitating BiP re-binding following nucleotide exchange. BiP binding disrupts the otherwise stable ERdj4:IRE1^{LD} complex. When present at adequate concentrations, ERdj4 re-binding to IRE1^{LD} dynamically maintains the BiP:IRE1^{LD} complex as demonstrated by the success in isolating the complex in the pull down system (Figure 3.03). However, in the BLI set-up ERdj4 stripped from IRE1^{LD}-bio by BiP is too dilute to rebind, allowing the BiP:IRE1^{LD} complex to dissipate through nucleotide exchange (last segment of green trace in figure 3.11).

The ability of ERdj4 and BiP to deplete the dimeric IRE1 population could occur through forcible disruption of pre-formed IRE1^{LD} dimers or by retention of monomers. To address whether the former mechanism occurred, pre-formed IRE1^{LD}-bio/IRE1^{LD}-TAM dimers were immobilised on streptavidin and confronted with BiP, GRP170, and ATP in the presence or absence of ERdj4 and monitored for the loss of bound IRE1^{LD}-TAM (Figure 3.14). Dissociated IRE1^{LD}-TAM was diluted in the large assay volume, minimising the effect of rebinding. ERdj4 accelerated the loss of IRE1^{LD}-TAM (Figure 3.15), indicating that ERdj4 empowered BiP to split pre-existing IRE1 dimers.

3.11

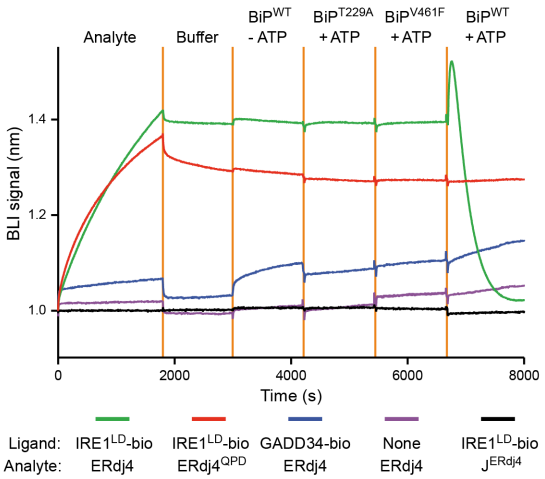

3.12

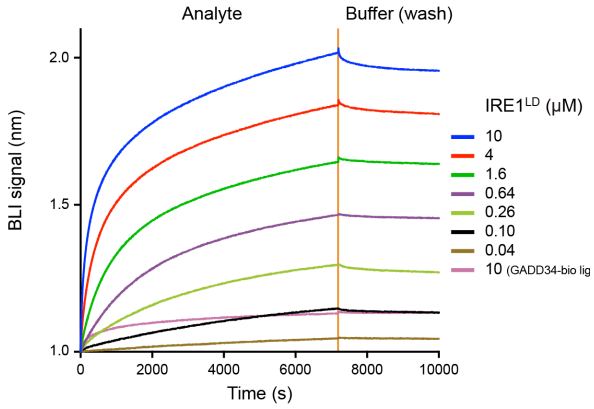

3.13

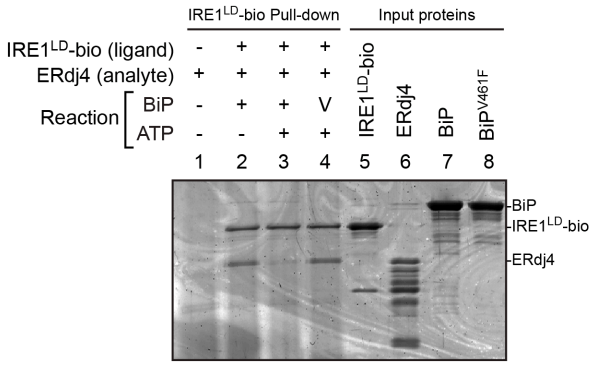

3.14

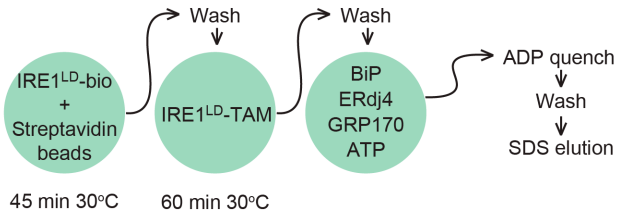

3.15

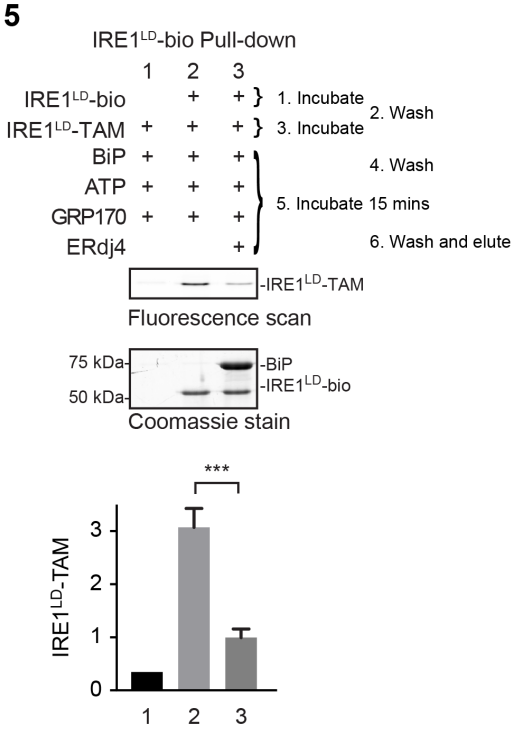

Figure 3.11 Bio-layer interferometry (BLI) signal of streptavidin sensors loaded with the indicated biotinylated ligand and reacted sequentially with the indicated solution of analyte, followed sequentially by the indicated solutions of BiP and ATP. Concentrations used were 1.5 μM ERdj4, 1 μM BiP, 2 mM ATP. Data for figure generated by Reuben Saunders.

Figure 3.12 BLI signal from streptavidin sensors pre-loaded with a biotinylated ERdj4 ligand (or with an irrelevant control biotinylated GADD34 ligand) and reacted with the indicated concentration of $IRE1^{LD}$ as an analyte and then transferred to a buffer only (wash) solution. Data for figure generated by Reuben Saunders.

Figure 3.13 Protein recovered from a BLI sensor lacking (lane 1) or containing an $IRE1^{LD}$-bio ligand (lanes 2-4). The sensor was incubated with an ERdj4 analyte and then with BiP or BiP^{V461F} ± ATP. Data for figure generated by Reuben Saunders.

Figure 3.14 Schema of the experiment shown in figure 3.15.

Figure 3.15 Fluorescence scans and Coomassie-stained SDS-PAGE gel of proteins recovered on immobilised streptavidin from reactions assembled from the indicated components. The $IRE1^{LD}$-bio-loaded streptavidin beads were pre-associated with $IRE1^{LD}$-TAM and then incubated in a solution of BiP, ERdj4, GRP170, and ATP. Bar chart shows mean $IRE1^{LD}$-TAM signal recovered with $IRE1^{LD}$-bio (± SD) from four independent experiments, ***p = 0.001 by parametric student's paired ratio t test. Concentrations used were 0.5 μM $IRE1^{LD}$-TAM, 8 μM ERdj4, 30 μM BiP, 1 μM GRP170, 2 mM ATP.

To determine if, as already hinted *in vivo* (Figure 2.28), ERdj4 could recruit BiP to dimeric IRE1^{LD} *in vitro* (a prerequisite for the forceful disruption suggested by figure 3.15), IRE1$^{LD\ Q105C}$ was purified, allowed to form Q105C-Q105C disulfides, and chemically labelled on lysine residues with biotin (indicated by a bio*) to form covalently stabilised biotinylated IRE1$^{LD\ Q105C}$-bio* dimers. ERdj4 bound IRE1, as seen by the BLI signal (Figure 3.16, initial ERdj4 association) and the direct analysis of the protein content of the BLI sensor (Figure 3.17, lane 3), and recruited BiP to disulfide-linked dimeric biotinylated IRE1$^{LD\ Q105C}$ (Figure 3.18). If as shown in these experiments ERdj4 and BiP are indeed able to bind to and disrupt IRE1 dimers they must bind at sites away from the dimer interface (which would be sterically inaccessible in the IRE1 dimers). This suggests the existence of an allosteric component to BiP-mediated inhibition of IRE1. BiP and ATP were also able to remove ERdj4 bound to the biotinylated disulfide-linked dimeric biotinylated IRE1$^{LD\ Q105C}$, indicating that IRE1 de-dimerisation is not a strict pre-requisite for BiP-mediated ERdj4 displacement (Figure 3.16, signal decay during the BiP/ATP incubation and subsequent ATP wash, Figure 3.17, lane 3 vs 4).

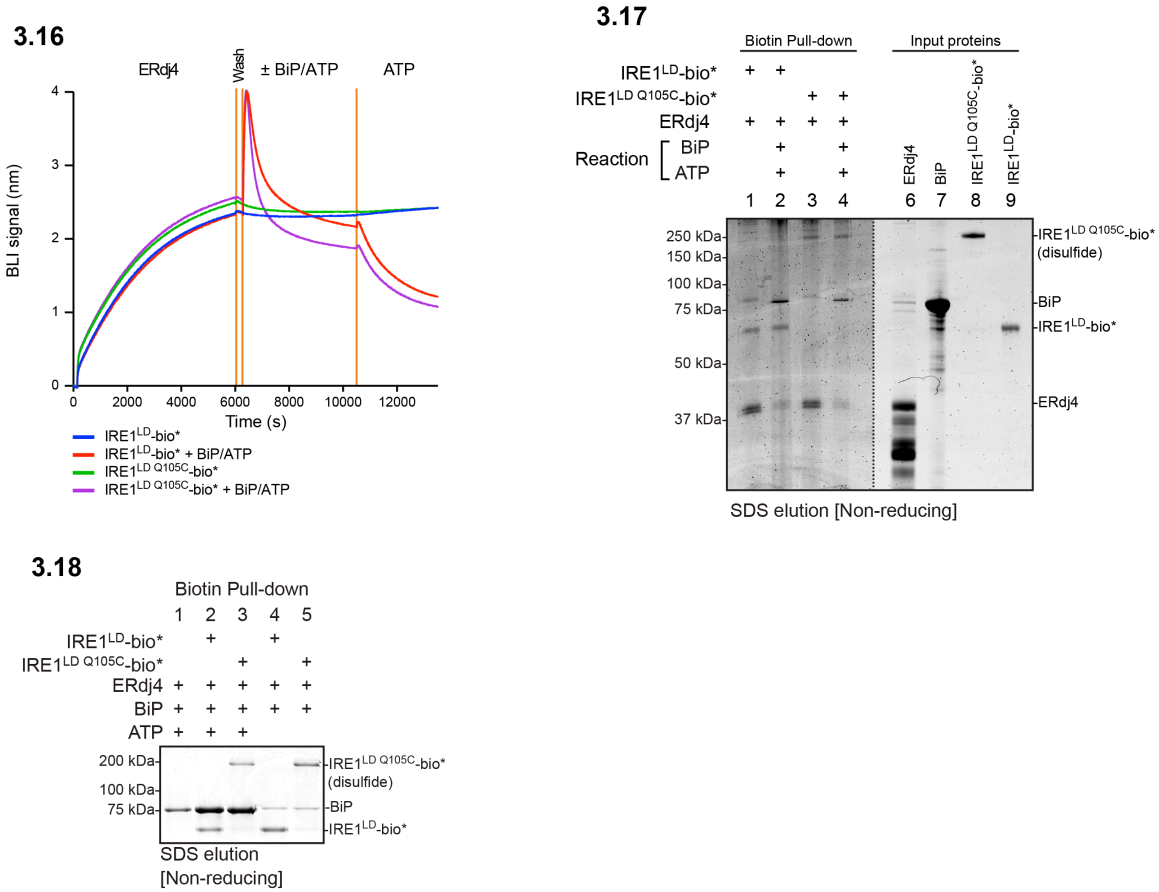

Figure 3.16 BLI signal of streptavidin sensors loaded with the wildtype biotinylated IRE1^{LD}, or covalent dimeric disulfide-linked biotinylated IRE1$^{LD\ Q105C}$ ligands and reacted with ERdj4, followed sequentially by the indicated solutions. Concentrations used were 1.7 µM ERdj4, 6 µM BiP, 2 mM ATP.

Figure 3.17 Coomasie-stained non-reducing SDS-PAGE gel of protein recovered by SDS sample buffer elution from the BLI sensors used in figure 3.16. The dotted line indicates the boundary at which the image contrast/brightness properties were treated differently to make the image clearer.

Note: To enable formation of Q105C-disulfide, without interference by other cysteines, both the WT IRE1^{LD} and the IRE1$^{LD\ Q105C}$ ligands were surface biotinylated on exposed lysine residues. This coupling chemistry likely accounts for the differences in kinetics of the BLI signal observed in this experiment as compared with figure 3.11, in which the IRE1^{LD} ligand was biotinylated on a single C-terminal cysteine residue (D443C) using maleimide biotin.

Figure 3.18 Coomassie stained non-reducing SDS-PAGE gel of IRE1 and BiP recovered on a streptavidin matrix from reactions constituted as in figure 3.02-3.03, but with IRE1^{LD}-bio* or covalent dimeric disulfide-linked IRE1$^{LD\ Q105C}$-bio*. Proteins were eluted with SDS sample buffer.

Unfolded protein substrates compete with IRE^{LD} for BiP, restoring IRE1^{LD} dimers

To monitor the disruption of IRE1^{LD} dimers in real time, a FRET-based assay was developed that reports on the IRE1^{LD} monomer-dimer equilibrium (Figure 3.19). IRE1^{LD} molecules labelled on a single cysteine introduced at R234 with an Oregon Green 488 donor were combined with molecules labelled on a single cysteine introduced at S112 with a TAM acceptor. A robust FRET signal (predicted by proximity of R234 and S112 in the human IRE1^{LD} dimer crystal structure), reflected by the quenching of donor fluorescence, was detected. Addition of unlabelled IRE1^{LD} restored donor fluorescence nearly to levels observed in absence of acceptor molecules, confirming the role of dimerisation in the quenched donor fluorescence (Figure 3.20).

Extended incubation of donor and acceptor-labelled IRE1^{LD} molecules with high concentrations of ADP-bound BiP (in the absence or presence of ERdj4) did not disrupt the FRET signal, indicating that IRE1^{LD} is a poor equilibrium BiP substrate (Figure 3.20, lower traces). However, addition of BiP, ERdj4, and ATP to pre-equilibrated donor/acceptor IRE1^{LD} reversed the FRET such that donor fluorescence nearly equalled that observed in the absence of acceptor molecules. BiP mutants defective in ATP hydrolysis (BiP^{T229A}) and

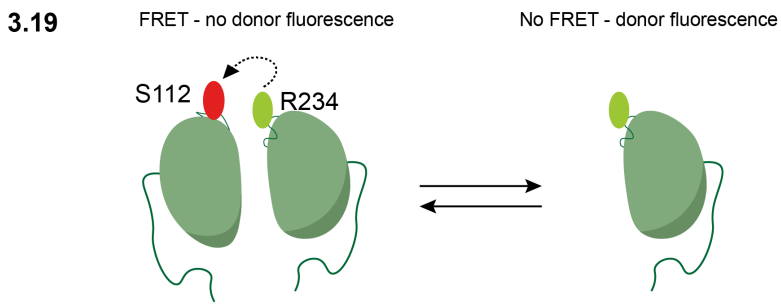

Figure 3.19 A cartoon outlining the FRET system. IRE1$^{LD\ S112C}$ and IRE1$^{LD\ R234C}$ molecules were labelled with the TAMRA (TAM) and Oregon Green (OG) fluorophores to create IRE1$^{LD\ TAM}$ and IRE1$^{LD\ OG}$ respectively. When IRE1$^{LD\ OG}$ exists in a dimer with IRE1$^{LD\ TAM}$ the OG fluorophore transfers its excitation energy to TAM via FRET and does not fluoresce. The OG IRE1$^{LD\ OG}$ not in a dimer with IRE1$^{LD\ TAM}$ is able to fluoresce. This system can therefore provide a readout for changes in the population distribution of IRE1 molecules.

substrate binding (BiP^{V461F}) and $ERdj4^{QPD}$ were inert, as was BiP^{AMP} that had been inactivated by AMPylation (Preissler et al., 2015a).

The inability of the isolated J-domain of ERdj4 to drive efficient monomerisation reveals the importance of the C-terminal targeting domain of ERdj4 in guiding it to load BiP onto relevant sites for inhibiting IRE1 dimerisation. Addition of the NEF GRP170 significantly increased the rate of $IRE1^{LD}$ monomerisation (Figure 3.21) highlighting how co-chaperones work together to enhance the efficiency of BiP function. Finally, BiP, ERdj4, and ATP also disrupted the FRET observed between donor/acceptor labelled IRE1 core luminal domain identifying this domain of IRE1 as being sufficient for the ERdj4 mediated monomerisation ($IRE1^{CLD}$, Figure 3.22).

In vivo the chaperone inhibition model relies on the basic tenet that BiP can be competed away from IRE1 by substrate to allow IRE1 dimerisation. This should still hold true *in vitro* and was addressed by introducing a BiP substrate (CH1 peptide HTFPAVL) (Marcinowski et al., 2011) into the FRET system after monomerisation of IRE1 by ERdj4 and BiP. Alone the substrate weakly restored the FRET signal to samples maintained in the monomeric state however, including sub-stoichiometric amounts of a second J-protein (devoid of $IRE1^{LD}$-binding activity), alongside the BiP substrate, markedly accelerated IRE1 dimerisation (Figure 3.23). These observations suggest that BiP binding to a substrate peptide directed by an orthogonal J-protein can indeed compete successfully for ERdj4-directed, BiP-mediated $IRE1^{LD}$ monomerisation and further supports the BiP:IRE1 complex being a canonical chaperone substrate interaction. The transitions between the monomeric “low FRET” and dimeric “high FRET” states (Figure 3.23) occur on a 30-60 minute time scale similar to that of the dissolution of the BiP:IRE1 complex in stressed cells and its reformation in cells recovering from stress (Bertolotti et al., 2000), suggesting that $IRE1^{LD}$, BiP, J-proteins, and a BiP substrate together can recapitulate in a simple *in vitro* assay a key aspect of UPR signalling.

The proposed model of IRE1 regulation by ERdj4 and BiP is shown (Figure 3.24).

Chapter 3 summary

Presented here are a series of experiments showing that *in vitro* ERdj4 promotes the formation of a canonical chaperone substrate interaction between BiP and the $IRE1^{CLD}$ which leads to monomerisation of the IRE1 population. The congruancy between these *in vitro* findings with the *in vivo* data from chapter two contests the idea that *in vivo* ERdj4 plays an indirect role in IRE1 repression and supports the physiological relevance of the *in vitro* observations. Though this *in vitro* system does lack many elements of the ER proteostasis machinery it has the advantage of being tolerant to various protein mutants (e.g. those of BiP), which can be used to provide mechanistic insight into IRE1 repression. Many of these mutants are difficult to exploit *in vivo*, due to their toxic effects on ER homeostasis, and the absence of a functional *in vitro* reconstitution of the chaperone inhibition model has therefore hindered progress in the UPR field.

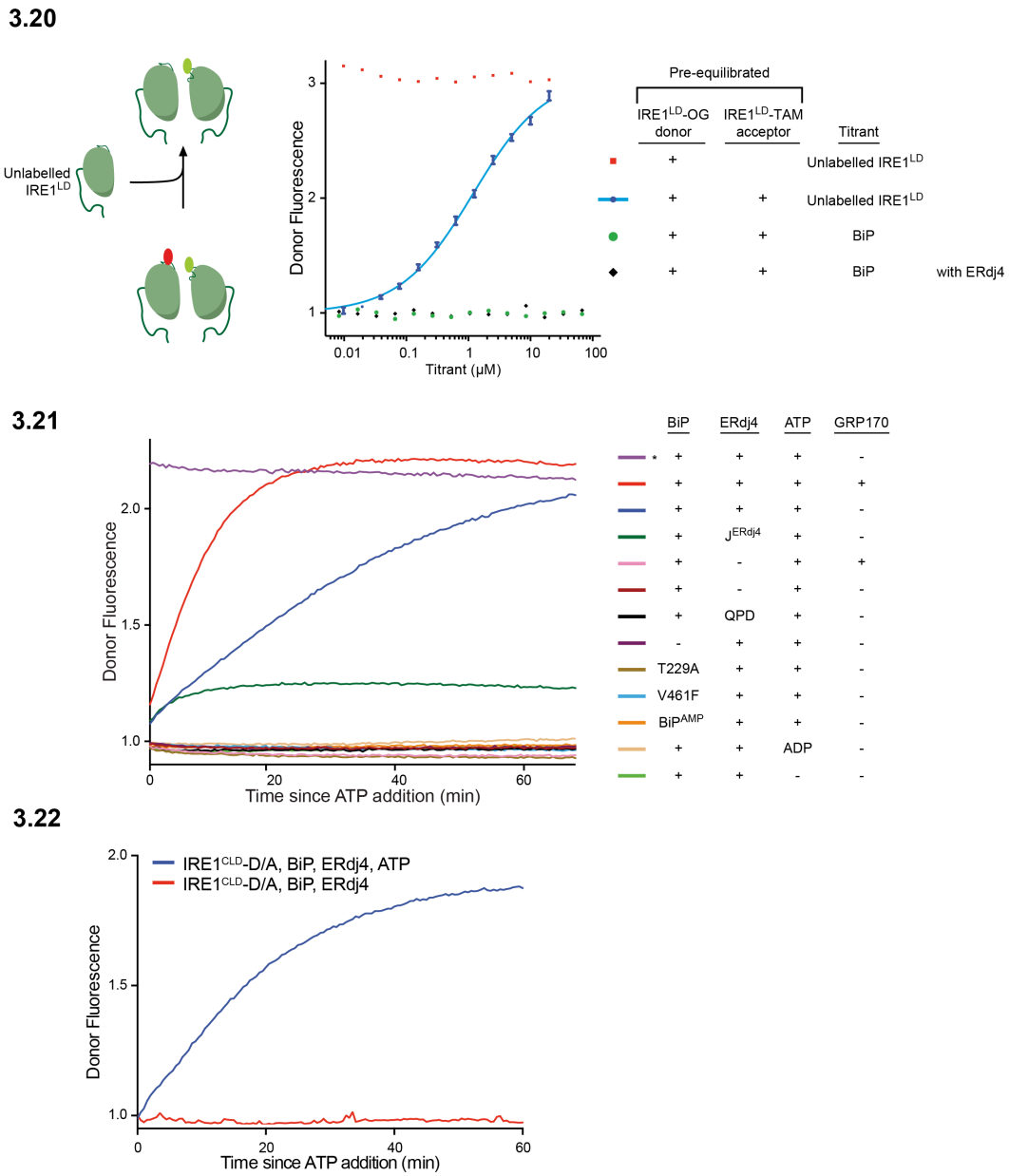

Figure 3.20 Donor fluorescence as a function of the concentration of competing unlabelled IRE1^{LD} equilibrated with a FRET pair (0.2 μM labeled IRE1^{LD}) consisting of an IRE1^{LD}-OG donor and IRE1^{LD}-TAM acceptor (blue trace). Also shown are titrations of unlabelled IRE1^{LD} into a mock FRET sensor (no IRE1^{LD}-TAM acceptor; red trace) and titration of BiP with 2 mM ADP (+/- ERdj4) into the pre-equilibrated FRET pair (green and black traces). Data for figure generated by Reuben Saunders.

Figure 3.21 Time-dependent change in donor fluorescence of the IRE1^{LD} FRET pair incubated at t=0 with indicated components. Concentrations used were 0.2 μM FRET IRE1^{LD}, 30 μM BIP, 2.5 μM ERdj4, 1 μM GRP170, and 2 mM ATP. J^{ERdj4} lacks the C-terminal targeting region. BiP^{AMP} is AMPylated BiP. *Reaction set up with a mock FRET sensor lacking the IRE1^{LD}-TAM acceptor. Data for figure generated by Reuben Saunders.

Figure 3.22 As in figure 3.21, but with OG488 and TAM-labeled IRE1^{CLD}. Data for figure generated by Reuben Saunders.

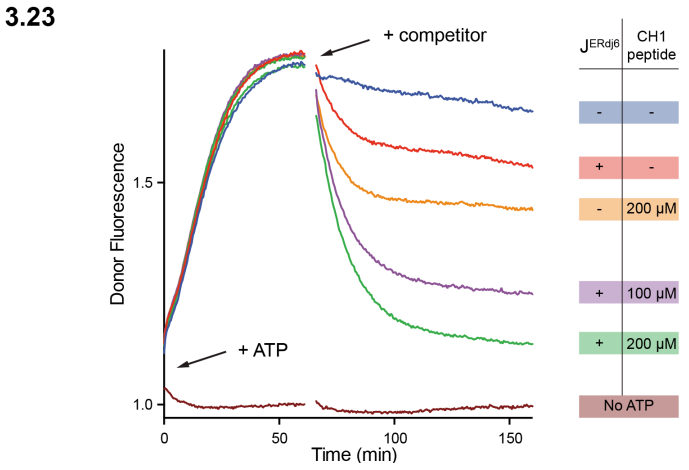

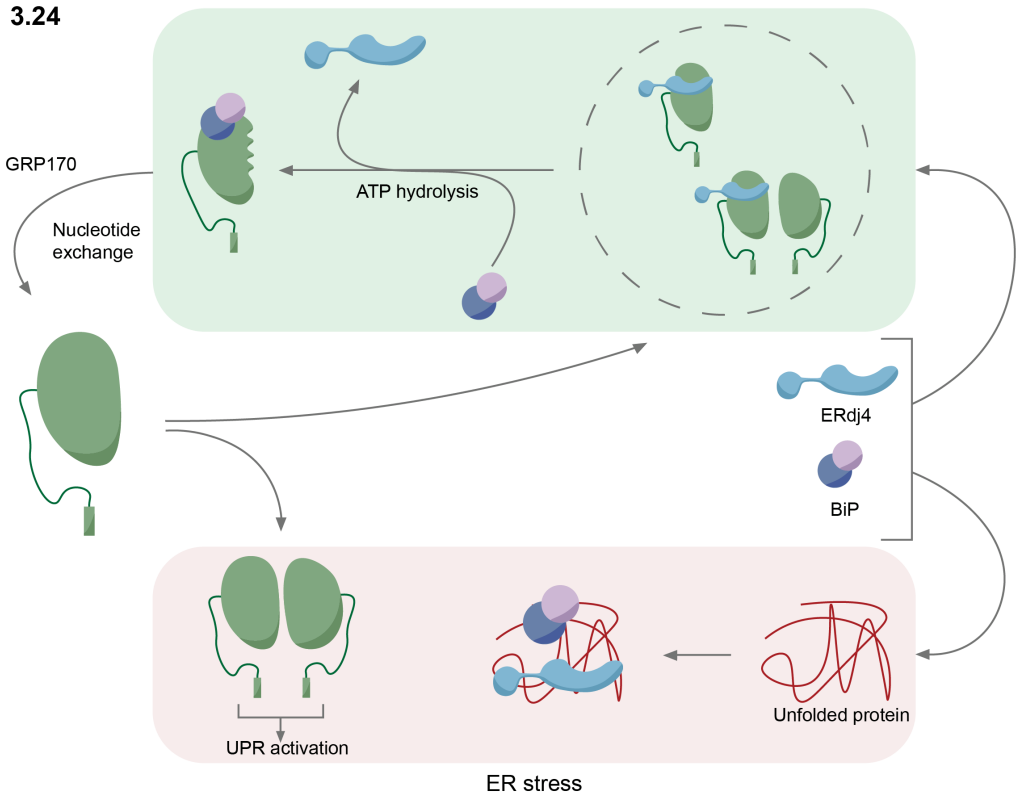

Figure 3.23 Time-dependent change in donor fluorescence of the IRE1^{LD} FRET pair exposed at t=0 to BiP, ERdj4 and ATP (arrow labeled “+ ATP”). Concentrations: 0.2 μM FRET IRE1^{LD}, 50 μM BIP, 2.5 μM ERdj4, 2 mM ATP. Following disruption of the FRET pair, at t=60, CH1 peptide and the J-domain of ERdj6 (2.5 μM) were added (arrow labeled “+ competitor”). Data for figure generated by Reuben Saunders.

Figure 3.24 In the unstressed ER (green box) ERdj4 binds IRE1 CLD via its targeting domain. ERdj4 stimulates BiP’s ATPase activity to drive BiP binding to IRE1, ejection of ERdj4, and formation of a repressive BiP:IRE1 complex with a disrupted dimer interface. This complex turns over by nucleotide exchange. Free ERdj4 and BiP recruit the released IRE1 (as monomer or dimer) in a kinetically maintained repressive cycle. Accumulating unfolded proteins during stress (red box) compete for BiP and/or ERdj4, interrupting the cycle of repression. IRE1 monomers are free to dimerise and activate downstream signals.

Chapter 4: Screening for de-repressing mutations in IRE1α

Tiling deletions and random mutagenesis of a gene can be a powerful tool to begin understanding the regions and residues required for regulation and function of the protein. The former has been employed to understand both yIRE1 and IRE1α (Kimata et al., 2004; Daisuke Oikawa et al., 2009).

A Cas9-CRISPR-mediated mutagenesis screen

With the advent of Cas9-CRISPR technology, it is now possible to carry out this technique at the endogenous locus, even in mammalian cells. As previously mentioned, repair of DSBs introduced by the Cas9 endonuclease can result in mutation of the DNA sequence and if two DSBs are introduced simultaneously, it can lead to larger deletions of the DNA sequence between them. By introducing a set of Cas9 guides that target a region of interest into cells, a semi random pool of mutants will be created containing small deletions, substitutions, and insertions around and between the DSB sites. The XBP1s::Turquoise reporter is a convenient tool for selecting rare clones that have a de-repressed IRE1 resulting from such a Cas9-CRISPR insult and the CHOP::GFP reporter can be used to avoid clones which have a general perturbation of ER protein homeostasis. Iterative rounds of FACS can enrich this XBP1s::Turquoise high population, allowing isolation of clones for genotyping and further analysis (Figure 4.01).

Mutation of the IRE1α tail

As described in the introduction, the tail of mammalian IRE1 (Figure 1.07) has been identified as being important for regulation of its activity. To explore this further, Cas9-CRISPR-mediated mutagenesis of the region was carried out.

Pools of WT cells were separately transfected with Cas9 and guides to introduce mutations across the coding sequence of the tail (Figure 4.02). The transfected cells were pooled to create Pop 0. Cells expressing elevated levels of XBP1s::Turquoise were collected by FACS to create Pop 1. A second round of FACS was used to further enrich for cells expressing elevated levels of XBP1s::Turquoise to create Pop 2. As well as selecting for clones with de-repressing mutations of IRE1, this procedure had the potential to enrich for

cells in which the XBP1::Turquoise reporter activity was deregulated independently of IRE1 activity. To address this possibility, Pop 2 was treated with the IRE1 inhibitor 4μ8c which revealed that about 70% of cells relied on IRE1 RNase activity to maintain high XBP1s::Turquoise expression whilst the remainder had acquired off pathway features affecting the reporter. Appropriate 4μ8c responsive clones from Pop2 were collected by a final round of FACS. An RT-PCR XBP1 splicing assay was carried out for one of the clones, showing that the endogenous XBP1 mirrored the constitutive splicing of the XBP1s::Turquoise reporter due to the de-repressed IRE1 (Figure 4.03).

Sequence analysis of the isolated clones (Table 4.01) revealed a common mutation that resulted in deletion of residues 403-441 of the IRE1α protein. To validate that this deletion causes de-repression of IRE1α, a strategy to reconstitute the endogenous locus with such a deletion was employed.

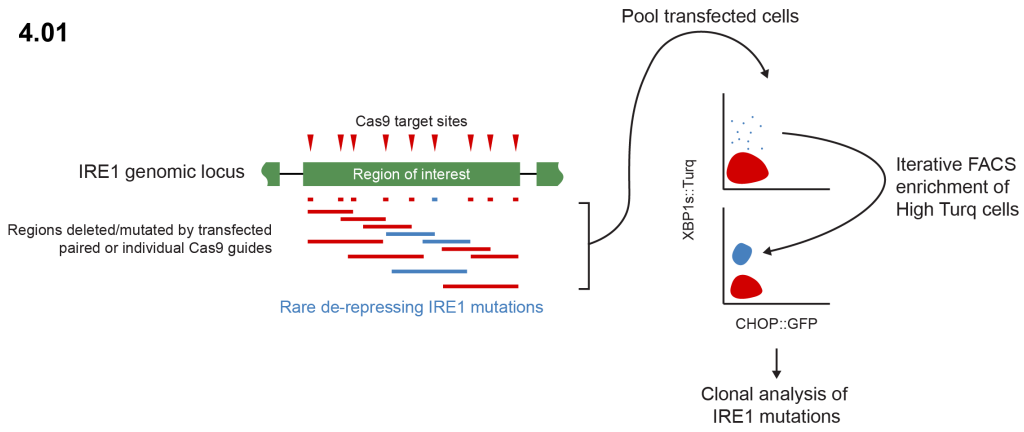

Figure 4.01 Cas9 guides (red triangles) can be selected at an even distribution across the IRE1 genomic locus encoding the protein's region of interest. Transfection of individual or pairs of guides will result in a series of directed mutations (blue and red lines). Cells harbouring rare de-repressing mutations of IRE1 (blue) can be selected for by rounds of FACS gating on cells expressing high XBP1s::Turquoise and low CHOP::GFP. The resultant clones can be genotyped and further analysed.

The endogenous IRE1 locus consists of 17 exons spanning ~60 kbp (with the luminal domain encoded by exons 2-12). To make mutations via Cas9 and HDR, a new repair template with new homology arms needs to be designed for each exon. Additionally, if desired mutations span several exons, extra steps are required to introduce all sets of mutations.

To make multiple mutations to the endogenous IRE1 locus, a more convenient system was therefore utilised, namely the ΔLD15 system (Figure 4.04)(Kono et al., 2017). The ΔLD15 system was created as follows. Appropriate Cas9-CRISPR guides were used to generate a large 50 kbp deletion between exons 2-11 in the endogenous IRE1α locus. This IRE1 null cell line (ΔLD15) can be reconstituted with IRE1 luminal domain variants using templates flanked by the same homology arms each time (Figure 4.05). The sequence of the alleles in the null cell line and the repair design are such that only one allele will be repaired with the IRE1 variant, meaning copy number is always constant between different clones.

The reconstitution of this locus with an IRE1 harbouring the deletion in the tail resulted in a de-repressed phenotype compared to when a WT sequence was introduced. This builds confidence in the importance of this region for IRE1 regulation as opposed to a clonal artefact (Figure 4.06).

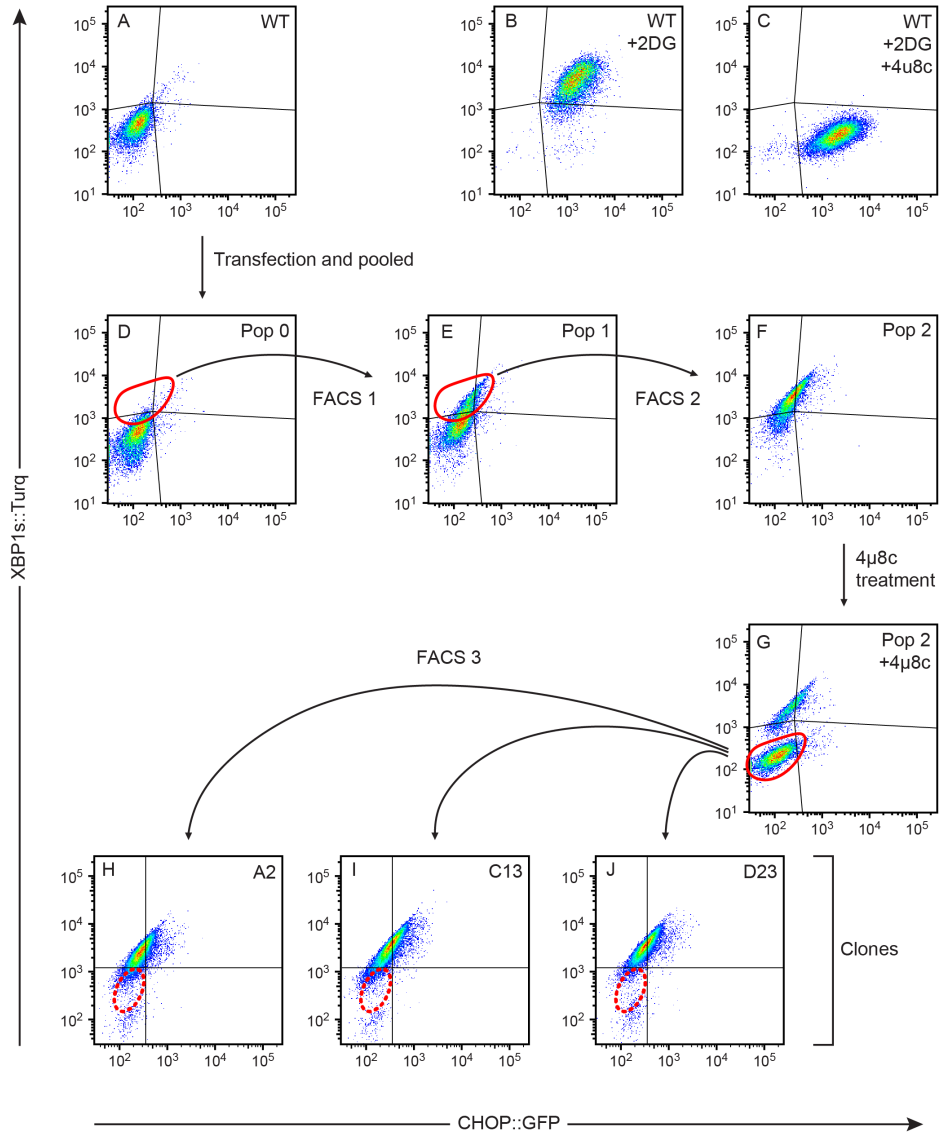

Figure 4.02 XBP1s::Turquoise and CHOP::GFP signals from the cell populations elaborated during the Cas9-CRISPR mutation screen targeting the tail of IRE1α as outlined in figure 4.01. Sets of WT cells (panel A) were separately transfected with Cas9 and guides and pooled (Pop 0 panel D). Pop0 cells with elevated levels of XBP1s::Turquoise were collected by FACS (Pop 1 panel E). A second FACS round enriched for cells with elevated reporter levels (Pop 2 panel F). Pop 2 was treated with the IRE1 inhibitor 4µ8c to identify undesirable cells with mutations that uncouple reporter expression from IRE1 activity (30% of Pop 2 panel G). Panels B+C show the efficacy of 4µ8c. 4µ8c responsive clones from Pop 2 were collected by a final round of FACS. The solid and dashed red lines indicate respectively the positions of the gates used for FACS, and the position of original WT cells as a reference for the extent of IRE1 de-repression in the final clones collected (panels H-J).

4.03

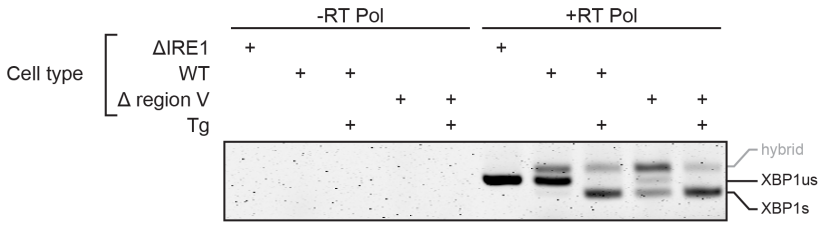

Table 4.01

Clone	Change to protein sequence
A2	Residues 403-441 deleted
B4	Residues 425-441 deleted
C13	Residues 403-441 substituted for QLLR residues
D23	Residues 403-441 substituted for PCI residues

4.04

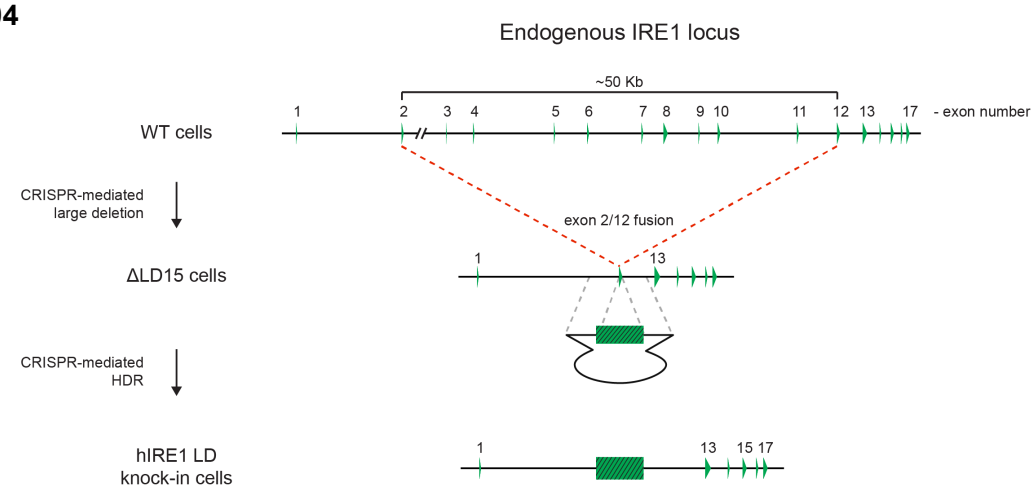

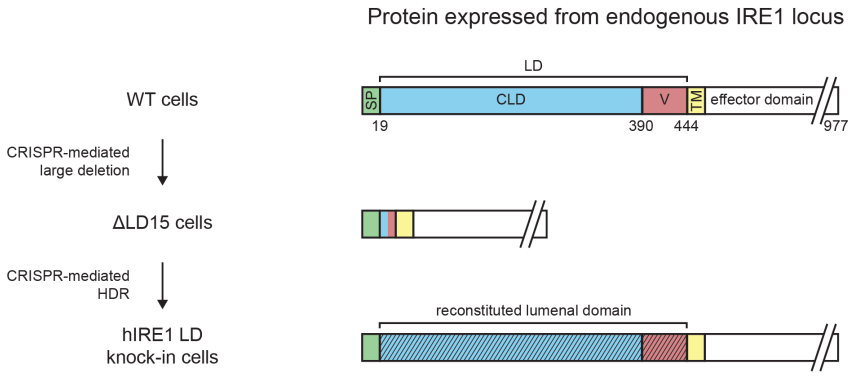

Figure 4.03 RT-PCR analysis of the extent of XBP1 splicing in the C13 clone compared to the WT parent cell line. The unspliced (XBP1us) and spliced (XBP1s) XBP1 species are annotated. In addition, a hybrid XBP1 species can be observed comprised of a strand of XBP1us annealed with a strand of XBP1s.

Table 4.01 The IRE1α protein mutations present in the indicated clones (isolated as in figure 4.02) as predicted by genomic and cDNA sequence analysis.

Figure 4.04 An overview of the ΔLD15 system. Appropriate Cas9-CRISPR guides were used to generate a large in-frame 50 kbp deletion between exons 2-11 in the WT endogenous IRE1α locus. The IRE1α locus in the resultant ΔLD15 cell line can be targeted with a unique Cas9 CRISPR guide and appropriate repair templates of the fused IRE1α exons 2-11 to introduce luminal domain variants. The in-frame deletion of the ΔLD15 cells results in the expression of IRE1α protein lacking the majority of the WT luminal domain.

Probing of the IRE1α tail

As previously described, the IRE1α tail is likely a flexible and potentially unstructured domain that connects the CLD to the TM. Shortening of such a flexible tether could well be imagined to restrict the space available that the CLD can explore, thus increasing the chance of dimerisation occurring. To test this theory, the hydrophobic amino acids (Ala, Leu, Ile, Met, Phe, Pro, Trp, Val) of the tail were mutated to alternating glycines or serines to interfere with binding sites for potential regulatory factors whilst retaining the overall length of the WT sequence (Figure 4.06). Mutation of these residues results in a de-repressed IRE1, suggesting that the composition of the tail is actually important and may provide a binding site for unknown regulatory factors.

A previous study of IRE1α had identified residues 390-408 as being important for repression of IRE1 (Daisuke Oikawa et al., 2009). Interestingly, these residues contain a predicted amphipathic α-helix (Figure 1.07 top), which may be important for facilitating interactions with regulatory factors in a manner dependent on its hydrophobic residues. Mutation of these hydrophobic residues (in the endogenous locus) to serines resulted in a moderate de-repression of IRE1 consistent with the hypothesis (Figure 4.06). However, the modest phenotype suggests that other residues of the IRE1 tail are involved in

repression or that this mutation of the helix was not sufficient to compromise the role it plays.

The other structural element of the IRE1 tail is the TM proximal amphipathic helix, which could also be involved in making interactions with regulatory factors. Single point mutations that disrupt the amphipathicity of this structure resulted in a strong derepression phenotype (Figure 4.07). Taken together these results suggest that multiple sequence elements of the IRE1α tail are important for repression of IRE1.

Mutation of IRE1α residues 312-353

Molecular details of the BiP:IRE1 interaction catalysed by ERdj4 could give an insight into how BiP binding destabilises IRE1 dimers. To obtain these details, BiP:IRE1 complexes (formed by ERdj4) were cross-linked and the covalent attachment sites identified by mass-spectrometry (data not shown). Analysis of the preliminary mass-spectrometry data suggest that BiP may bind residues 312-353 of IRE1α, which are not resolved in the IRE1α crystal structure (Figure 4.08). A Cas9-CRISPR screen (Figure 4.01) was implemented to identify mutations in this region that de-repress IRE1α activity (Figure 4.09) and though a promising 4μ8c-responsive de-repressed population is seen (compare figure 4.09 panel G to figure 4.02 panel E), interpretation of this awaits sequence analysis and further control experiments.

Chapter 4 summary

This set of mutational analyses of the endogenous IRE1α locus reveal the potential importance of amino acid stretches 312-353 and 403-441 in allowing repression of IRE1. Though it remains to be experimentally determined, both regions are likely required for the formation of a repressive BiP:IRE1 complex. The luminal domains of these IRE1 mutants retain the ability to dimerise (inferred by the requirement of this event for XBP1us splicing) which builds confidence that the mutations do not significantly disrupt the global structure of IRE1 but rather interfere with specific sites required for binding of regulatory factors. It will be of particular interest to assess the ability of ERdj4 to load BiP onto the region 312-353 mutants both *in vitro* and *in vivo* once the sequence analysis of the clones has been completed.

4.05

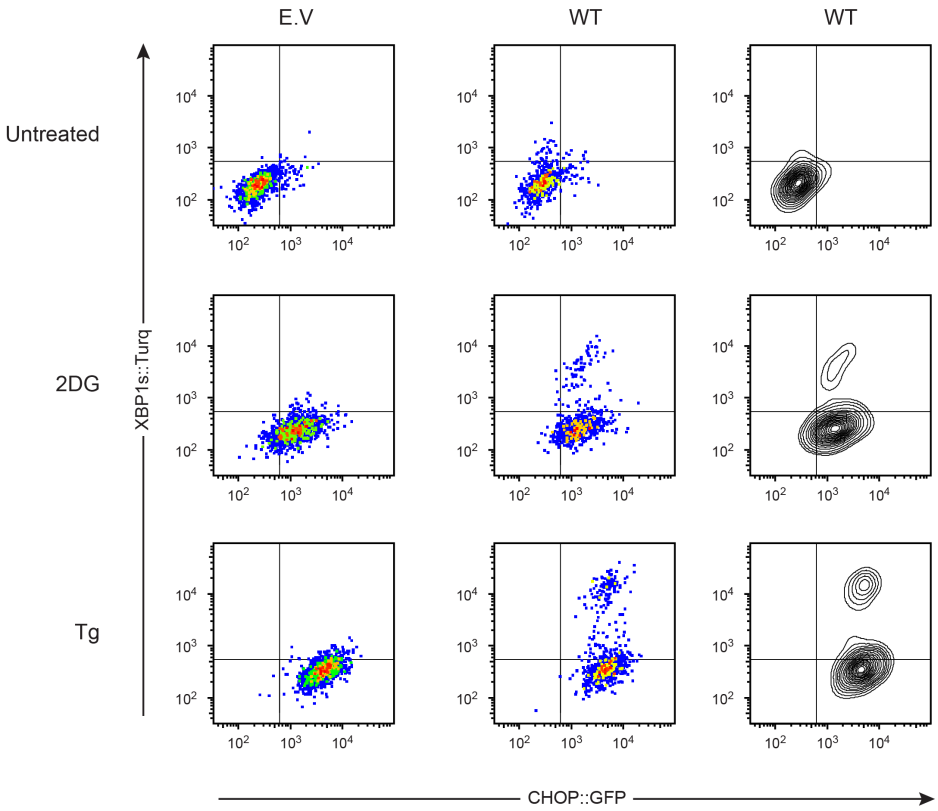
E.V
WT
WT
Untreated
2DG
Tg
XBP1s::Turq
CHOP::GFP

4.06

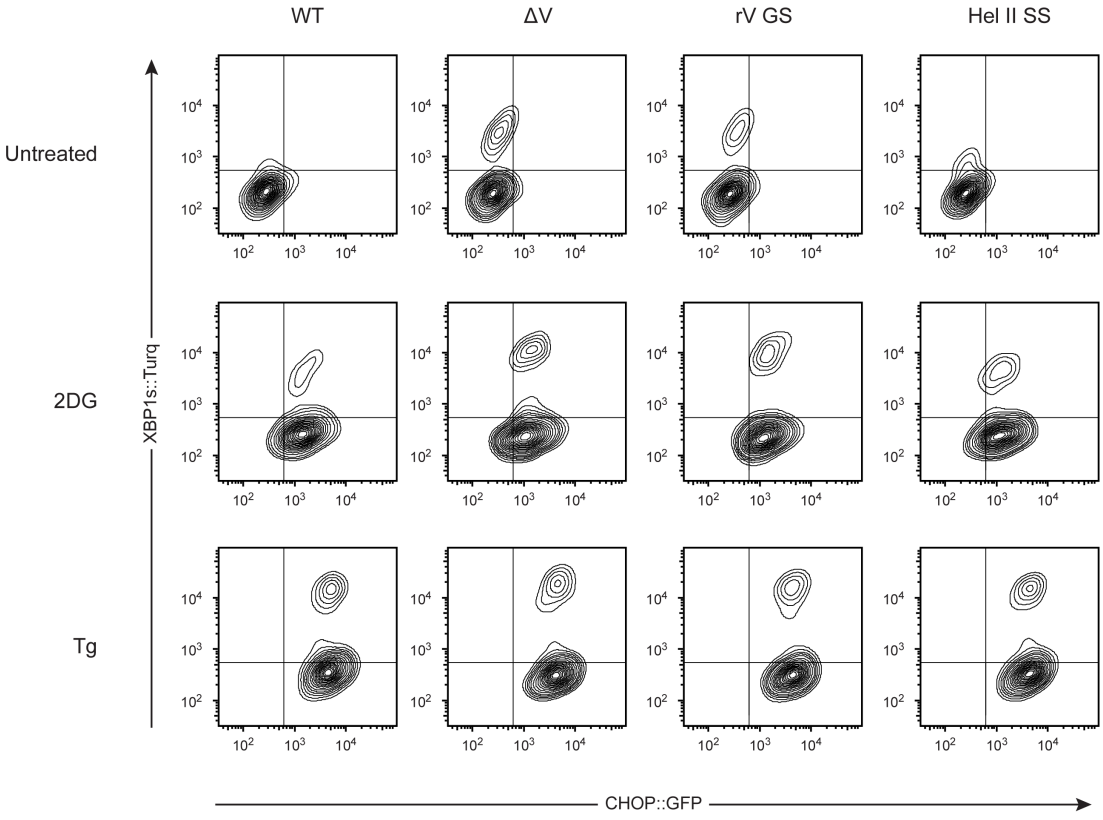
WT
ΔV
rV GS
Hel II SS
Untreated
2DG
Tg
XBP1s::Turq
CHOP::GFP

4.07

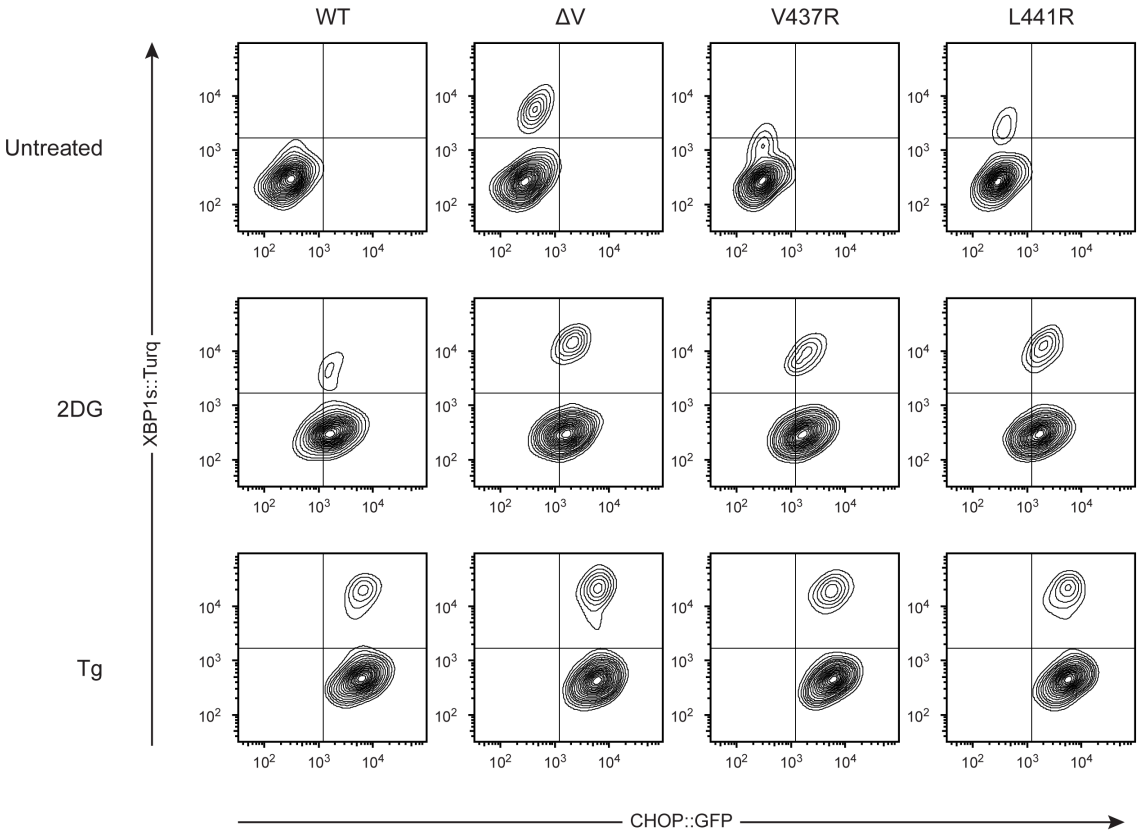

Figure 4.05 Dual channel flow cytometry plots of the XBP1s::Turquoise and CHOP::GFP gene reporters of ΔLD15 cells with the endogenous IRE1 locus reconstituted with WT IRE1 treated with the indicated ER stressors. To better visualise the repaired population, the contour plot mode of displaying raw flow cytometry data was chosen (far right plots) instead of the classical pseudo colour dot plot.

Figure 4.06 Dual channel flow cytometry plots of the XBP1s::Turquoise and CHOP::GFP gene reporters of ΔLD15 cells with the endogenous IRE1 locus reconstituted with the indicated IRE1 variant: ΔV –deletion of IRE1 residues 403-441, rv GS - hydrophobic resides within residues 403-441 mutated to alternating gly/ser, Hel IISS – mutation of the α helix (figure 1.07) with F400S, V403S, I404S, L406S mutations. Cells were treated with 2DG or Tg to reveal the extent of reconstitution and the response still afforded by the IRE1 variants. Note that the efficiency of reconstitution is comparable for the IRE1 variants.

Figure 4.07 Dual channel flow cytometry plots of the XBP1s::Turquoise and CHOP::GFP gene reporters of cells with the endogenous IRE1 locus reconstituted with the indicated IRE1 variant: ΔV –deletion of IRE1 residues 403-441, V437R and L441R. Cells were treated with 2DG or Tg to reveal the extent of reconstitution and the response still afforded by the IRE1 variants. Note that the efficiency of reconstitution is comparable for the IRE1 variants. Initial finding of figure by Nozomu Kono.

4.08

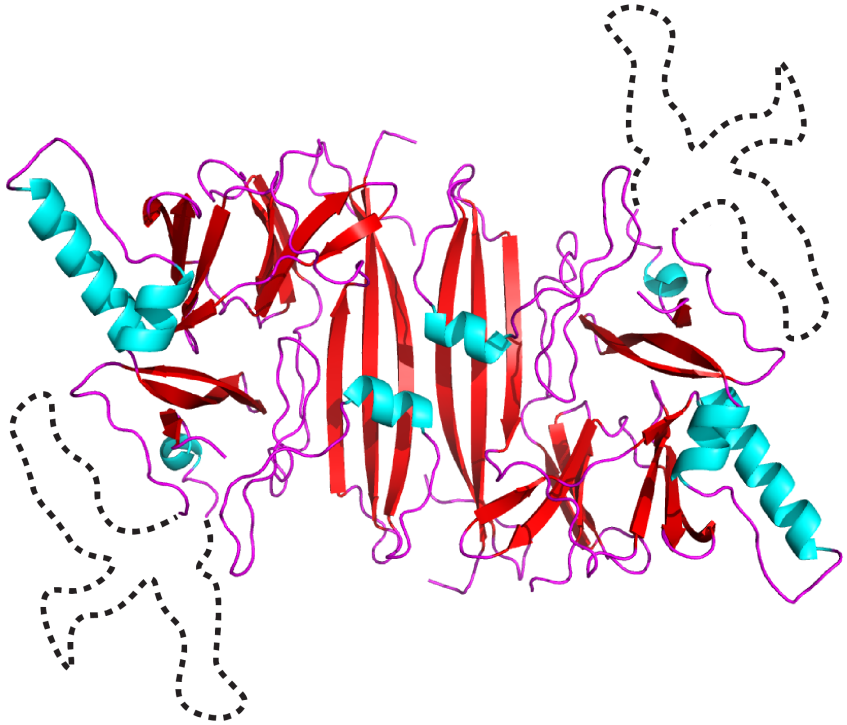

4.09

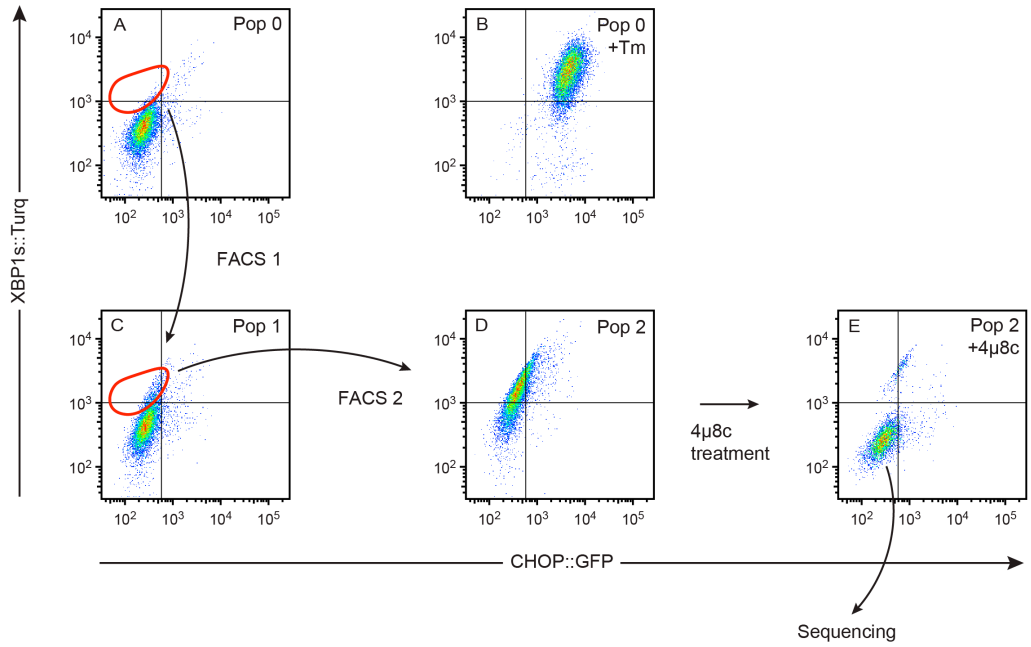

Figure 4.08 hIRE1α LD crystal structure with dashed lines giving an impression of the approximate size and location of the unstructured region of residues 312-353.

Figure 4.09 XBP1s::Turquoise and CHOP::GFP signals from the various cell populations elaborated during the on-going Cas9-CRISPR mutation screen targeting residues 312-353 of IRE1 as outlined in figure 4.01. Sets of WT cells were separately transfected with Cas9 and guides and pooled (Pop 0 panel A). Pop0 cells with elevated levels of XBP1s::Turquoise were collected by FACS (Pop 1 panel C). A second FACS round enriched for cells with elevated reporter levels (Pop 2 panel D). Pop 2 was treated with the IRE1 inhibitor 4µ8c to identify undesirable cells with mutations that uncouple the reporter from IRE1 activity (5% of Pop 2 panel E). The red lines indicate the gates used for FACS.

Chapter 5: *In vitro* experiments addressing the direct binding of unfolded proteins to IRE1α

Whilst model unfolded proteins have been described to activate IRE1α signalling when expressed *in vivo*, until recently, the absence of known specific sequence elements that can drive IRE1α activation has prevented *in vitro* assays assessing facets of this regulatory mechanism. Recently, however, a peptide sequence was identified that reportedly binds the IRE1α peptide-binding groove (Karagöz et al., 2017). This peptide (MPZN) was derived from the model unfolded protein myelin protein zero (MPZ) and has a mix of hydrophobic and hydrophilic residues (LIRYAWLRRQAALQRRLIRYAWLRRQAA) making it sufficiently soluble for *in vitro* binding assays. Karagöz et al measured the binding of IRE1 and MPZN by using a fluorescently MPZN variant in a series of fluorescence polarisation anisotropy experiments. They then performed NMR and analytical ultracentrifugation experiments to assess the consequences of MPZN binding on IRE1's oligomeric status. The regulation of IRE1 by ERdj4-mediated BiP binding does not exclude a regulatory role for direct binding of unfolded proteins to IRE1 and it is of interest to study their relative roles in regulation. Prior to endeavouring to investigate this, it was first attempted to reproduce key findings of Karagöz et al and to further probe the mechanistic details of peptide binding further probed.

MPZN binds IRE1α with an occluded peptide-binding groove

If the binding site for this peptide is indeed the peptide-binding groove then, no binding signal should be obtained when it is incubated with disulfide linked IRE1^{Q105C}, which based on the dimer crystal structure of WT IRE1 would be predicted to have an occluded peptide-binding groove. To test this hypothesis, the fluorescently labeled MPZN peptide (FAM-MPZN) described by Karagöz et al was used in anisotropy experiments. As reported by Karagöz et al, a robust increase in anisotropy is observed when the peptide is incubated with IRE1α (Figure 5.01). However, this increase in anisotropy is still observed when the peptide is incubated with disulfide linked IRE1^{Q105C} (Figure 5.02-5.03). This is

strong evidence that the peptide does not bind in the peptide-binding groove of IRE1α in the manner suggested by the direct binding model.

The MPZN peptide binds non-specifically to IRE1α

The effect the peptide has on IRE1 oligomerisation nevertheless still has the potential to be physiologically relevant and the actual binding site is therefore of interest. To verify that the binding of peptide to IRE1 occurred via a specific site increasing concentrations of unlabelled peptide were included in the anisotropy assay to compete with the labelled peptide for binding to IRE1. However, the presence of this unlabelled peptide does not compete with the labeled peptide to prevent the increase in anisotropy (Figure 5.04). Therefore, there is no single specific binding site for this peptide on IRE1.

Chapter 5 summary

The data shown here suggest that the MPZN peptide does not bind specifically to one site on IRE1 nor that binding to IRE1 requires an accessible peptide-binding groove. Provided that the anisotropy readings obtained here report on the same events as reported by Karagöz et al these data indicate that a specific peptide sequence that drives IRE1α oligomerisation by engaging the peptide-binding groove is still lacking from the field.

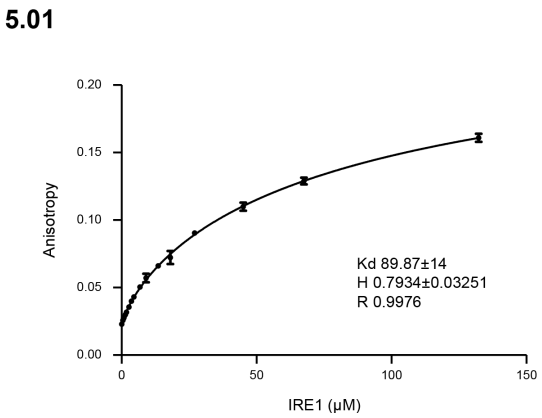

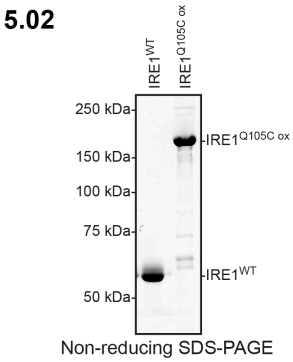

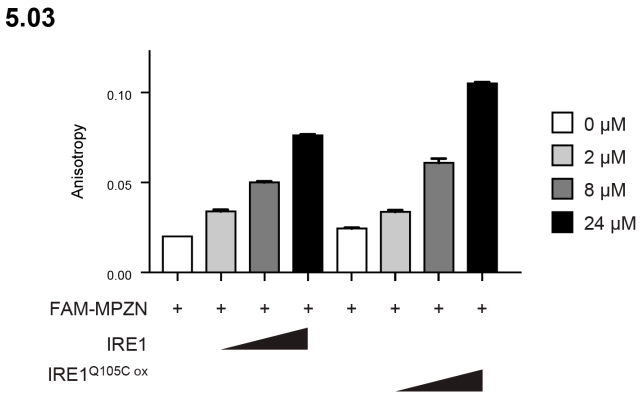

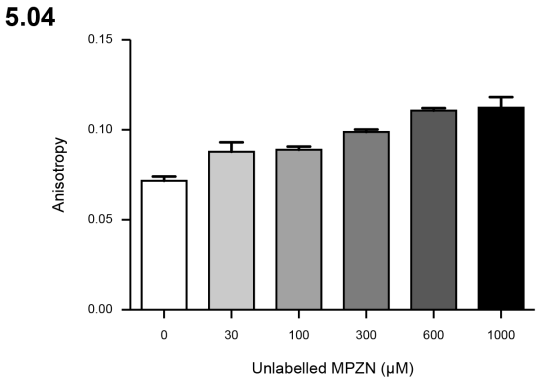

Figure 5.01 Change in anisotropy of 100 nM FAM-MPZN in response to increasing concentrations of WT-IRE1. Shown are mean anisotropy values ± SD from three independent experiments. Anisotropy is calculated as $(I_{para} – I_{perp})/(I_{para} + 2*I_{perp})$

Figure 5.02 Coomassie stained non-reducing SDS-PAGE gel of WT-IRE1 and IRE1$^{Q105C\ ox}$.

Figure 5.03 Anisotropy of 100 nM FAM-MPZN in the presence of the indicated concentration (µM) of WT-IRE1 or IRE1$^{Q105C\ ox}$. Shown are mean anisotropy values ± SD from three independent experiments.

Figure 5.04 Anisotropy of 100 nM FAM-MPZN in the presence of 27 µM WT-IRE1 and the indicated concentration (µM) of unlabelled MPZN competitor. Shown are mean anisotropy values ± SD from three independent experiments.

Chapter 6

Discussion

Summary

The data presented here describe the *in vivo* to *in vitro* journey of identifying and validating ERdj4 as an IRE1α repressor which it achieves through its ability to interact with IRE1α and stimulate the ATP-hydrolysis of BiP thereby guiding BiP to bind IRE1. This thesis also shows how mutational analysis of IRE1α can identify regions of potential importance for the mechanisms responsible for IRE1 regulation. Finally, experimental data are presented that call in to question the current evidence for the direct binding model of IRE1α regulation.

What is the stress sensor?

BiP abundance in the ER

In eukaryotic cells, BiP is highly abundant (>200 μM), whereas IRE1 is scarce (Ghaemmaghami et al., 2003; Kim et al., 2014). Given this stoichiometry, it has been argued that BiP repression cannot be reconciled with the high sensitivity of the UPR (Pincus et al., 2010). However, this argument does not acknowledge the importance of "free" BiP (BiP available to engage with substrate) in repressing IRE1. *In vitro* this is exemplified by the ability of the GRP170 NEF to increase both the amount of BiP recruited to $IRE1^{LD}$ and the rate of $IRE1^{LD}$ monomerisation as explained by GRP170's ability to recover BiP molecules that have futilely hydrolysed ATP without recruitment onto $IRE1^{LD}$, thereby increasing the concentration of ATP-bound, i.e. "free", BiP.

This principle holds true *in vivo* where analysis of cell lysates suggests that the pool of "free" BiP is small: most of the BiP detectable on native gels is either substrate bound, engaged in inactive BiP oligomers or inactivated by AMPylation (Freiden et al., 1992; Preissler et al., 2015a; Preissler et al., 2015b). Therefore, despite the abundance of BiP protein, the buffer of "free" BiP available to repress IRE1 is likely rather modest, thus explaining the sensitivity of the system to stress.

Even if the amount of “free” BiP were not so carefully regulated the discovery of the role played by ERdj4 in IRE1 regulation provides an alternate solution to the high sensitivity to stress exhibited by the UPR branches.

Depletion of co-chaperone rather than chaperone

The strict requirement for a J-protein for repressive complex formation suggests that competition may also occur at the level of the co-chaperone. ERdj4, far less abundant than BiP, likely possess affinity for certain unfolded proteins through its C-terminal targeting domain (Shen et al., 2002; Dong et al., 2008). Since ERdj4 is similarly dependent on this domain to repress IRE1, both *in vitro* and *in vivo*, it follows that the canonical chaperone substrate interaction underlying IRE1 repression could be out-competed by non-IRE1 ERdj4 ligands and serve as selective activators of the IRE1 branch of the UPR. Currently ERdj4 has been shown to bind to a single known substrate: the misfolded substrate protein SP-C$^{\Delta exon4}$ via its C-terminal domain (Dong et al., 2008). SP-C$^{\Delta exon4}$ is indeed seen to be an activator of the UPR, though it does not display selectivity for the IRE1 branch (Maguire et al., 2012; Nguyen and Uhal 2016). Going forward it would be of interest to identify whether the IRE1 branch is particularly sensitive to SP-C$^{\Delta exon4}$ when expressed at low levels and if other ERdj4 substrates exist.

Selective regulation of the mammalian UPR branches

The discovery of ERdj4’s role in IRE1 repression ties in to the prevalent understanding that differential activation of the UPR branches elicits different consequences for the cell and resolution of the initial stress insult (Chiang et al., 2012; Shoulders et al., 2013; Hetz et al., 2015; Adamson et al., 2016).

This is not so surprising given that, despite some overlap, each branch has unique elements to its transcriptional programme e.g. the IRE1/XBP1 branch is essential for the strong upregulation of ERdj4 and ERdj6 whilst the ATF6 branch is primarily responsible for the upregulation of BiP (Lee et al., 2003; Shoulders et al., 2013).

For example, one could imagine instances where the increased folding capacity of the ER by IRE1 and ATF6 activation without decreasing global protein synthesis through PERK activation could be beneficial.

ERdj4 is among other cofactors suggested to play a role in UPR branch specific regulation and, in some cases, pathogens have evolved to exploit these during infection (X. Shen et al., 2005; Gupta et al., 2010; Kato et al., 2012; Chen et al., 2014; Taguchi et al., 2015).

It seems plausible that the different mammalian UPR branches evolved such that subtly different UPR programmes could be initiated that were tailored to respond to the stress that activated them. Does ERdj4 respond to a particular type of stress that other ERdj proteins do not? For example, does ERdj4's *in vitro* dependence on a disulfide between its cysteine residues connect physiological changes in the redox state of the ER to IRE1 activation? Further studies that scrutinise ERdj4 during stress conditions are required to address this.

Redundancy in IRE1 repression

ERdj4 is not the sole repressor of IRE1

The data presented here show that ERdj4 is required for repression of IRE1α in the absence of stress and this repression is alleviated during stress.

There exist further hints in the literature that there is a special relationship between ERdj4 and the IRE1 branch as the ERdj4 gene is selectively up-regulated by IRE1/XBP1 activity (Adamson et al., 2016; Lee et al., 2003) and the phenotype of ERdj4 inactivation in mice mimics XBP1 overexpression (Fritz and Weaver 2014).

However, there is clearly redundancy in the regulation of IRE1 given that ER stressors can further activate IRE1 in cells lacking ERdj4 (Figure 2.08-2.09+2.11) and mutations in region V (a region not involved in the mechanism of ERdj4 repression) result in de-repression of IRE1 (Figure 4.06-4.07). But what are these other mechanisms of IRE1 regulation? The direct binding mechanism may be involved in further activation of IRE1 during stress,

however, it is currently proposed to involve only the CLD thus eliminating it as a candidate for explaining the de-repressing mutations of region V.

In the absence of other mechanisms of IRE1 activation by protein stress, only the chaperone inhibition mechanism remains, raising the possibility of a role for other ERdj proteins in regulating IRE1 activity (by contributing to BiP repression of IRE1). Unlike ERdj4, which appears to act on the CLD, these alternate ERdj proteins may bind to the IRE1 tail and load BiP onto sites similar or distinct from those used by ERdj4.

ERdj2, the translocon and IRE1

From the ERdj knock out screen, ERdj2 emerges as an additional candidate for IRE1 regulation, though it is not clear whether this is due to global perturbation of ER proteostasis or de-repression of the IRE1 and PERK branches that arises independently of any increase in the burden of unfolded proteins (Figure 2.02). It is worth considering that ERdj2 may play a specific role in chaperone inhibition, especially given its association with the translocon complex, a convenient position as a sensor for the protein folding load of the ER.

The Sec translocon complex is responsible for the co-translational insertion of proteins into the ER membrane or lumen. The translocon consists of several components, some more essential than others to the function of the whole. The relevant components for this discussion are the Sec61 heterotrimer and Sec63 (i.e. ERdj2). Sec61, consisting of α, β, and γ subunits, forms the core pore complex that facilitates access from the cytosol into the ER (Johanna Dudek et al., 2015). Sec63/ERdj2, is a J-domain-containing, multipass-transmembrane protein whose main role is thought to be to load BiP onto the nascent polypeptide emerging from the translocon to aid its import into the lumen and folding (Brodsky et al., 1995; Lyman and Schekman 1995; Craven et al., 1996; Matlack et al., 1999).

A link between IRE1 regulation and the translocon is suggested by recent papers. Genetic evidence comes from a screen for genes that, when knocked out, activate the IRE1 branch, which identified the major translocon components, including the Sec61 subunits and ERdj2 (Adamson et al., 2016).

More directed work has been carried out by the Malaiyalam Mariappan lab who report that an interaction between IRE1 and the translocon is important for regulating the activity of IRE1 as reported in Plumb et al., 2015 and Sundaram et al., 2017.

Plumb et al., report on an interaction of IRE1α with ERdj2 and Sec61 subunits. The Sec61:IRE1 interaction is dependent on the luminal IRE1 residues 434-443 and, unlike the BiP:IRE1 interaction, is insensitive to stress. Analysis of these mutants and Sec61α-siRNA knock down experiments suggested that the Sec61:IRE1 interaction is important for efficient splicing of XBP1us mRNA by IRE1 during stress.

The translated XBP1us contains a pseudo-TM domain that is partially inserted into the ER membrane (Yanagitani et al., 2009; Yanagitani et al., 2011). Additionally, the XBP1us mRNA contains a translation pause sequence after the pseudo-TM domain. Combined these features result in increased localisation of the XBP1us mRNA to the ER membrane in close proximity to the translocon.

Building on this and further experiments, Plumb et al concluded that the translocon serves as a hub to confine XBP1us mRNA and IRE1 together such that during stress splicing can proceed more swiftly and efficiently.

The finding that the Δ434-443 IRE1 splices less XBP1us than WT but has higher basal phosphorylation levels led Sundaram et al to further explore the Sec61:IRE1 interaction using IRE1 mutants with either disrupted or enhanced interaction with Sec61. They found that the strength of the Sec61:IRE1 interaction correlates positively with the ability to splice XBP1us and correlates inversely with the propensity for IRE1 to activate (phosphorylation and cluster formation). The Mariappan lab interpret their data to mean that the Sec61:IRE1 interaction favours repression of IRE1 activity (at the level of auto-phosphorylation) whilst enhancing the efficiency of XBP1 splicing by activated IRE1.

The sites of IRE1α that facilitate the interaction with the translocon are located in the tail region which, as described in the introduction, has been implicated in Kar2/BiP binding and IRE1 activity.

It is interesting to note that Myc-PERK harbouring a LD deletion adjacent to the TM has fewer BiP molecules associated with it than WT and has elevated levels of auto-phosphorylation (Ma et al., 2002).

Taking into account the described published literature and the data presented in this thesis it is tempting to propose that translocon-associated ERdj2 may couple IRE1/PERK signalling directly to the flux of proteins imported into the ER. When the flux is low, ERdj2 recruits BiP to IRE1/PERK^{LD}. During periods of high secretory activity, ERdj2 is engaged facilitating translocation, thereby allowing IRE1/PERK to dimerise and activate. Through this coupling, the UPR may activate even before unfolded proteins begin to accumulate in the ER. Such a pre-emptive UPR activation would be very advantageous to the cell.

In this thesis, deletions in the IRE1α tail region are seen to increase IRE1's basal activity as measured by XBP1 splicing (Figure 4.06) which contrasts with Mariappan and Iwawaki lab observations (Daisuke Oikawa et al., 2009; Plumb et al., 2015; Sundaram et al., 2017). It is difficult to reconcile these differences but the simplest explanation is that cellular expression levels are hard to maintain reproducibly at endogenous levels in the experimental systems used in these studies (transient transfections and leaky expression from a doxycycline regulated promoter). As previously mentioned, IRE1 expression levels can dramatically influence its activity and exogenous expression of IRE1 therefore has the potential to yield misleading data (Daisuke Oikawa et al., 2009) and even Sundaram et al themselves show the importance of IRE1 expression levels.

This discussion of expression levels potentially yielding misleading experimental outcomes raises an important issue. The advent of Cas9-CRISPR technology has revolutionised cell biology and should set new standards for experiments assessing gene function *in vivo*. Using Cas9-CRISPR, it is now easier to consistently ensure homogenous protein expression at physiologically relevant endogenous levels within a perturbed cell population, as opposed to expression experiments relying on transient transfections (Figure 2.06) or random genome integration events. Knock down and over-expression systems need no longer be the only techniques used to manipulate gene expression.

Key experiments in this thesis therefore make use of the Cas9-CRISPR technology to introduce mutations into the endogenous gene locus of IRE1, such that its expression levels remain correctly regulated and physiologically relevant.

Currently, ERdj2 is the most plausible candidate for additional ERdj-mediated regulation of IRE1 (and PERK) but ERdj2 may behave very differently to ERdj4 in the manner in which it represses signalling. In contrast to the direct contacts made by ERdj4, ERdj2 is not thought to interact directly with its substrate (nascent polypeptides), yet it is still able to load BiP onto them. Spatial positioning of ERdj2 in proximity to substrate is instead important and this could well be the case if ERdj2 is required for IRE1/PERK regulation (sequence elements in the tail of IRE1 may be required to ensure the correct positioning of IRE1 relative to ERdj2). The lack of a direct interaction between ERdj2 and substrates, coupled with it being a multipass membrane protein may make *in vitro* studies of its role in IRE1/PERK regulation very difficult.

Roles of the other ERdj proteins

The diverse nature of the ERdj proteins means they are involved in a range of different ER proteostasis events. For example, ERdj1 (like ERdj2) is thought to be important for co-translational import into the ER, ERdj3 and ERdj6 potentially play a role in chaperoning folding and ERdj5 is involved in altering disulfides and ERAD. Despite this, the ER environment is not obviously perturbed when these ERdj proteins (other than ERdj2) are individually knocked out suggesting a surprisingly large degree of redundancy in the roles they play, at least in CHO cells used in our study (Figure 2.02). This redundancy may have masked any role played by the other ERdjs in IRE1 or PERK branch regulation and raises interesting questions about ERdj4 and why the burden of IRE1 regulation seems predominantly borne by it. Combinatorial knock outs would be required to assess the extent of redundancy between the ERdj co-chaperones and how they cooperate to maintain ER proteostasis.

The yeast genome encodes four ERdj proteins, Scj1, Sec63, Jem1 and ERj5 (some of which have mammalian homologues) and one or more may be

required to facilitate formation of a Kar2:IRE1 complex. Some evidence for a de-repressed UPR can be seen in yeast lacking either Scj1 or Jem1 consistent with a role of these ERdjs in repressing IRE1 (Silberstein et al., 1998; Famá et al., 2007). Experiments similar to those outlined in this thesis may be a suitable starting point to understanding whether yeast ERdjs play a role in IRE1 regulation and provide further support to the chaperone inhibition model.

Other reported aspects of IRE1 regulation

The direct binding model vs chaperone inhibition

There is a large body of literature, mainly focused on yIRE1, championing the direct binding model as being crucial to IRE1 regulation. Several UPR activating model-unfolded protein substrates have been reported to bind IRE1 and drive oligomerisation. The group of Peter Walter has thoroughly probed such proteins for the peptide sequences facilitating their interaction with IRE1. For yIRE1, the sequence of model unfolded protein mutant CPY was screened for sequences that bind yIRE1 and the highest affinity peptide (F17) was a 15mer which bound with a $K_{1/2}$ of 172 μM (Gardner and Walter 2011)[6]. More recently, proinsulin, MPZ and 8PI were similarly interrogated for sequences that bind IRE1α and the highest affinity peptide was the 12mer MPZN, which bound with a $K_{1/2}$ of 16 μM (Karagöz et al., 2017).

The data presented in this thesis suggest that the MPZN peptide is unlikely to bind solely across the MHC-like peptide-binding groove of IRE1α, as its binding is not disrupted by a disulfide bond that occludes the groove (Figure

[6] A peptide with higher binding affinity than F17 was also identified by Gardener et al., 2011. This peptide, ΔEspP, is a signal peptide and has a K1/2 of 0.75 μM. The mutation of the MFY residues of yIRE1 increases the K1/2 to 42 μM, though this is still a higher affinity than F17 displays for yIRE1. Signal peptides are not normally expected to be present in the ER lumen and it is still unclear whether relevant high-affinity peptides that drive yIRE1 oligomerisation exist.

5.03). This finding, together with the observation that activation of IRE1α^{Q105C}, in cells favours formation of a disulfide (Figure 2.23), argues against an important role for peptide binding in IRE1 activation.

Karagöz et al also discovered that the 2xMPZN peptide, consisting of two joined copies of the MPZN peptide, has a higher affinity for IRE1α ($K_{1/2}$ of 0.6 μM). At concentrations equal to or below that of IRE1α, presence of the peptide stabilises soluble oligomers. Presence of 2xMPZN in molar excess of IRE1α, however, results in precipitation of IRE1α (data not shown and correspondence with Elif Karagöz). It is currently unclear whether precipitation occurs due to formation of stress-relevant oligomers or non-specific aggregates and the effect may still be manifest at lower concentrations of 2xMPZN relative to IRE1.

A competition experiment (as carried out in figure 5.04) is also lacking from the study identifying peptides that drive oligomerisation of yIRE1 (Gardner and Walter 2011). Given the importance of the *in vitro* fluorescent polarisation experiments in the Gardner and Karagöz papers as evidence supporting a role for direct binding of peptides to IRE1 for regulation, it is important to determine to what extent they are reliable indicators of a single, specific binding site as proposed by the direct binding model. If it holds true that MPZN (and the yIRE1 equivalent) indeed bind IRE1 non-specifically at multiple sites and drive it into non-physiologically relevant aggregates then little convincing published data remains supporting the direct binding model.

To regain support for the direct binding model a peptide sequence motif would need to be identified that: binds specifically to and drives dimerisation of IRE1 both *in vivo* and *in vitro*, is present and exposed in model unfolded proteins, and is found in high abundance in the ER proteome to ensure that the UPR is sensitive to the accumulation of any type of unfolded protein. Crosslinking or crystallography experiments could be useful to better characterise the binding sites for such peptides on IRE1.

ERdj4-directed BiP repression is played out at the level of the minimal structured core IRE1^{LD}, sufficient for UPR regulation (Daisuke Oikawa et al., 2009). In pure solution, core IRE1^{LD} protomers have a high affinity for each other and dimerise without addition of peptides (Zhou et al., 2006).

Furthermore, as noted above, the formation a stress-dependent $IRE1^{LD\ Q105C}$ disulfide is difficult to reconcile with an extended unfolded protein engaging the proposed peptide-binding groove of $IRE1^{LD}$ as the initiator of $IRE1^{LD}$ dimerisation.

Given the current experimental data, it seems likely that chaperone inhibition is the main regulator of IRE1α and if unfolded protein binding contributes, it seems it does so not by altering the monomer-dimer equilibrium, which lies at the heart of the UPR, but rather by influencing the formation of higher order IRE1α oligomers, whose function remains to be determined. Whilst chaperone inhibition and direct binding mechanisms are not mutually exclusive, it does not seem necessary at this stage to produce a contrived model of IRE1α regulation encompassing both mechanisms given that chaperone inhibition seems both necessary and sufficient to describe the behaviour of IRE1α.

yIRE1 compared to the mammalian IRE1 isoforms

Yeast and mammals last shared a common ancestor ~1.2 billion years ago. It would not be surprising to find that different mechanisms of IRE1 regulation have evolved since that divergence. The most convincing data supporting chaperone inhibition and direct binding/IRE1 oligomerisation come from mammalian and yeast IRE1 studies respectively. *In vitro* experiments exploring the role of chaperone inhibition of yIRE1 are still lacking but the current consensus is that binding of Kar2 to region V attenuates yIRE1 activity during prolonged stress (Pincus et al., 2010; Ishiwata-Kimata et al., 2013; Mathuranyanon et al., 2015) and potentially desensitises yIRE1 to stress (Pincus et al., 2010). Attenuation of IRE1 activity may influence cell survival during the UPR, as seen by the increased mortality of cells expressing yIRE1 mutants lacking region V exposed to ethanol or heat-stress (Kimata et al., 2004).

Generally yeast and mammalian IRE1 have not been directly compared in a single study, however, the few that have done this see clear differences in the properties of the two proteins that may be linked to their mechanism of regulation. Such studies have led to the suggestion that yIRE1 is regulated by both chaperone inhibition and direct binding and that these regulatory

mechanisms have been partitioned between the mammalian IRE1 isoforms. This compromise suggests that IRE1α is regulated by chaperone inhibition, and not direct binding, whilst the converse is true for IRE1β (Daisuke Oikawa et al., 2012). This is supported by the observation that IRE1β performs more efficiently in anti-aggregation assays (*in vitro*) and interacts more with model unfolded proteins in pull down assays compared to IRE1α (Daisuke Oikawa et al., 2012). It is unclear whether a stress-sensitive BiP:IRE1β complex forms (Bertolotti et al., 2000; Daisuke Oikawa et al., 2012) but there seem to be clear differences between the cytosolic events catalysed by IRE1α vs IRE1β. Over expression of IRE1β is seen to increase cell apoptosis relative to IRE1α (Iwawaki et al., 2001). In addition, the substrate specificity of the IRE1β and IRE1α RNase domains differ allowing IRE1β to cleave for example 28S rRNA to decrease the synthesis of secreted proteins (Iwawaki et al., 2001; Imagawa et al., 2008; Nakamura et al., 2011).

As further work is done to understand the mechanisms of yIRE1 and IRE1α regulation, the reported differences described here and in the introduction may persist and demonstrate how regulation of conserved proteins can diverge.

The molecular detail of chaperone inhibition

BiP and ERdj4 binding sites on IRE1

It will be exciting to pursue a high-resolution map of the interaction sites between IRE1 with ERdj4 and BiP, and the following predictions can already be made regarding these interaction sites. Binding sites sufficient for ERdj4 binding and for repressive BiP binding exist in the CLD (Figure 3.22). Both sites are accessible in Q105C disulfide linked IRE1 dimers and therefore the binding sites are unlikely to be at the dimer interface suggesting the repressive mechanism is allosteric rather than a steric blocking of the interface (Figure 3.16-3.18). The binding site of BiP is likely on an exposed loop protruding from the core globular $IRE1^{CLD}$ due to the structural constraints of BiP substrate binding, which favours interactions with extended polypeptides (Zhu et al., 1996; Rüdiger et al., 1997).

These predictions marry well with preliminary experimental data from the mass-spectrometry and mutagenesis approaches indicating a role for IRE1α residues 312-353 in binding BiP. Given their absence from the crystal structure, these residues are likely unstructured or flexible making them a more accessible substrate for BiP.

Though algorithms exist for predicting the sites of BiP binding in proteins (Blond-Elguindi et al., 1993; Schneider et al., 2016), these were created using data of unregulated binding of BiP to peptides and may therefore not be informative for identifying the sites of ERdj-directed BiP substrate binding.

In vitro multiple BiP molecules associate with a single IRE1 molecule, possibly through multiple binding sites on IRE1 and/or BiP oligomers binding to IRE1 (Figure 3.06). Given the difficulty of measuring the stoichiometry of the endogenous BiP:IRE1 complex, it is difficult to assess whether the *in vitro* observations on stoichiometry mirror the *in vivo* system. As discussed, the *in vivo* pool of “free” BiP is likely small and significant amounts of BiP oligomers are only known to actively assemble in response to the stress of ER calcium depletion (Preissler et al., 2015b). Therefore, if multiple BiP molecules do associate with IRE1 *in vivo*, it seems unlikely that the repressive endogenous BiP:IRE1 complex comprises of oligomeric BiP. It is more likely that multiple binding sites on IRE1 for BiP exist and could provide a mechanism for the gradual activation of IRE1 in response to mounting stress.

Whilst there is hope that the BiP:IRE1 interaction can be properly characterised, it will likely not be as simple to establish the binding site for ERdj4 on IRE1 given the difficulty of working with this protein. However, some details of the interaction can still be discussed in light of the data presented here.

The nature of the ERdj4:IRE1 interaction

BLI data reproducibly reports on a very high affinity interaction between IRE1 and ERdj4 and is independent of which component is used as the biotinylated ligand (Figure 3.11-3.12). This interaction is disrupted by ERdj4-mediated loading of BiP onto IRE1 and requires hydrolysis of ATP. Hints of this high-affinity interaction have also been observed indirectly via the FRET system.

ERdj4^{QPD} is a strong inhibitor of ERdj4/BiP/ATP disruption of IRE1 dimers consistent with the idea that ERdj4^{QPD} binds to IRE1 and cannot activate BiP to displace itself from IRE1, thereby blocking ERdj4^{WT} from binding and loading BiP to inhibit dimerisation (data not shown). This displacement of ERdj by BiP from its substrate has some precedent with a QPD ERdj3 and immunoglobulin light chain intermediates (Y. Shen and Hendershot 2005).

Some puzzling aspects of the ERdj4:IRE1 interaction remain to be understood. In contradiction to the displacement of ERdj4 by BiP seen *in vitro, in vivo* co-immunoprecipitation reveals a reproducible interaction between IRE1^{LD}-GST and ERdj4^{WT} but not ERdj4^{QPD} (data not shown). This finding may represent an uninformative and confusing experimental artefact (as both the IRE1 and the ERdj4 partners of this interaction are over-expressed), however it may also be explained by accumulation of ERdj4 specific substrate in *ΔERdj4* cells. When ERdj4^{WT} is expressed these substrates bind ERdj4 and are cleared, leaving ERdj4 free again. However, in the absence of a functional J-domain, the pool of ERdj4^{QPD} instead becomes sequestered by these substrates with fewer molecules available to associate with the IRE1 luminal domain. The idea that ERdj4 may be involved in aspects of proteostasis other than repressing IRE1 via BiP loading is supported by the finding that over-expression of ERdj4^{QPD} in *ΔERdj4* cells retains some ability to repress the de-regulated IRE1, which is not seen *in vitro* (Figure 2.05).

An ERdj4:IRE1 interaction is not always apparent *in vitro.* The pull-down system used in this thesis does not reproducibly reveal an ERdj4:IRE1 interaction above the background binding of purified recombinant ERdj4 to the streptavidin beads used. This suggests that further optimisation of the binding conditions is required before drawing conclusions. In addition, a stable ERdj4:IRE1 complex in the size exclusion chromatography data set was not detected (Figure 3.06), which is difficult to reconcile with the very low off rates of the complex observed in the BLI experiment (Figure 3.11+3.12).

The repressive BiP:IRE1 complex forms through a canonical chaperone-substrate interaction

The work in this thesis provides evidence that the repressive BiP:IRE1 complex is formed through a canonical chaperone substrate interaction as directed by a co-chaperone rather than a non-canonical alternative. This is difficult to reconcile with the data presented by the group of Maruf Ali who have published a comprehensive set of *in vitro* experiments showing the BiP-IRE1 interaction to be NBD-mediated, SBD independent and nucleotide insensitive (Carrara et al., 2015b; Kopp et al., 2018).

Though few BiP-IRE1 *in vitro* experiments have been published, some information about the nature of the BiP:IRE1 interaction can be gleaned from *in vivo* studies, which support it being a canonical chaperone substrate interaction (Bertolotti et al., 2000; Kimata et al., 2003; Liu et al., 2003). The findings of the Ali group are partly supported by the *in vivo* study of Todd-Corlett et al, who show that presence of glycans around the Kar2 NBD but not the SBD are able to prevent the BiP:IRE1 interaction. This data and further mutational analysis suggests that the Kar2 NBD is responsible for mediating the interaction with yIRE1 (Todd-Corlett et al., 2007). It is important to note that to date, other than those of the Ali group, studies supporting that the BiP:IRE1 interaction is non-canonical do not suggest that it is insensitive to nucleotide (Todd-Corlett et al., 2007; Sou et al., 2012).

Some of the findings of Carrara et al may be reconciled by taking into account the different experimental conditions used. For the striking pull down data BiP variants were incubated with 500 μM (150 μM for Kopp et al., 2018) of binding partner (IRE1 etc.), which may facilitate non-physiological interactions between the components. In addition, the Ali group may not see association of SBD with IRE1 because of the short incubation time (1 hr) used in all binding experiments which, due to the low k_{on} of the isolated (un-regulatable) BiP SBD, is likely not enough to be able to claim that no binding occurs.

It should again be emphasised that *in vivo* the capacity of BiP to function is thought to be completely dependent on regulation by ERdj and NEF co-chaperones (Otero et al., 2010). Whilst the Ali group convincingly show that

under certain experimental conditions BiP-NBD but not BiP-SBD can bind IRE1, the data presented in this thesis and the current knowledge of the Hsp70 field all suggest that NBD binding and the observed nucleotide insensitivity is not physiologically relevant to IRE1 regulation *in vivo*.

The validity of IRE1^{Q105C} as a tool

Some important conclusions of this thesis rest on the validity of disulfide linked IRE1^{Q105C} representing stress relevant IRE1 dimers, namely the ability of ERdj4 to favour IRE1 monomers *in vivo* (Figure 2.27) and the ability of ERdj4 to load BiP onto IRE1 dimers *in vitro* (Figure 3.16-3.18).

Though it has not been proven that the endogenous IRE1^{Q105C} forms Q105C-Q105C homodimers rather than heterodimers with an unknown entity, the existence of the former when overexpressed (Figure 2.26) and *in vitro* (Figure 5.02) makes it reasonable to assume that it does.

As described the endogenous IRE1^{Q105C} also contains the C109S mutation, which could be corrupting to the protein however previous studies have determined that C109 is not important to IRE1α's function. In total, the WT IRE1α^{LD} has 3 endogenous cysteines, C109, C148 and C332, and disulfide linked IRE1α species have been observed which are dependent on C148 and C332. However, formation of these disulfides is not important for IRE1α folding or dimerisation (Liu et al., 2002; Liu et al., 2003; Daisuke Oikawa et al., 2009)[7].

---

[7] As mentioned IRE1α LD disulfides are not thought to be a critical post-translational modification for its function. IRE1α LD also has a single predicted N-linked glycosylation site which has been seen to be glycosylated, however the folding and dimerisation of IRE1α is not dependent on the integrity of this site (Chuan Yin Liu et al., 2002). The insensitivity of IRE1α functionality and structure to its glycosylation and disulfide states makes it a robust protein to tolerate and continue functioning under ER stress conditions that may impair

Disulfide bond formation between IRE1 molecules or other proteins may have subtle effects on IRE1α e.g. slower attenuation of IRE1α activity during/post stress due to an inability to interact with PDIA6 (via C148) which has been reported to dissociate from IRE1α in response stress before reassociating during stress resolution and IRE1α attenuation (Eletto et al., 2014).

All this being said, it seems likely that IRE1Q105C is indeed a suitable tool for providing a stress-relevant disulfide linked IRE1 dimer.

---

glycosylation machinery or the redox environment of the ER and is likely an evolved/selected for trait.

A proposed model for IRE1 regulation

A final model for the mechanism of IRE1α regulation is shown incorporating the data from this thesis and observations from the literature (Figure 6.05). In the absence of stress, when the folding load is low, there is sufficient available J-activity (from ERdj2 and ERdj4) and “free” BiP to maintain the IRE1 population in inactive monomers. The monomer population is stabilised through active disruption of IRE1 dimers and through the inability of BiP-IRE1 monomers to dimerise. Both of these are achieved through a dynamic, non-equilibrium, ATP-consuming process of J-protein-driven cycles of BiP rebinding to $IRE1^{LD}$ and release following nucleotide exchange. During stress, available J-activity and “free” BiP is depleted by the increased folding load and becomes insufficient to maintain the inactive IRE1 population.

The J-protein driven ATP hydrolysis of BiP provides the energy for the described mechanism of IRE1 inactivation. The dynamic nature of this mechanism, provided by NEF, allows the system to continually sample the ER environment, which is required for sensitivity to changes. At the heart of this mechanism is that the ERdj-mediated BiP:IRE1 complex is a canonical co-chaperone formed chaperone-substrate complex as it allows unfolded proteins to compete for the same pool of chaperone and co-chaperone.

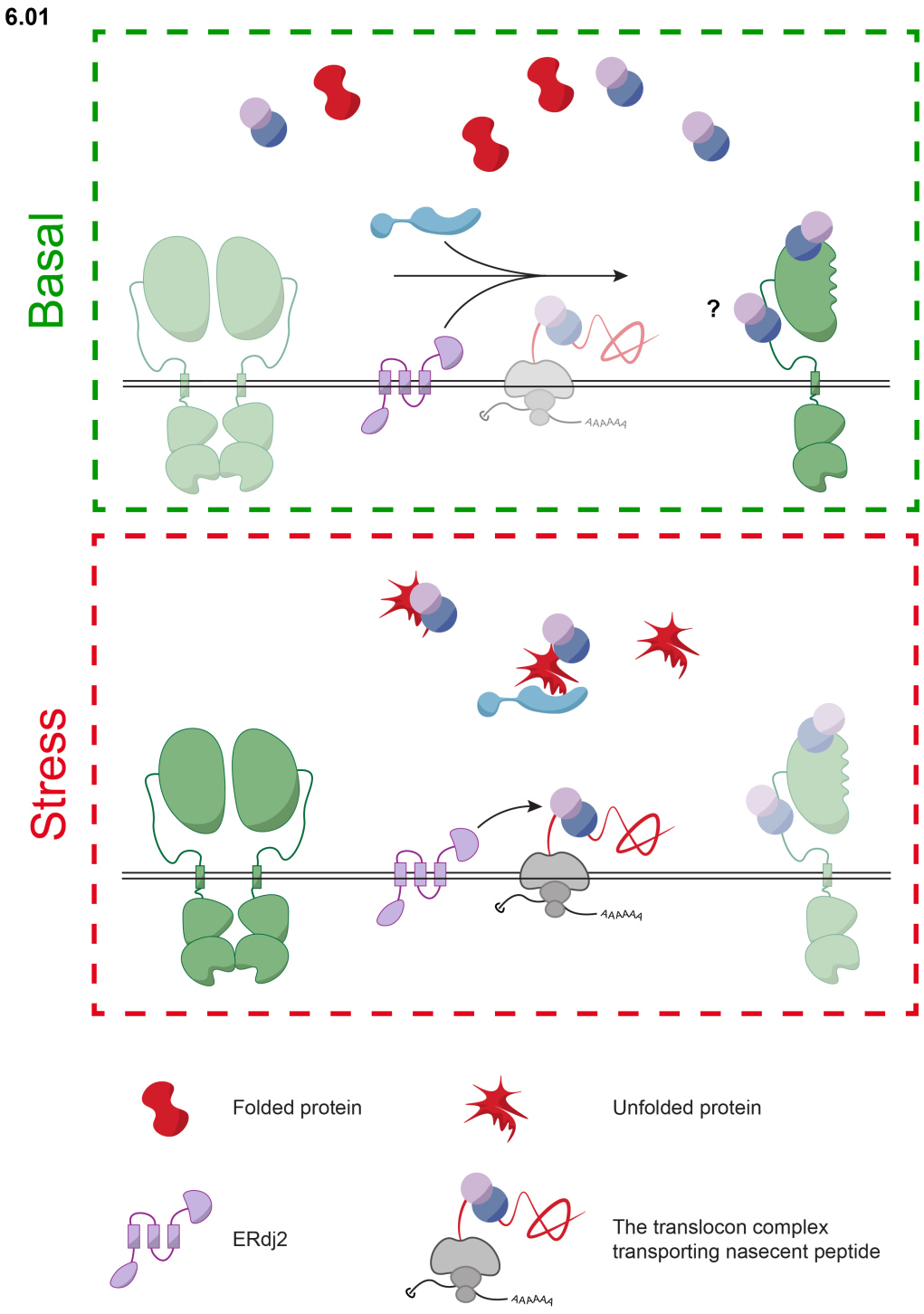

6.01 The proposed model of IRE1α regulation (see main body text for full description). The question mark in the above panel indicates uncertainty about the role of BiP in binding the IRE1α tail in regulating IRE1 activity. Faded images indicate a decreased abundance of the respective species.

Conclusion

Since the discovery of the eukaryotic unfolded protein response, the mechanism by which ER proteostasis is monitored has been sought. The discovery of an ER-localised J-protein that selectively represses IRE1 activity has, for the first time, allowed reconstitution of a UPR that is based on sensor repression by free BiP and de-repression by accumulating unfolded proteins. By incorporating this missing component the experiments presented in this thesis have closed an important gap between the finding that activity of the UPR transducers in cells correlates inversely with the amount of associated BiP and a plausible explanation for how this might come about.

Though direct binding originally emerged as an elegant hypothesis for IRE1 regulation this thesis reveals that the most compelling published data supporting it are potentially misleading. Consequently, direct binding remains a mere model that awaits further experimentation to restore it to being an accepted mechanism for IRE1α regulation.

By exploiting the diversity of functionalities associated with J-proteins, BiP-mediated repression of ER stress transducers throughout eukaryotes may have developed as a conserved, sensitive and potentially versatile mechanism for coupling changes in unfolded protein burden to signalling – the essence of the UPR.

Methods

Information on key oligonucleotides and plasmids used in this thesis is provided in appendix tables 1 and 2.

CHO cell line

A parental stock of Chinese Hamster Ovary CHO-K1 cells (ATCC, CCL-61) was used. Its identity has been validated by the presence of auxotrophic markers and by deep sequencing of the genome.

CHOP::GFP and *XBP1::Turquoise* reporters were introduced sequentially under G418 and puromycin selection to generate the previously-described derivative CHO-K1 S21 clone (Sekine et al., 2016). The puromycin resistance marker was subsequently lost, rendering CHO-K1 S21 cells sensitive to puromycin.

Adherent Chinese hamster ovary (CHO) cell-lines were grown in Ham's nutrient mixture F12 (Sigma). All cell media was supplemented with 10% Hyclone FetalClone-2 serum (FetalClone II, Hyclone-GE Healthcare Life Sciences, South Logan, UT Lot# ABB214492), 2 mM glutamine (Sigma), 100 U/ml penicillin and 100 µg/ml streptomycin (Sigma). Cells were grown at 37°C in 5% atmospheric CO_2.

Bacterial culture

Proteins were expressed in BL21 C3013 *E. coli* cells or Origami B(DE3) cells (NEB). Bacterial cultures were grown at 37˚C in LB medium containing 100 µg/ml ampicillin to an OD_{600nm} of 0.6-0.8. Expression was induced with 0.5 mM isopropylthio β-D-1-galactopyranoside (IPTG) and the cells were incubated for 16 hours at 18˚C.

DNA amplification PCR/RT-PCR

RNA was extracted as per a standard phenol:chloroform extraction. Briefly RNA STAT 60 was used to lyse cells and gDNA sheared with needle. 0.3 M NaOAc was added and two sequential phenol:chloroform extractions performed. The RNA was then precipitated in isopropanol and washed in 70% EtOH before resuspending in RNase-free water. The reverse transcription

reaction was primed with oligo dT and the subsequent PCR reaction primed with primes 5 and 1470.

Cell culture

Thapsigargin (Calbiochem) treatment was at 0.5 µM. Tunicamycin (Melford) treatment was at 2.5 µg/ml for 16 hours unless otherwise stated. 2-Deoxyglucose (Sigma) treatment was at 4 mM for 16 hours. Dithiothreitol (DTT) (Sigma) treatment was at 2 mM for 15 minutes. 4µ8c (Cross et al., 2012) treatment was at 10 µM for 12 days.

Transfection

Cells were transfected using Lipofectamine LTX (Life Technologies) with the reduced serum medium Opti-MEM (Life Technologies) according to manufacturer's instructions.

Gene manipulation and allele analysis

Cas9 guide design was aided in part by the online resource "CRISPy" (Ronda et al., 2014) several guides were designed manually following standard guidelines (Ran et al., 2013). Cells were transfected with the Cas9 and guide constructs and grown for a week before analysis by flow cytometry and sorting.

For genotyping, genomic DNA was extracted from cells by incubation in proteinase K solution (100 mM Tris pH 8.5, 5 mM EDTA, 200 mM NaCl, 0.25% SDS, 0.2 mg/ml Proteinase K) overnight at 50°C. Proteinase K was then heat inactivated at 98°C for 20 minutes before the supernatant was collected and used as a template in PCR reactions before sequencing. To aid in interpreting sequencing data of genes modified by Cas9 the changes in size of the target gene alleles were determined by cappilary electrophoresis on a 3730xl DNA analyser (Applied Biosystems). Samples to be analysed by the DNA analyser were generated through PCR reactions where one of the oligonucleotides had a 5' 6-carboxyfluorescein (FAM) flurophore modification. Genomic information of the clones elaborated, is provided in appendix table 3.

Creating the endogenous IRE1^{Q105C}

The endogenous IRE1 locus was challenged with Cas9 guide UK1558 to generate a loss of function indel and fluorescence-activated cell sorting (FACS) was used to select for XBP1s::Turquoise dull cells after 2-deoxyglucose (2DG) treatment. The resultant clones were genotyped with oligonucleotides 1100/1125 and 1101. After sequencing, a clone (NC6) that was apparently homozygous for a single frameshift nucleotide deletion was selected. To introduce the Q105C and C109S mutations, the new IRE1 locus was challenged with Cas9 guide UK1559 and a PCR-knitting generated repair template (oligonucleotides used: 1097, 1098, 1116, 1117 to PCR from CHO genomic DNA, see appendix table 4 for repair template sequence). Cells that successfully repaired the IRE1 locus were selected using FACS to collect cells that were XBP1s::Turquoise bright after 2DG treatment. Resultant clones were genotyped with oligonucleotides 1100/1125 and 1101. Two clones (CV1 and CV8) were idenitfied by sequencing as homozygous for the repair sequence and were used for subsequent experiments.

Flow cytometry and FACS

Flow cytometry was carried out on a BD LSRFortessa. Adherent CHO cells were washed once in PBS and then incubated for 5 minutes in PBS + 4 mM EDTA before harvesting and fixing in PBS + 1.1% paraformaldehyde. Cell sorting was carried out on a Beckman Coulter MoFlo Cell sorter. Adherent CHO cells were washed once in PBS and then incubated 5 minutes in PBS + 4 mM EDTA + 0.5% BSA before sorting into fresh media. CHOP::GFP fluorescence was measured by excitation at 488 nm and monitoring emission at 530/30 nm. XBP1s::Turquoise fluorescence was measured by excitation 405 nm and monitoring emission 450/50 nm.

Mammalian cell lysis

Adherent cells were grown in 10-cm dishes and treated as described above. The dishes were then transferred to ice and cells were washed in PBS and harvested in PBS + 1 mM EDTA with a cell scraper. The collected cells were spun at 370 *g* for 5 minutes at 4°C. Cells were lysed in 1% Triton X-100, 150

mM NaCl, 20 mM HEPES-KOH pH 7.5, 10% glycerol, 1 mM EDTA, 1 mM phenylmethylsulphonyl fluoride (PMSF), 4 µg/ml Aprotinin and 2 g/ml Pepstatin A and 2 µM Leupeptin. For BiP coimmunoprecipitation experiments the lysis buffer lacked EDTA and was further supplemented with 10 mM $MgCl_2$, 6 mg/ml glucose and 2 mg/ml Hexokinase (Sigma) to deplete ATP and stabilise BiP substrate interactions. For analysis of IRE1 phosphorylation by Phostag gel electrophoresis (Yang et al., 2010), the lysis buffer was further supplemented with 10 mM tetrasodium pyrophosphate, 100 mM sodium fluoride and 17.5 mM β-glycerophosphate. For analysis of $IRE1^{Q105C}$ disulfide linked species the lysis buffer was further supplemented with 20 mM N-Ethylmaleimide (NEM). After 5 minutes of lysis on ice cells were spun at 21,130 *g* for 10 minutes at 4°C. The supernatant was transferred to a fresh tube and, when necessary, protein concentration measured with BioRad protein assay (Bio-Rad).

To reduce the non-specific binding of BiP to protein-A sepharose beads the experiments shown in figure 2.10+2.18 included an additional digitonin permeabilisation step (Le Gall et al., 2003) to remove non-membrane associated BiP from cells prior to lysis. After harvesting cells were washed in HNC buffer (50 mM HEPES-KOH pH 7.5, 150 mM NaCl, 2 mM $CaCl_2$) and then incubated in HNC with 0.1% (w/v) digitonin (Calbiochem) for 10 minutes. Cells were then washed in HNE buffer (50 mM HEPES-KOH pH 7.5, 150 mM NaCl, 1 mM EGTA) before proceeding to the lysis step as described above.

Antibodies

Anti-mouse IRE1α serum (NY200) and anti-mouse PERK serum (NY97 & NY201) was used for immunoprecipitation and immunoblot detection of endogenous IRE1α, PERK and PERK-P respectively (Bertolotti et al., 2000). Anti-hamster BiP serum was used for immunoblot detection of endogenous BiP (Avezov et al., 2013). Anti-GST serum was used for immunoblot detection of GST fusion proteins (Ron and Habener 1992). Anti-FLAG-M2 monoclonal antibody was used for immunoblot detection of FLAG fusion proteins (Sigma F1804).

Immunoprecipitation and GSH pull-down assays

Protein A sepharose 4B beads (Zymed Invitrogen), and appropriate antisera (against IRE1 and PERK), or Glutathione (GSH) Sepharose 4B beads (GE Healthcare) were equilibrated in lysis buffer. For BiP immunoprecipitation anti-BiP chicken IgY antibodies were covalently bound to UltraLink Hydrazine Resin (Pierce cat. # 53,149) according to the manufacturer's instructions. 20 µl beads/resin per sample was added to lysates and left rotating for 1 hour at 4°C. The beads/resin was then washed in lysis buffer and residual liquid was removed using a syringe. The protein from the beads/resin was eluted in SDS sample buffer containing 20 mM DTT or 20 mM NEM (for non reducing gels).

SDS-PAGE/Phos-tag SDS-PAGE and immunoblotting

Samples were separated on standard polyacrylamide Tris-HCl gels and transferred to Immobilon-P PVDF membrane (Pore size 0.45 µm, Sigma). The membrane was then blocked in 5% (w/v) dried skimmed milk in PBS. For the non-reducing gels of endogenous IRE1α the membrane was treated with GDHCl buffer (6 M Guanidine-HCl, 250 mM NaCl, 50 mM Tris pH 7.5, 10% glycerol) with added 0.2% SDS and 100 mM DTT for 30 minutes then washed in GDHCl buffer, and finally treated with GDHCl buffer with added 40 mM NEM for 30 minutes. The membranes were then washed three times in TBS (50 mM Tris pH 7.5, 150 mM NaCl) and blocked in 5% (w/v) dried skimmed milk in PBS before continuing with the standard procedure. After blocking the membranes were washed in TBS with 0.1% Tween-20 and stained with various primary antibodies/antisera followed by staining with IRDye fluorescently labelled secondary antibodies or horse radish peroxidase (HRP) labelled secondary antibodies (G21234, ThermoFisher). Super Signal West Pico Chemiluminescent substrate (Thermo Scientific) was used as an HRP substrate. Imaging was carried out with either a LICOR CLx Odyssey infrared imager or by film. For Phos-tag gels, 50 µM Phos-tag acrylamide (NARD) and 100 µM $MnCl_2$ were included in the gel recipe as described (Kinoshita et al., 2009). Transfer was carried out according to the standard protocol except that

prior to transferring, the Phos-tag gel was washed in transfer buffer supplemented with 1 mM EDTA.
Coomassie-staining was carried out with Instant Blue (Expedeon) and imaged on the above-mentioned LICOR. $IRE1^{LD}$-TAM in SDS-PAGE gels was imaged with a typhoon trio imager with a 532 nm laser and monitoring emission at 580/30 nm.

Protein Purification

Human IRE1LD

$IRE1^{LD}$ (UK2007), $IRE1^{LD}$-cys (UK1915) and $IRE1^{CLD}$-cys (UK1998) used to make $IRE1^{LD}$-biotin (UK1915 and UK2007), $IRE1^{LD}$-OG (UK1915) and $IRE1^{CLD}$-biotin (UK1998), were encoded on pGEX vectors (GE Healthcare) as GST fusion proteins and expressed in BL21 C3013 *E. coli* cells (NEB). Bacterial cultures were grown at 37˚C in LB medium containing 100 µg/ml ampicillin to an OD_{600nm} of 0.6-0.8. Expression was induced with 0.5 mM IPTG and the cells were incubated for 16 hours at 18˚C. The cells were sedimented by centrifugation and the pellets were resuspended in TNGMT buffer (50 mM Tris pH 7.4, 500 mM NaCl, 10% glycerol, 1 mM $MgCl_2$, 1 mM TCEP). The cell suspension was supplemented with 0.1 mg/ml DNaseI and protease inhibitors [2 mM PMSF, 4 µg/ml pepstatin, 4 µg/ml leupeptin, 8 µg/ml aprotinin] and lysed by repeated passage through a high-pressure homogeniser (EmulsiFlex-C3, Avestin). The lysates were cleared by centrifugation at 20,000 *g* for 60 minutes. The supernatant was removed, supplemented with 0.5% (v/v) Triton X-100, and incubated for 60 minutes at 4˚C with glutathione sepharose beads (GE Healthcare; 0.5 ml per litre of bacterial culture). The beads were washed four times with 50 ml of TNGMT buffer (supplemented with 0.05% Triton X-100) and incubated for 20 minutes with 2 bed volumes of TNTGsh buffer (50 mM Tris pH 7.4, 150 mM NaCl, 40 mM GSH, 1mM TCEP). The slurry was passed through a table-top column and the flow-through was collected after a wash with 1 bed volume of TNTGsh elution buffer. Tobacco Etch Virus protease (TEV) was added (1:100 mol:mol) and the eluate was incubated overnight at 4˚C to remove the GST tag. The eluted and cleaved proteins were concentrated and passed through a Superdex 200 10/300 GL gel filtration

column (GE Healthcare) connected in series with a 1 ml GSTrap FF column (GE Healthcare) equilibrated in HKG buffer (50 mM HEPES-KOH pH 7.6, 150 mM KCl, 10% glycerol). For IRE1^{LD}-cys, the buffer was supplemented with 1 mM TCEP and 0.1 mM EDTA. Appropriate fractions were collected, concentrated, and flash frozen.

IRE1^{LD}-cys (UK1915) and IRE1^{CLD}-cys (UK1998) were labelled with a 3-fold molar excess of biotin-maleimide (Sigma) to make IRE1^{LD}-biotin and IRE1^{CLD}-biotin, respectively. IRE1^{LD}-cys was labelled with a 1:100 (mol:mol) ratio of Oregon Green-iodoacetic acid (ThermoFisher) to make IRE1^{LD}-OG. The reaction proceeded at room temperature in the dark for two hours and was quenched by the addition of 5 mM DTT. The reaction mixture was passed through a CentiPure P10 gravity-desalting column (Generon) equilibrated in HKG buffer and through a Superdex 200 10/300 GL gel filtration column equilibrated in HKG buffer. Appropriate fractions were collected, concentrated, and flash frozen.

The IRE1^{LD} R234C (UK2048) and IRE1^{LD} S112C (UK2076) used to make IRE1^{LD}-donor and IRE1^{LD}-acceptor, respectively, were encoded on a pET-derived vector (Novagen) as a His-Smt3 fusion protein and expressed as described above. Cells were harvested in HNKIGT buffer (25 mM HEPES-KOH pH 7.5, 400 mM NaCl, 100 mM KCl, 25 mM imidazole, 10% glycerol, 1 mM TCEP) and lysed and clarified as above. The lysates were cleared by centrifugation at 20,000 *g* for 60 minutes. The supernatant was removed, supplemented with 0.5% (v/v) Triton X-100, and incubated for 60 minutes at 4˚ C with Ni-NTA Agarose beads (ThermoFisher; 0.75 ml per liter of bacterial culture). The beads were washed four times with 50 ml of HNKIGT buffer (supplemented with 0.05% Triton X-100) and eluted with HNKIGT buffer supplemented with 250 mM imidazole. The eluate was concentrated, passed through a gravity desalting column equilibrated with HKG supplemented with 1 mM TCEP and 0.1 mM EDTA, concentrated and labelled overnight at room temperature with a 3-fold molar excess of TAM-maleimide (Sigma; S112C) or Oregon Green-iodoacetic acid (ThermoFisher; R234C). The reaction mixtures were quenched, passed through a gravity desalting column, and passed through an S200 column as described above and the appropriate fractions

were concentrated and flash frozen. IRE1^{CLD}-S112C (UK2117) and IRE1^{CLD}-R234C (UK2118) were expressed, purified, and labelled similarly.
The IRE1$^{LD\ Q105C}$ (UK2045) used to make disulfide-linked dimeric IRE1^{LD}-bio was expressed as an His6-Smt3 fusion protein in Origami B(DE3) cells (Novagen) and purified without reducing agent as described above. Dimeric IRE1^{LD}-^{Q105C} and standard IRE1^{LD} (UK2007) were labelled at a 1:10 (mol:mol) ratio with biotin-NHS ester (Sigma) for one hour at room temperature to create disulfide-linked dimeric IRE1^{LD}-bio and wild-type IRE1^{LD}-bio, respectively. Reactions were quenched by the addition of 5 mM Tris-HCl pH 8.

Hamster ERdj4

ERdj4 and variants were expressed as fusion proteins with an N-terminal His6-Smt3 (UK2012 for WT, UK2040 for QPD) or with both an N-terminal His6-Smt3 and C-terminal MBP (UK2108 for WT, UK2119 for QPD). Proteins were expressed in Origami B(DE3) cells. ERdj4 proteins expressed in BL21 (DE3) cells were not soluble, suggesting that ERdj4 may have a stabilising disulfide between its two cysteines therefore, no reducing agent was used in purification of Erdj4 or its variants. Cells were grown and lysed as described above for His6-Smt3 tagged proteins. Media of cells expressing His6-Smt3-ERdj4-AviTag (UK2098) was supplemented with 0.2 mM Biotin (to allow the endogenous biotinylation enzymes of the bacteria to biotinylate the Erdj4 protein). The lysates were purified by Ni affinity chromatography as described above. His6-Smt3-ERdj4 was aliquoted immediately after elution from the Ni matrix. It was found to precipitate immediately upon cleavage of Smt3 by Ulp1. His6-Smt3-ERdj4-MBP was loaded onto an S200 10/300 GL column equilibrated in HKG buffer. Fractions containing His6-Smt3-ERdj4-MBP were collected, aliquotted, and flash-frozen.

Human GRP170

N-terminally His6-tagged human GRP170 (UK1264) was expressed in BL21 (DE3) cells and induced, lysed, bound to a Ni-NTA agarose beads as described above however, no detergent was present in any of the buffers and all buffers contained 5 mM ATP. The beads were sequentially washed with two bed volumes of HNIGβA buffer (50 mM HEPES-KOH pH 7.4, 300 mM

NaCl, 5% glycerol, 10 mM imidazole, 5 mM β-mercaptoethanol, 5 mM ATP) supplemented with 0.5 M NaCl, 3 mM Mg^{2+}-ATP, 0.25 M Tris pH 7.5, and 35 mM imidazole. The protein was then eluted in buffer HNIGβA supplemented with 240 mM imidazole. The eluted protein was loaded onto an Superdex S200 10/300 GL column equilibrated in HKMA buffer (50 mM HEPES-KOH pH 7.4, 150 mM KCl, 10 mM $MgCl_2$, 0.5 mM ATP). GRP170-containing fractions were aliquotted and flash-frozen.

BiP

BiP and BiP variants were purified as previously described (Petrova et al., 2008; Preissler et al., 2015a). Briefly, His6-BiP (WT and variants) was expressed and purified from BL21 C3013 *E. coli* cells as described above for His6-Smt3-IRE1. Cells were lysed in TNGMTr buffer (50 mM Tris pH 7.4, 500 mM NaCl, 10% glycerol, 1 mM $MgCl_2$, 0.2% (v/v) Triton X-100, 20 mM imidazole) containing protease inhibitors and DnaseI as above. Prior to elution of BiP from the Ni-NTA agarose beads, the beads were washed with TNGMTr sequentially supplemented with 30 mM imidazole, 1% (v/v) Triton X-100, 1 M NaCl, 5 mM Mg2+-ATP and 0.5 M Tris–HCl pH 7.5. BiP was eluted in TNGMIz buffer (50 mM Tris–HCl pH 7.5, 500 mM NaCl, 1 mM MgCl2, 10% (v/v) glycerol, 250 mM imidazole) and dialysed against HKM buffer (50 mM HEPES-KOH pH 7.4, 150 mM KCl, 10 mM MgCl2).

BiP NBD was purified as described for His6-Smt3-IRE1. After elution the protein was concentrated and passed through a CentiPure gravity-desalting column into 50 mM HEPES pH 7.4, 150 mM KCl, 10% glycerol and 0.1 mM EDTA.

AMPylation of purified BiP proteins was performed as previously described with minor modifications (Preissler et al., 2015a). Purified BiP was incubated for 6 hours at 30°C with 0.25 mg bacterially expressed $FICD^{E234G}$ per 20 mg of BiP protein in presence of 3 mM ATP in buffer I [25 mM HEPES-KOH pH 7.4, 100 mM KCl, 10 mM $MgCl_2$, 1 mM $CaCl_2$, 0.1% (v/v) Triton X-100] followed by binding to Ni-NTA agarose beads for 1 hour at 25°C. The beads were washed with buffer I, and eluted in buffer I containing 350 mM imidazole for 45 minutes at 25°C. The eluate was desalted using a CentriPure column equilibrated in HKM buffer.

ERdj6 J-domain

The J-domain of ERdj6 (UK185) was purified as previously described (Petrova et al., 2008). Briefly, the J-domain of ERdj6 was expressed as a GST fusion protein and purified as described above for GST fusion proteins. The protein was eluted in buffer H [50 mM HEPES-KOH pH 7.4, 100 mM KCl, 4 mM $MgCl_2$, 1 mM $CaCl_2$, 0.1% (v/v) Triton X-100, 1 mM DTT, 10% (v/v) glycerol, 40 mM reduced glutathione] and dialysed over night against HKM buffer.

GADD34-bio

GADD34-bio (UK1920) was purified as previously described (Crespillo-Casado et al., 2017). Briefly, GADD34-bio (PPP1R15A) was purified as above for GST tagged proteins with the modification that the TNGMT lysis buffer was supplemented with 1 mM $MnCl_2$. Following the initial GST based purification and overnight incubation with TEV, cleaved GADD34 was bound to amylose beads (New England Biolabs) for 1–2 hr at 4°C. The amylose beads were washed with TNGMT and protein eluted with HEPES buffer (20 mM HEPES, 100 mM NaCl, 0.2 mM CaCl2, 0.2 mM ATP, 0.2 mM TCEP, 0.5 mM MnCl2, 100 µM PMSF, 20 mTIU/ ml aprotonin, 2 µM leupeptin, and 2 µg/ml pepstatin) and 10 mM maltose. The eluted GADD34 was then biotinylated using BirA (BirA UK1881 purified as described above for GST fusion proteins) in the presence of 2 mM $MgCl_2$, 2 mM ATP, 0.01% Triton X-100, excess biotin (1:2 molar ratio to substrate protein) and BirA ($1/20^{th}$ molar ratio of substrate protein). Following biotinylation GADD34-bio was passed through a CentiPure gravity-desalting column into HEPES buffer to remove excess of biotin that would interfere with the Bio-Layer Interferometry measurements.

Streptavidin pull-down assays

Assessing ERdj4 loading BiP onto IRE1

Schema shown in figure 3.02. 20 µl Dynabeads MyOne Streptavidin C1 (Thermo Fisher Scientific) per sample were used. Reactions were carried out in 150 mM KCl, 50 mM HEPES-KOH pH 7.4, 10 mM $MgCl_2$, 1 mM $CaCl_2$, 0.1% Triton X-100. Reactions contained 5 µM $IRE1^{LD}$-bio, 8 µM ERdj4 or variants, 30 µM BiP or variants, and 2 mM ATP. Reactions proceeded for 20

minutes at 30°C before quenching with an excess of ice cold 1 mM ADP and clarification at 21,130 *g* for 5 minutes, followed by the addition of magnetic beads to supernatant. Binding was carried out for 15 minutes before washes and elution in first 5 mM ATP followed by 1x SDS sample buffer. Pull-down experiments with the nucleotide binding domain of BiP were conducted similarly, but the ATP elution was skipped.

Assessing ERdj4's effect on IRE1 dimerisation

Schema shown in figure 3.10. Beads were first preloaded with $IRE1^{LD}$-bio and then washed extensively. Beads were then incubated with the reaction mixtures containing 0.5 µM $IRE1^{LD}$-TAM with 8 µM ERdj4 or variants, 30 µM BiP or variants, and 2 mM ATP. Where indicated, reactions also contained 1 µM GRP170. Reactions were quenched as described above. The beads were washed and the protein was eluted in SDS sample buffer.

Assessing the disruption of IRE1 dimers

Schema shown in figure 3.14. Beads were first pre-loaded with $IRE1^{LD}$-bio and then washed extensively. Beads were incubated with 0.5 µM $IRE1^{LD}$-TAM for one hour at 30˚ C, washed extensively, and then incubated with a solution of 30 µM BiP, 8 µM ERdj4, 1 µM GRP170, and 2 mM ATP at 30˚C for 15 minutes. The reaction was quenched as described above and the beads were washed and eluted in SDS sample buffer.

Size-exclusion chromatography

Sample were run through a SEC-3 300A, 4.6x300 mm column (Agilent 5190-2513) on an Agilent infinity HPLC system. Samples were run in HKM buffer (150 mM KCl, 50 mM HEPES-KOH pH 7.4, 10 mM $MgCl_2$). Reactions proceeded in 20 µl for 20 minutes at 30°C before clarification at 21,130 *g* for 5 minutes and subsequent injection.

Bio-Layer Interferometry experiments

Experiments were performed on an Octet RED96 (Pall ForteBio). Experiments were performed in HKMGTr buffer (50 mM HEPES-KOH pH 7.6, 150 mM KCl, 10 mM $MgCl_2$, 10% glycerol, 0.05% Triton X-100).

In the sequential dipping experiment (Figure 3.11), streptavidin biosensors were loaded with IRE1^{LD}-bio or GADD34-bio to approximately 1 nm shift, washed in buffer, and then sequentially dipped in wells containing 1.5 μM Smt3-ERdj4 or variants, 1 μM BiP with no nucleotide, 1μM BiP^{T229A} with 2 mM ATP, 1 μM BiP^{V461F} with 2 mM ATP, and 1 μM BiP. Data were decimated, background-subtracted, and normalised to the signal after the first wash step.
In the titration experiment (Figure 3.12), streptavidin biosensors were loaded with Smt3-ERdj4-bio to approximately 1 nm shift, washed in buffer, and then dipped in wells containing the indicated concentration of IRE1^{LD}. Data were decimated and normalised to the signal after the first wash step
In the sequential dipping experiment (Figure 3.13), streptavidin biosensors were loaded with IRE1^{LD}-bio to approximately 1 nm shift, washed in buffer, and then dipped in wells containing the indicated concentration of Smt3-ERdj4. Data were decimated, background subtracted, and normalised to the signal after the first wash step.
In the elution experiments (Figure 3.13), streptavidin biosensors were loaded with IRE1^{LD}-bio to a shift of approximately 7.5 nm. The biosensors were washed in buffer and then dipped in wells containing 1.2 μM Smt3-ERdj4. The biosensors were washed in buffer and then dipped in wells containing either: 6 μM BiP with no ATP, 6 μM BiP with 2 mM ATP, or 6 μM BiP^{V461F} with 2 mM ATP. The biosensors were then washed in buffer with 2 mM ATP and the protein eluted in SDS sample buffer.

In the sequential dipping and elution experiment (Figure 3.16), streptavidin biosensors were loaded with IRE1^{LD}-bio (UK2007) or IRE1$^{LD\ Q105C}$-bio (UK2045) to a shift of approximately 2.5 nm. The biosensors were washed in buffer and then dipped in wells containing 1.7 μM Smt3-ERdj4. The biosensors were washed in buffer and then dipped in wells containing: 6 μM BiP with 2 mM ATP, or just buffer. The biosensors were then washed in buffer with 2 mM ATP and the protein eluted in SDS sample buffer and ran on a non-reducing SDS-PAGE gel. The BLI data was decimated and normalised to the signal after the first wash step.

FRET equilibrium experiments

In figure 3.20 $IRE1^{LD}$-donor and $IRE1^{LD}$-acceptor were combined at a 1:2 ratio and incubated at room temperature in the dark for two hours. $IRE1^{LD}$-donor/acceptor (0.2 μM total) was combined with unlabelled $IRE1^{LD}$ at the specified concentration in HKMGTw buffer (50 mM HEPES-KOH pH 7.6, 150 mM KCl, 10 mM $MgCl_2$, 10% glycerol, 0.05% TWEEN 20) and incubated for 3 hours. The samples were transferred to a black low volume 384-well plate and donor fluorescence was recorded with a CLARIOstar platereader (BMG), exciting at 470-15 nm and reading emission at 524-20 nm. Alternatively, $IRE1^{LD}$-donor/acceptor was combined with BiP at the specified concentration in HKMGTw buffer and incubated for 24 hours. Fluorescence was recorded as described above. Fluorescence was normalised to that of $IRE1^{LD}$-donor/$IRE1^{LD}$ acceptor absent titrant.

FRET kinetic experiments

$IRE1^{LD}$-donor and $IRE1^{LD}$-acceptor were combined at a 1:2 ratio and incubated at room temperature in the dark for two hours. In figure 3.21-3.22 on a black low volume 384-well plate, BiP, Smt3-ERdj4-MBP, and $IRE1^{LD}$-donor/acceptor were combined in HKMGTw buffer. The concentrations used were 30 μM BiP variants, 2.5 μM ERdj4 variants, and 0.2 μM $IRE1^{LD}$-donor/acceptor. After incubation for 30 minutes, 2 mM ATP with an ATP regeneration system (8 mM phosphocreatine, 0.016 mg/ml creatine kinase) was added to initiate the reaction. In indicated wells, 1 μM GRP170 was added along with ATP and the regeneration system. In figure 3.23, 50 μM BiP, 2.5 μM Smt3-ERdj4-MBP, and 0.2 μM equilibrated $IRE1^{LD}$-donor/acceptor were combined in HKMGTw buffer. After incubation for 30 minutes, 2 mM ATP with the ATP regeneration system was added to initiate the reaction. At the indicated time, buffer, CH1 heptapeptide (HTFPAVL, a model BiP substrate) at the indicated concentration, and/or 2.5 μM ERdj6 J-domain was added. In all kinetic experiments, donor fluorescence was followed with a CLARIOstar plate reader (excitation: 470-15 nm / emission: 524-20 nm) recording fluorescence every 30 seconds. Fluorescence was normalised to the level at t=0.

Peptide binding anisotropy experiments

FAM labelled and unlabelled MPZN (LIRYCWLRRQAA) peptides (as described in Karagöz et al., 2017 were purchased from Genscript.

Anisotropy was measured using a CLARIOstar plate reader. Parallel and perpendicular fluorescence of the FAM fluorophore was measured using excitation at 496 nm and measuring emission at 519-550 nm.

FAM-MPZN was kept at 100 nM in reactions. The concentrations of IRE1 variants and unlabelled MPZN used are detailed in the figure legends. Components were mixed together in 25 µl and then 20 µl transferred to a black flat bottomed 384 well plate and incubated for 30 minutes prior to reading. Fluorescence readings were corrected by subtracting fluorescence from a well containing only buffer. The average of 6 readings (spaced at 30 s intervals) per well was taken as one repeat and the average of three independent repeats was used for the final data presented.

Anisotropy is calculated as: $(I_{para} - I_{perp})/(I_{para} + 2*I_{perp})$

The data in figure 5.01 was fit to the equation $r_{free} + (r_{max} - r_{free})[X]^h/([X]^h+K^h)$ where r_{free} is the anisotropy in the absence of protein, r_{max} is the theoretical maximal anisotropy, [X] is the protein concentration and h is the hill-coefficient.

References

Abravaya, Klara, Michael P. Myers, Shawn P. Murphy, and Richard I. Morimoto. 1992. “The Human Heat Shock Protein hsp70 Interacts with HSF, the Transcription Factor That Regulates Heat Shock Gene Expression.” *Genes & Development* 6 (7): 1153–64. doi:10.1101/gad.6.7.1153 Genes & Dev. 1992. 6: 1153-1164.

Adamson, Britt, Thomas M. Norman, Marco Jost, Min Y. Cho, James K. Nuñez, Yuwen Chen, Jacqueline E. Villalta, et al., 2016. “A Multiplexed Single-Cell CRISPR Screening Platform Enables Systematic Dissection of the Unfolded Protein Response.” *Cell* 167 (7): 1867–1882.e21. doi:10.1016/j.cell.2016.11.048.

Aragón, Tomás, Eelco van Anken, David Pincus, Iana M Serafimova, Alexei V Korennykh, Claudia a Rubio, and Peter Walter. 2009. “Messenger RNA Targeting to Endoplasmic Reticulum Stress Signalling Sites.” *Nature* 457 (7230): 736–40. doi:10.1038/nature07641.

Avezov, Edward, Benedict C.S. S Cross, Gabriele S. Kaminski Schierle, Mikael Winters, Heather P. Harding, Eduardo Pinho Melo, Clemens F. Kaminski, and David Ron. 2013. “Lifetime Imaging of a Fluorescent Protein Sensor Reveals Surprising Stability of ER Thiol Redox.” *The Journal of Cell Biology* 201 (2): 337–49. doi:10.1083/jcb.201211155.

Behnke, Julia, Matthias J. Feige, and Linda M. Hendershot. 2015. *BiP and Its Nucleotide Exchange Factors Grp170 and Sil1: Mechanisms of Action and Biological Functions*. *Journal of Molecular Biology*. Vol. 427. Academic Press. doi:10.1016/j.jmb.2015.02.011Review.

Bertelsen, E. B., L. Chang, J. E. Gestwicki, and E. R. P. Zuiderweg. 2009. “Solution Conformation of Wild-Type E. Coli Hsp70 (DnaK) Chaperone Complexed with ADP and Substrate.” *Proceedings of the National Academy of Sciences* 106 (21): 8471–76. doi:10.1073/pnas.0903503106.

Bertolotti, A, Y Zhang, L M Hendershot, H P Harding, and D Ron. 2000. “Dynamic Interaction of BiP and ER Stress Transducers in the Unfolded-Protein Response.” *Nature Cell Biology* 2 (6). Macmillan Magazines Ltd.: 326–32. doi:10.1038/35014014.

Blond-Elguindi, S, S E Cwirla, W J Dower, R J Lipshutz, S R Sprang, J F

Sambrook, and M J Gething. 1993. “Affinity Panning of a Library of Peptides Displayed on Bacteriophages Reveals the Binding Specificity of BiP.” *Cell* 75 (4): 717–28.

Brodsky, J L, J Goeckeler, and R Schekman. 1995. “BiP and Sec63p Are Required for Both Co- and Posttranslational Protein Translocation into the Yeast Endoplasmic Reticulum.” *Proceedings of the National Academy of Sciences of the United States of America* 92 (21): 9643–46.

Calfon, Marcella, Huiqing Zeng, Fumihiko Urano, Jeffery H Till, Stevan R Hubbard, Heather P Harding, Scott G Clark, and David Ron. 2002. “IRE1 Couples Endoplasmic Reticulum Load to Secretory Capacity by Processing the XBP-1 mRNA.” *Nature* 415 (6867): 92–96. doi:10.1038/415092a.

Carla Famá, M, David Raden, Nicolás Zacchi, Darío R Lemos, Anne S Robinson, and Susana Silberstein. 2007. “The Saccharomyces Cerevisiae YFR041C/ERJ5 Gene Encoding a Type I Membrane Protein with a J Domain Is Required to Preserve the Folding Capacity of the Endoplasmic Reticulum.” *Biochimica et Biophysica Acta* 1773 (2). NIH Public Access: 232–42. doi:10.1016/j.bbamcr.2006.10.011.

Carrara, M., F. Prischi, P. R. Nowak, and M. M. Ali. 2015. “Crystal Structures Reveal Transient PERK Luminal Domain Tetramerization in Endoplasmic Reticulum Stress Signaling.” *The EMBO Journal* 34 (11). EMBO Press: 1589–1600. doi:10.15252/embj.201489183.

Carrara, Marta, Filippo Prischi, Piotr R Nowak, Megan C Kopp, and Maruf Mu Ali. 2015. “Noncanonical Binding of BiP ATPase Domain to Ire1 and Perk Is Dissociated by Unfolded Protein CH1 to Initiate ER Stress Signaling.” *eLife* 4 (January). eLife Sciences Publications Limited: e03522. doi:10.7554/eLife.03522.

Chang, S C, A E Erwin, and A S Lee. 1989. “Glucose-Regulated Protein (GRP94 and GRP78) Genes Share Common Regulatory Domains and Are Coordinately Regulated by Common Trans-Acting Factors.” *Molecular and Cellular Biology* 9 (5): 2153–62.

Chen, L, S Xu, L Liu, X Wen, Y Xu, J Chen, and J Teng. 2014. “Cab45S

Inhibits the ER Stress-Induced IRE1-JNK Pathway and Apoptosis via GRP78/BiP." *Cell Death & Disease* 5 (5). Nature Publishing Group: e1219. doi:10.1038/cddis.2014.193.

Chiang, Wei-Chieh, Nobuhiko Hiramatsu, Carissa Messah, Heike Kroeger, and Jonathan H Lin. 2012. "Selective Activation of ATF6 and PERK Endoplasmic Reticulum Stress Signaling Pathways Prevent Mutant Rhodopsin Accumulation." *Investigative Ophthalmology & Visual Science* 53 (11). Association for Research in Vision and Ophthalmology: 7159–66. doi:10.1167/iovs.12-10222.

Cohen, Nir, Michal Breker, Anush Bakunts, Kristina Pesek, Ainara Chas, Josepmaria Argemí, Andrea Orsi, et al., 2017. "Iron Affects Ire1 Clustering Propensity and the Amplitude of Endoplasmic Reticulum Stress Signaling." *Journal of Cell Science*.

Cox, J S, and P Walter. 1996. "A Novel Mechanism for Regulating Activity of a Transcription Factor That Controls the Unfolded Protein Response." *Cell* 87 (3): 391–404.

Cox, Jeffery S., Caroline E. Shamu, and Peter Walter. 1993. "Transcriptional Induction of Genes Encoding Endoplasmic Reticulum Resident Proteins Requires a Transmembrane Protein Kinase." *Cell* 73 (6): 1197–1206. doi:10.1016/0092-8674(93)90648-A.

Craig, Elizabeth A., and Jaroslaw Marszalek. 2017. "How Do J-Proteins Get Hsp70 to Do So Many Different Things?" *Trends in Biochemical Sciences*. doi:10.1016/j.tibs.2017.02.007.

Craven, R A, M Egerton, and C J Stirling. 1996. "A Novel Hsp70 of the Yeast ER Lumen Is Required for the Efficient Translocation of a Number of Protein Precursors." *The EMBO Journal* 15 (11): 2640–50.

Credle, Joel J, Janet S Finer-Moore, Feroz R Papa, Robert M Stroud, and Peter Walter. 2005. "On the Mechanism of Sensing Unfolded Protein in the Endoplasmic Reticulum." *Proceedings of the National Academy of Sciences of the United States of America* 102 (52): 18773–84. doi:10.1073/pnas.0509487102.

Crespillo-Casado, Ana, Joseph E Chambers, Peter M Fischer, Stefan J Marciniak, and David Ron. 2017. “PPP1R15A-Mediated Dephosphorylation of eIF2a Is Unaffected by sephin1 or Guanabenz.” *eLife* 6 (April). eLife Sciences Publications Limited: 6681–88. doi:10.7554/eLife.26109.

Cross, Benedict C S, Peter J Bond, Pawel G Sadowski, Babal Kant Jha, Jaroslav Zak, Jonathan M Goodman, Robert H Silverman, et al., 2012. “The Molecular Basis for Selective Inhibition of Unconventional mRNA Splicing by an IRE1-Binding Small Molecule.” *Proceedings of the National Academy of Sciences of the United States of America* 109 (15): E869-78. doi:10.1073/pnas.1115623109.

Daugaard, Mads, Mikkel Rohde, and Marja Jäättelä. 2007. “The Heat Shock Protein 70 Family: Highly Homologous Proteins with Overlapping and Distinct Functions.” *FEBS Letters* 581 (19): 3702–10. doi:10.1016/j.febslet.2007.05.039.

De Los Rios, Paolo, and Alessandro Barducci. 2014. “Hsp70 Chaperones Are Non-Equilibrium Machines That Achieve Ultra-Affinity by Energy Consumption.” *eLife* 3 (May). eLife Sciences Publications, Ltd: e02218. doi:10.7554/ELIFE.02218.

Dong, Mei, James P. Bridges, Karen Apsley, Yan Xu, and Timothy E. Weaver. 2008. “ERdj4 and ERdj5 Are Required for Endoplasmic Reticulum-Associated Protein Degradation of Misfolded Surfactant Protein C.” *Molecular Biology of the Cell* 19 (6): 2620–30. doi:10.1091/mbc.E07-07-0674.

Dorner, a J, L C Wasley, and R J Kaufman. 1992. “Overexpression of GRP78 Mitigates Stress Induction of Glucose Regulated Proteins and Blocks Secretion of Selective Proteins in Chinese Hamster Ovary Cells.” *The EMBO Journal* 11 (4): 1563–71.

Dudek, J., J. Benedix, S. Cappel, M. Greiner, C. Jalal, L. Müller, and R. Zimmermann. 2009. “Functions and Pathologies of BiP and Its Interaction Partners.” *Cellular and Molecular Life Sciences* 66 (9). Birkhäuser-Verlag: 1556–69. doi:10.1007/s00018-009-8745-y.

Dudek, Johanna, Stefan Pfeffer, Po-Hsien Lee, Martin Jung, Adolfo Cavalié, Volkhard Helms, Friedrich Förster, and Richard Zimmermann. 2015. “Protein Transport into the Human Endoplasmic Reticulum.” *Journal of Molecular Biology* 427 (6): 1159–75. doi:10.1016/j.jmb.2014.06.011.

Eletto, Davide Daniela, Devin Dersh, Tali Gidalevitz, and Yair Argon. 2014. “Protein Disulfide Isomerase A6 Controls the Decay of IRE1α Signaling via Disulfide-Dependent Association.” *Molecular Cell* 53 (4). Elsevier Inc.: 562–76. doi:10.1016/j.molcel.2014.01.004.

Flynn, G C, J Pohl, M T Flocco, and J E Rothman. 1991. “Peptide-Binding Specificity of the Molecular Chaperone BiP.” *Nature* 353 (6346): 726–30. doi:10.1038/353726a0.

Freiden, P J, J R Gaut, and L M Hendershot. 1992. “Interconversion of Three Differentially Modified and Assembled Forms of BiP.” *The EMBO Journal* 11 (1): 63–70.

Fritz, Jill M, and Timothy E Weaver. 2014. “The BiP Cochaperone ERdj4 Is Required for B Cell Development and Function.” *PloS One* 9 (9). Public Library of Science: e107473. doi:10.1371/journal.pone.0107473.

Gamer, J, G Multhaup, T Tomoyasu, J S McCarty, S Rüdiger, H J Schönfeld, C Schirra, H Bujard, and B Bukau. 1996. “A Cycle of Binding and Release of the DnaK, DnaJ and GrpE Chaperones Regulates Activity of the Escherichia Coli Heat Shock Transcription Factor sigma32.” *The EMBO Journal* 15 (3). European Molecular Biology Organization: 607–17.

Gardner, Brooke M, and Peter Walter. 2011. “Unfolded Proteins Are Ire1-Activating Ligands That Directly Induce the Unfolded Protein Response.” *Science (New York, N.Y.)* 333 (6051): 1891–94. doi:10.1126/science.1209126.

Gething, Mary-Jane J. 1999. “Role and Regulation of the ER Chaperone BiP.” *Seminars in Cell & Developmental Biology* 10 (5): 465–72. doi:10.1006/scdb.1999.0318.

Ghaemmaghami, Sina, Won-Ki Huh, Kiowa Bower, Russell W. Howson, Archana Belle, Noah Dephoure, Erin K. O’Shea, and Jonathan S.

Weissman. 2003. “Global Analysis of Protein Expression in Yeast.” *Nature* 425 (6959). Nature Publishing Group: 737–41. doi:10.1038/nature02046.

Gupta, Sanjeev, Ayswaria Deepti, Shane Deegan, Fernanda Lisbona, Claudio Hetz, and Afshin Samali. 2010. “HSP72 Protects Cells from ER Stress-Induced Apoptosis via Enhancement of IRE1alpha-XBP1 Signaling through a Physical Interaction.” *PLoS Biology* 8 (7): e1000410. doi:10.1371/journal.pbio.1000410.

Halbleib, Kristina, Kristina Pesek, Roberto Covino, Harald F. Hofbauer, Dorith Wunnicke, Inga Hänelt, Gerhard Hummer, and Robert Ernst. 2017. “Activation of the Unfolded Protein Response by Lipid Bilayer Stress.” *Molecular Cell*, July. doi:10.1016/j.molcel.2017.06.012.

Harding, Heather P, Yuhong Zhang, Huiquing Zeng, Isabel Novoa, Phoebe D Lu, Marcella Calfon, Navid Sadri, et al., 2003. “An Integrated Stress Response Regulates Amino Acid Metabolism and Resistance to Oxidative Stress.” *Molecular Cell* 11 (3): 619–33.

Hardwick, K G, M J Lewis, J Semenza, N Dean, and H R Pelham. 1990. “ERD1, a Yeast Gene Required for the Retention of Luminal Endoplasmic Reticulum Proteins, Affects Glycoprotein Processing in the Golgi Apparatus.” *EMBO J* 9 (3). European Molecular Biology Organization: 623–30.

Haze, K, H Yoshida, H Yanagi, T Yura, and K Mori. 1999. “Mammalian Transcription Factor ATF6 Is Synthesized as a Transmembrane Protein and Activated by Proteolysis in Response to Endoplasmic Reticulum Stress.” *Molecular Biology of the Cell* 10 (11): 3787–99.

Hetz, Claudio, Eric Chevet, and Scott A Oakes. 2015. “Proteostasis Control by the Unfolded Protein Response.” *Nature Cell Biology*. NIH Public Access. doi:10.1038/ncb3184.

Hollien, Julie, and Jonathan S Weissman. 2006. “Decay of Endoplasmic Reticulum-Localized mRNAs during the Unfolded Protein Response.” *Science (New York, N.Y.)* 313 (5783): 104–7. doi:10.1126/science.1129631.

Hou, Nicole S, Aljona Gutschmidt, Daniel Y Choi, Keouna Pather, Xun Shi, Jennifer L Watts, Thorsten Hoppe, and Stefan Taubert. 2014. “Activation of the Endoplasmic Reticulum Unfolded Protein Response by Lipid Disequilibrium without Disturbed Proteostasis in Vivo.” *Proceedings of the National Academy of Sciences of the United States of America* 111 (22): E2271-80. doi:10.1073/pnas.1318262111.

Imagawa, Yusuke, Akira Hosoda, Shin-ichi Sasaka, Akio Tsuru, and Kenji Kohno. 2008. “RNase Domains Determine the Functional Difference between IRE1α and IRE1β.” *FEBS Letters* 582 (5): 656–60. doi:10.1016/j.febslet.2008.01.038.

Ishiwata-Kimata, Yuki, Thanyarat Promlek, Kenji Kohno, and Yukio Kimata. 2013. “BiP-Bound and Nonclustered Mode of Ire1 Evokes a Weak but Sustained Unfolded Protein Response.” *Genes to Cells : Devoted to Molecular & Cellular Mechanisms* 18 (4): 288–301. doi:10.1111/gtc.12035.

Iwawaki, Takao, Ryoko Akai, and Kenji Kohno. 2010. “IRE1?? Disruption Causes Histological Abnormality of Exocrine Tissues, Increase of Blood Glucose Level, and Decrease of Serum Immunoglobulin Level.” *PLoS ONE* 5 (9). Public Library of Science: e13052. doi:10.1371/journal.pone.0013052.

Iwawaki, Takao, Ryoko Akai, Kenji Kohno, and Masayuki Miura. 2004. “A Transgenic Mouse Model for Monitoring Endoplasmic Reticulum Stress.” *Nature Medicine* 10 (1): 98–102. doi:10.1038/nm970.

Iwawaki, Takao, Akira Hosoda, Tetsuo Okuda, Yusuke Kamigori, Chizumi Nomura-Furuwatari, Yukio Kimata, Akio Tsuru, and Kenji Kohno. 2001. “Translational Control by the ER Transmembrane Kinase/ribonuclease IRE1 under ER Stress.” *Nature Cell Biology* 3 (2). Nature Publishing Group: 158–64. doi:10.1038/35055065.

Jurkin, Jennifer, Theresa Henkel, Anne Færch Nielsen, Martina Minnich, Johannes Popow, Therese Kaufmann, Katrin Heindl, Thomas Hoffmann, Meinrad Busslinger, and Javier Martinez. 2014. “The Mammalian tRNA Ligase Complex Mediates Splicing of XBP1 mRNA and Controls Antibody

Secretion in Plasma Cells." *The EMBO Journal*, November. doi:10.15252/embj.201490332.

Kampinga, Harm H., and Elizabeth A. Craig. 2010. "The HSP70 Chaperone Machinery: J Proteins as Drivers of Functional Specificity." *Nature Reviews. Molecular Cell Biology* 11 (8). Nature Publishing Group, a division of Macmillan Publishers Limited. All Rights Reserved.: 579–92. doi:10.1038/nrm2941.

Karagöz, Gülsün Elif, Diego Acosta-Alvear, Hieu T Nguyen, Crystal P Lee, Feixia Chu, and Peter Walter. 2017. "An Unfolded Protein-Induced Conformational Switch Activates Mammalian IRE1." *eLife* 6 (October). eLife Sciences Publications Limited: e30700. doi:10.7554/eLife.30700.

Kassenbrock, C K, and R B Kelly. 1989. "Interaction of Heavy Chain Binding Protein (BiP/GRP78) with Adenine Nucleotides." *The EMBO Journal* 8 (5): 1461–67.

Kato, H, S Nakajima, Y Saito, S Takahashi, R Katoh, and M Kitamura. 2012. "mTORC1 Serves ER Stress-Triggered Apoptosis via Selective Activation of the IRE1-JNK Pathway." *Cell Death and Differentiation* 19 (2). Macmillan Publishers Limited: 310–20. doi:10.1038/cdd.2011.98.

Kim, Min-Sik, Sneha M Pinto, Derese Getnet, Raja Sekhar Nirujogi, Srikanth S Manda, Raghothama Chaerkady, Anil K Madugundu, et al., 2014. "A Draft Map of the Human Proteome." *Nature* 509 (7502): 575–81. doi:10.1038/nature13302.

Kimata, Yukio, Yuki Ishiwata-Kimata, Tatsuhiko Ito, Aiko Hirata, Tomohide Suzuki, Daisuke Oikawa, Masato Takeuchi, and Kenji Kohno. 2007. "Two Regulatory Steps of ER-Stress Sensor Ire1 Involving Its Cluster Formation and Interaction with Unfolded Proteins." *The Journal of Cell Biology* 179 (1). The Rockefeller University Press: 75–86. doi:10.1083/jcb.200704166.

Kimata, Yukio, Yuki I Kimata, Yusuke Shimizu, Hiroshi Abe, Ileana C Farcasanu, Masato Takeuchi, Mark D Rose, and Kenji Kohno. 2003. "Genetic Evidence for a Role of BiP / Kar2 That Regulates Ire1 in Response to Accumulation of Unfolded Proteins." *Molecular Biology of*

the Cell 14 (June): 2559–69. doi:10.1091/mbc.E02.

Kimata, Yukio, Daisuke Oikawa, Yusuke Shimizu, Yuki Ishiwata-Kimata, and Kenji Kohno. 2004. “A Role for BiP as an Adjustor for the Endoplasmic Reticulum Stress-Sensing Protein Ire1.” *The Journal of Cell Biology* 167 (3): 445–56. doi:10.1083/jcb.200405153.

Kinoshita, Eiji, Emiko Kinoshita-Kikuta, and Tohru Koike. 2009. “Separation and Detection of Large Phosphoproteins Using Phos-Tag SDS-PAGE.” *Nature Protocols* 4 (10): 1513–21. doi:10.1038/nprot.2009.154.

Kitai, Yuto, Hiroyuki Ariyama, Nozomu Kono, Daisuke Oikawa, Takao Iwawaki, and Hiroyuki Arai. 2013. “Membrane Lipid Saturation Activates IRE1α without Inducing Clustering.” *Genes to Cells : Devoted to Molecular & Cellular Mechanisms* 18 (9): 798–809. doi:10.1111/gtc.12074.

Kityk, Roman, Jürgen Kopp, and Matthias P Mayer. 2017. “Molecular Mechanism of J-Domain-Triggered ATP Hydrolysis by Hsp70 Chaperones.” *Molecular Cell* 0 (0). Elsevier. doi:10.1016/j.molcel.2017.12.003.

Kityk, Roman, Jürgen Kopp, Irmgard Sinning, and Matthias P. Mayer. 2012. “Structure and Dynamics of the ATP-Bound Open Conformation of Hsp70 Chaperones.” *Molecular Cell* 48 (6). Cell Press: 863–74. doi:10.1016/j.molcel.2012.09.023.

Kono, N., N. Amin-Wetzel, and D. Ron. 2017. “Generic Membrane-Spanning Features Endow IRE1α with Responsiveness to Membrane Aberrancy.” *Molecular Biology of the Cell* 28 (17). doi:10.1091/mbc.E17-03-0144.

Kono, Nozomu, Niko Amin-Wetzel, and David Ron. 2017. “Generic Membrane-Spanning Features Endow IRE1α with Responsiveness to Membrane Aberrancy.” *Molecular Biology of the Cell* 28 (17). American Society for Cell Biology: 2318–32. doi:10.1091/mbc.E17-03-0144.

Kopp, Megan C, Piotr R Nowak, Natacha Larburu, Christopher J Adams, and Maruf MU Ali. 2018. “In Vitro FRET Analysis of IRE1 and BiP Association and Dissociation upon Endoplasmic Reticulum Stress.” *eLife* 7 (January). eLife Sciences Publications Limited: e30257. doi:10.7554/eLife.30257.

Korennykh, Alexei, and Peter Walter. 2012. “Structural Basis of the Unfolded Protein Response.” *Annual Review of Cell and Developmental Biology* 28 (1). Annual Reviews : 251–77. doi:10.1146/annurev-cellbio-101011-155826.

Korennykh, Alexei V, Pascal F Egea, Andrei a Korostelev, Janet Finer-Moore, Chao Zhang, Kevan M Shokat, Robert M Stroud, and Peter Walter. 2009. “The Unfolded Protein Response Signals through High-Order Assembly of Ire1.” *Nature* 457 (7230). Nature Publishing Group: 687–93. doi:10.1038/nature07661.

Korennykh, Alexei V, Andrei a Korostelev, Pascal F Egea, Janet Finer-Moore, Robert M Stroud, Chao Zhang, Kevan M Shokat, and Peter Walter. 2011. “Structural and Functional Basis for RNA Cleavage by Ire1.” *BMC Biology* 9 (1). BioMed Central Ltd: 47. doi:10.1186/1741-7007-9-47.

Kozutsumi, Y, M Segal, K Normington, M J Gething, and J Sambrook. 1988. “The Presence of Malfolded Proteins in the Endoplasmic Reticulum Signals the Induction of Glucose-Regulated Proteins.” *Nature*. doi:10.1038/332462a0.

Laufen, T, M P Mayer, C Beisel, D Klostermeier, A Mogk, J Reinstein, and B Bukau. 1999. “Mechanism of Regulation of hsp70 Chaperones by DnaJ Cochaperones.” *Proceedings of the National Academy of Sciences of the United States of America* 96 (10): 5452–57.

Le Gall, S., Andrea Neuhof, and Tom Rapoport. 2003. “The Endoplasmic Reticulum Membrane Is Permeable to Small Molecules.” *Molecular Biology of the Cell* 15 (2): 447–55. doi:10.1091/mbc.E03-05-0325.

Lee, A.-H. Ann-Hwee, Neal N Iwakoshi, and Laurie H Glimcher. 2003. “XBP-1 Regulates a Subset of Endoplasmic Reticulum Resident Chaperone Genes in the Unfolded Protein Response.” *Molecular and Cellular Biology* 23 (21). American Society for Microbiology: 7448–59. doi:10.1128/MCB.23.21.7448-7459.2003.

Lee, Albert, Anthony K Henras, and Guillaume Chanfreau. 2005. “Multiple RNA Surveillance Pathways Limit Aberrant Expression of Iron Uptake mRNAs and Prevent Iron Toxicity in S. Cerevisiae.” *Molecular Cell* 19 (1):

39–51. doi:10.1016/j.molcel.2005.05.021.

Lee, Kenneth P.K., Madhusudan Dey, Dante Neculai, Chune Cao, Thomas E. Dever, and Frank Sicheri. 2008. “Structure of the Dual Enzyme Ire1 Reveals the Basis for Catalysis and Regulation in Nonconventional RNA Splicing.” *Cell* 132 (1): 89–100. doi:10.1016/j.cell.2007.10.057.

Li, Han, Alexei V Korennykh, Shannon L Behrman, and Peter Walter. 2010. “Mammalian Endoplasmic Reticulum Stress Sensor IRE1 Signals by Dynamic Clustering.” *Proceedings of the National Academy of Sciences of the United States of America* 107 (37): 16113–18. doi:10.1073/pnas.1010580107.

Liberek, K, J Marszalek, D Ang, C Georgopoulos, and M Zylicz. 1991. “Escherichia Coli DnaJ and GrpE Heat Shock Proteins Jointly Stimulate ATPase Activity of DnaK.” *Proceedings of the National Academy of Sciences of the United States of America* 88 (7). National Academy of Sciences: 2874–78.

Liu, C Y, M Schröder, and R J Kaufman. 2000. “Ligand-Independent Dimerization Activates the Stress Response Kinases IRE1 and PERK in the Lumen of the Endoplasmic Reticulum.” *The Journal of Biological Chemistry* 275 (32): 24881–85. doi:10.1074/jbc.M004454200.

Liu, Chuan Yin, Hetty N Wong, Joseph A Schauerte, and Randal J Kaufman. 2002. “The Protein Kinase/endoribonuclease IRE1alpha That Signals the Unfolded Protein Response Has a Luminal N-Terminal Ligand-Independent Dimerization Domain.” *The Journal of Biological Chemistry* 277 (21): 18346–56. doi:10.1074/jbc.M112454200.

Liu, Chuan Yin, Zhaohui Xu, and Randal J Kaufman. 2003. “Structure and Intermolecular Interactions of the Luminal Dimerization Domain of Human IRE1alpha.” *The Journal of Biological Chemistry* 278 (20): 17680–87. doi:10.1074/jbc.M300418200.

Lu, Yanyan, Feng-Xia Liang, and Xiaozhong Wang. 2014. “A Synthetic Biology Approach Identifies the Mammalian UPR RNA Ligase RtcB.” *Molecular Cell* 55 (5). NIH Public Access: 758–70. doi:10.1016/j.molcel.2014.06.032.

Lyman, S K, and R Schekman. 1995. “Interaction between BiP and Sec63p Is Required for the Completion of Protein Translocation into the ER of Saccharomyces Cerevisiae.” *The Journal of Cell Biology* 131 (5): 1163–71.

Ma, Kun, Krishna M Vattem, and Ronald C Wek. 2002. “Dimerization and Release of Molecular Chaperone Inhibition Facilitate Activation of Eukaryotic Initiation Factor-2 Kinase in Response to Endoplasmic Reticulum Stress.” *The Journal of Biological Chemistry* 277 (21): 18728–35. doi:10.1074/jbc.M200903200.

Maguire, Jean Ann, Surafel Mulugeta, and Michael F Beers. 2012. “Multiple Ways to Die: Delineation of the Unfolded Protein Response and Apoptosis Induced by Surfactant Protein C BRICHOS Mutants.” *The International Journal of Biochemistry & Cell Biology* 44 (1). NIH Public Access: 101–12. doi:10.1016/j.biocel.2011.10.003.

Marcinowski, Moritz, Matthias Höller, Matthias J Feige, Danae Baerend, Don C Lamb, and Johannes Buchner. 2011. “Substrate Discrimination of the Chaperone BiP by Autonomous and Cochaperone-Regulated Conformational Transitions.” *Nature Structural & Molecular Biology* 18 (2). Nature Publishing Group: 150–58. doi:10.1038/nsmb.1970.

Mathuranyanon, Rubwad, Tomoko Tsukamoto, Asumi Takeuchi, Yuki Ishiwata-Kimata, Yuichi Tsuchiya, Kenji Kohno, and Yukio Kimata. 2015. “Tight Regulation of the Unfolded Protein Sensor Ire1 by Its Intramolecularly Antagonizing Subdomain.” *Journal of Cell Science* 128 (9): 1762–72. doi:10.1242/jcs.164111.

Matlack, K E, B Misselwitz, K Plath, and T A Rapoport. 1999. “BiP Acts as a Molecular Ratchet during Posttranslational Transport of Prepro-Alpha Factor across the ER Membrane.” *Cell* 97 (5): 553–64.

Mayer, Marcus, Jochen Reinstein, and Johannes Buchner. 2003. “Modulation of the ATPase Cycle of BiP by Peptides and Proteins.” *Journal of Molecular Biology* 330 (1): 137–44.

Mayer, Matthias P. 2013. “Hsp70 Chaperone Dynamics and Molecular Mechanism.” *Trends in Biochemical Sciences*. Elsevier Current Trends.

doi:10.1016/j.tibs.2013.08.001.

McCarty, J S, and G C Walker. 1991. “DnaK as a Thermometer: Threonine-199 Is Site of Autophosphorylation and Is Critical for ATPase Activity.” *Proceedings of the National Academy of Sciences of the United States of America* 88 (21): 9513–17.

Misselwitz, Benjamin, Oliver Staeck, and Tom A Rapoport. 1998. “J Proteins Catalytically Activate Hsp70 Molecules to Trap a Wide Range of Peptide Sequences.” *Molecular Cell* 2 (5): 593–603. doi:10.1016/S1097-2765(00)80158-6.

Mori, Kazutoshi, Wenzhen Ma, M J Gething, and J Sambrook. 1993. “A Transmembrane Protein with a cdc2+/CDC28-Related Kinase Activity Is Required for Signaling from the ER to the Nucleus.” *Cell* 74 (4): 743–56. doi:10.1016/0092-8674(93)90521-Q.

Nakamura, Daisuke, Akio Tsuru, Kentaro Ikegami, Yusuke Imagawa, Naoko Fujimoto, and Kenji Kohno. 2011. “Mammalian ER Stress Sensor IRE1β Specifically down-Regulates the Synthesis of Secretory Pathway Proteins.” *FEBS Letters* 585 (1): 133–38. doi:10.1016/j.febslet.2010.12.002.

Nguyen, Hang, and Bruce D. Uhal. 2016. “The Unfolded Protein Response Controls ER Stress-Induced Apoptosis of Lung Epithelial Cells through Angiotensin Generation.” *American Journal of Physiology - Lung Cellular and Molecular Physiology* 311 (5).

Nikawa, Jun-Ichi, and Satoshi Yamashita. 1992. “IRE1 Encodes a Putative Protein Kinase Containing a Membrane-Spanning Domain and Is Required for Inositol Phototrophy in Saccharomyces Cerevisiae.” *Molecular Microbiology* 6 (11): 1441–46. doi:10.1111/j.1365-2958.1992.tb00864.x.

Oikawa, Daisuke, Yukio Kimata, and Kenji Kohno. 2007. “Self-Association and BiP Dissociation Are Not Sufficient for Activation of the ER Stress Sensor Ire1.” *Journal of Cell Science* 120 (Pt 9): 1681–88. doi:10.1242/jcs.002808.

Oikawa, Daisuke, Yukio Kimata, Kenji Kohno, and Takao Iwawaki. 2009. "Activation of Mammalian IRE1alpha upon ER Stress Depends on Dissociation of BiP rather than on Direct Interaction with Unfolded Proteins." *Experimental Cell Research* 315 (15): 2496–2504. doi:10.1016/j.yexcr.2009.06.009.

Oikawa, Daisuke, Akira Kitamura, Masataka Kinjo, and Takao Iwawaki. 2012. "Direct Association of Unfolded Proteins with Mammalian ER Stress Sensor, IRE1β." Edited by F. Gisou van der Goot. *PloS One* 7 (12). Public Library of Science: e51290. doi:10.1371/journal.pone.0051290.

Oikawa, D, Y Kimata, M Takeuchi, and K Kohno. 2005. "An Essential Dimer-Forming Subregion of the Endoplasmic Reticulum Stress Sensor Ire1." *Biochemical and Biophysical Research Communications* 391 (October). Portland Press Ltd.: 135–42.

Okamura, K, Y Kimata, H Higashio, A Tsuru, and K Kohno. 2000. "Dissociation of Kar2p/BiP from an ER Sensory Molecule, Ire1p, Triggers the Unfolded Protein Response in Yeast." *Biochemical and Biophysical Research Communications* 279 (2): 445–50. doi:10.1006/bbrc.2000.3987.

Otero, Joel H, Beáta Lizák, and Linda M Hendershot. 2010. "Life and Death of a BiP Substrate." *Seminars in Cell & Developmental Biology* 21 (5): 472–78. doi:10.1016/j.semcdb.2009.12.008.

Petrova, Kseniya, Seiichi Oyadomari, Linda M Hendershot, and David Ron. 2008. "Regulated Association of Misfolded Endoplasmic Reticulum Lumenal Proteins with P58/DNAJc3." *The EMBO Journal* 27 (21). European Molecular Biology Organization: 2862–72. doi:10.1038/emboj.2008.199.

Pincus, David, Michael W Chevalier, Tomás Aragón, Eelco van Anken, Simon E Vidal, Hana El-Samad, and Peter Walter. 2010. "BiP Binding to the ER-Stress Sensor Ire1 Tunes the Homeostatic Behavior of the Unfolded Protein Response." *PLoS Biology* 8 (7): e1000415. doi:10.1371/journal.pbio.1000415.

Plumb, Rachel, Zai-Rong Zhang, Suhila Appathurai, and Malaiyalam Mariappan. 2015. "A Functional Link between the Co-Translational

Protein Translocation Pathway and the UPR." *eLife* 4 (May). eLife Sciences Publications Limited: e07426. doi:10.7554/eLife.07426.

Preissler, Steffen, Joseph E. Chambers, Ana Crespillo-Casado, Edward Avezov, Elena Miranda, Juan Perez, Linda M. Hendershot, Heather P. Harding, and David Ron. 2015. "Physiological Modulation of BiP Activity by Trans -Protomer Engagement of the Interdomain Linker." *eLife* 4 (OCTOBER2015). doi:10.7554/eLife.08961.

Preissler, Steffen, Cláudia Rato, Ruming Chen, Robin Antrobus, Shujing Ding, Ian M. Fearnley, and David Ron. 2015. "AMPylation Matches BiP Activity to Client Protein Load in the Endoplasmic Reticulum." *eLife* 4 (DECEMBER2015): e12621. doi:10.7554/eLife.12621.

Promlek, Thanyarat, Yuki Ishiwata-Kimata, Masahiro Shido, Mitsuru Sakuramoto, Kenji Kohno, and Yukio Kimata. 2011. "Membrane Aberrancy and Unfolded Proteins Activate the Endoplasmic Reticulum Stress Sensor Ire1 in Different Ways." *Molecular Biology of the Cell* 22 (18): 3520–32. doi:10.1091/mbc.E11-04-0295.

Ran, Ann F, Patrick D Hsu, Jason Wright, Vineeta Agarwala, David A Scott, and Feng Zhang. 2013. "Genome Engineering Using the CRISPR-Cas9 System." *Nature Protocols* 8 (11): 2281–2308. doi:10.1038/nprot.2013.143.Genome.

Robblee, Megan M., Charles C. Kim, Jess Porter Abate, Martin Valdearcos, Karin L.M. Sandlund, Meera K. Shenoy, Romain Volmer, Takao Iwawaki, and Suneil K. Koliwad. 2016. "Saturated Fatty Acids Engage an IRE1α-Dependent Pathway to Activate the NLRP3 Inflammasome in Myeloid Cells." *Cell Reports* 14 (11): 2611–23. doi:10.1016/j.celrep.2016.02.053.

Rodriguez, Fernanda, Florence Arsène-Ploetze, Wolfgang Rist, Stefan Rüdiger, Jens Schneider-Mergener, Matthias P. Mayer, and Bernd Bukau. 2008. "Molecular Basis for Regulation of the Heat Shock Transcription Factor σ32 by the DnaK and DnaJ Chaperones." *Molecular Cell* 32 (3): 347–58. doi:10.1016/j.molcel.2008.09.016.

Ron, D, and J F Habener. 1992. "CHOP, a Novel Developmentally Regulated Nuclear Protein That Dimerizes with Transcription Factors C/EBP and

LAP and Functions as a Dominant-Negative Inhibitor of Gene Transcription." *Genes & Development* 6 (3): 439–53.

Ronda, Carlotta, Lasse Ebdrup Pedersen, Henning Gram Hansen, Thomas Beuchert Kallehauge, Michael J Betenbaugh, Alex Toftgaard Nielsen, and Helene Faustrup Kildegaard. 2014. "Accelerating Genome Editing in CHO Cells Using CRISPR Cas9 and CRISPy, a Web-Based Target Finding Tool." *Biotechnology and Bioengineering* 111 (8): 1604–16. doi:10.1002/bit.25233.

Rubio, Claudia, David Pincus, Alexei Korennykh, Sebastian Schuck, Hana El-Samad, and Peter Walter. 2011. "Homeostatic Adaptation to Endoplasmic Reticulum Stress Depends on Ire1 Kinase Activity." *The Journal of Cell Biology* 193 (1). The Rockefeller University Press: 171–84. doi:10.1083/jcb.201007077.

Rüdiger, S, A Buchberger, and B Bukau. 1997. "Interaction of Hsp70 Chaperones with Substrates." *Nature Structural Biology* 4 (5): 342–49.

Sagara, Y, and G Inesi. 1991. "Inhibition of the Sarcoplasmic Reticulum Ca2+ Transport ATPase by Thapsigargin at Subnanomolar Concentrations." *The Journal of Biological Chemistry* 266 (21): 13503–6.

Schneider, Markus, Mathias Rosam, Manuel Glaser, Atanas Patronov, Harpreet Shah, Katrin Christiane Back, Marina Angelika Daake, Johannes Buchner, and Iris Antes. 2016. "BiPPred: Combined Sequence- and Structure-Based Prediction of Peptide Binding to the Hsp70 Chaperone BiP." *Proteins: Structure, Function and Bioinformatics*, October. doi:10.1002/prot.25084.

Sekine, Yusuke, Alisa Zyryanova, Ana Crespillo-Casado, Niko Amin-Wetzel, Heather P. Harding, and David Ron. 2016. "Paradoxical Sensitivity to an Integrated Stress Response Blocking Mutation in Vanishing White Matter Cells." Edited by Eric Jan. *PLoS ONE* 11 (11). Cold Spring Harbor Laboratory Press: e0166278. doi:10.1371/journal.pone.0166278.

Shamu, C E, and P Walter. 1996. "Oligomerization and Phosphorylation of the Ire1p Kinase during Intracellular Signaling from the Endoplasmic Reticulum to the Nucleus." *The EMBO Journal* 15 (12): 3028–39.

Shen, Jingshi, Erik L. Snapp, Jennifer Lippincott-Schwartz, and Ron Prywes. 2005. “Stable Binding of ATF6 to BiP in the Endoplasmic Reticulum Stress Response.” *Molecular and Cellular Biology* 25 (3). American Society for Microbiology (ASM): 921–32. doi:10.1128/MCB.25.3.921-932.2005.

Shen, Xiaohua, Ronald E Ellis, Kenjiro Sakaki, and Randal J Kaufman. 2005. “Genetic Interactions due to Constitutive and Inducible Gene Regulation Mediated by the Unfolded Protein Response in C. Elegans.” *PLoS Genetics* 1 (3): e37. doi:10.1371/journal.pgen.0010037.

Shen, Y., and Linda M Hendershot. 2005. “ERdj3, a Stress-Inducible Endoplasmic Reticulum DnaJ Homologue, Serves as a CoFactor for BiP’s Interactions with Unfolded Substrates.” *Molecular Biology of the Cell* 16 (1): 40–50. doi:10.1091/mbc.E04-05-0434.

Shen, Ying, Laurent Meunier, and Linda M Hendershot. 2002. “Identification and Characterization of a Novel Endoplasmic Reticulum (ER) DnaJ Homologue, Which Stimulates ATPase Activity of BiP in Vitro and Is Induced by ER Stress.” *The Journal of Biological Chemistry* 277 (18): 15947–56. doi:10.1074/jbc.M112214200.

Shoulders, Matthew D., Lisa M. Ryno, Joseph C. Genereux, James J. Moresco, Patricia G. Tu, Chunlei Wu, John R. Yates, Andrew I. Su, Jeffery W. Kelly, and R. Luke Wiseman. 2013. “Stress-Independent Activation of XBP1s And/or ATF6 Reveals Three Functioanally Diverse ER Proteostasis Environments.” *Cell Reports* 3 (4). Elsevier: 1279–92. doi:10.1016/j.celrep.2013.03.024.

Sidrauski, Carmela, and Peter Walter. 1997. “The Transmembrane Kinase Ire1p Is a Site-Specific Endonuclease That Initiates mRNA Splicing in the Unfolded Protein Response.” *Cell* 90 (6): 1031–39. doi:10.1016/S0092-8674(00)80369-4.

Silberstein, S, G Schlenstedt, P A Silver, and R Gilmore. 1998. “A Role for the DnaJ Homologue Scj1p in Protein Folding in the Yeast Endoplasmic Reticulum.” *The Journal of Cell Biology* 143 (4). The Rockefeller University Press: 921–33.

Sou, Si Nga, Kristina M Ilieva, and Karen M Polizzi. 2012. “Binding of Human BiP to the ER Stress Transducers IRE1 and PERK Requires ATP.” *Biochemical and Biophysical Research Communications* 420 (2): 473–78. doi:10.1016/j.bbrc.2012.03.030.

Sriburi, Rungtawan, Suzanne Jackowski, Kazutoshi Mori, and Joseph W Brewer. 2004. “XBP1: A Link between the Unfolded Protein Response, Lipid Biosynthesis, and Biogenesis of the Endoplasmic Reticulum.” *The Journal of Cell Biology* 167 (1): 35–41. doi:10.1083/jcb.200406136.

Sundaram, Arunkumar, Rachel Plumb, Suhila Appathurai, and Malaiyalam Mariappan. 2017. “The Sec61 Translocon Limits IRE1α Signaling during the Unfolded Protein Response.” *eLife* 6 (May). eLife Sciences Publications Limited: e27187. doi:10.7554/eLife.27187.

Swain, Joanna F., Gizem Dinler, Renuka Sivendran, Diana L. Montgomery, Mathias Stotz, and Lila M. Gierasch. 2007. “Hsp70 Chaperone Ligands Control Domain Association via an Allosteric Mechanism Mediated by the Interdomain Linker.” *Molecular Cell* 26 (1). Cell Press: 27–39.

Taguchi, Yuki, Koichi Imaoka, Michiyo Kataoka, Akihiko Uda, Daiki Nakatsu, Sakuya Horii-Okazaki, Rina Kunishige, Fumi Kano, and Masayuki Murata. 2015. “Yip1A, a Novel Host Factor for the Activation of the IRE1 Pathway of the Unfolded Protein Response during Brucella Infection.” *PLoS Pathogens* 11 (3): e1004747. doi:10.1371/journal.ppat.1004747.

Takatsuki, A, K Kohno, and G Tamura. 1975. “Inhibition of Biosynthesis of Polyisoprenol Sugars in Chick Embryo Microsomes by Tunicamycin.” *Agric. Biol. Chem*, no. 39: 2089–91.

Tirasophon, W., a. a. Welihinda, and R. J. Kaufman. 1998. “A Stress Response Pathway from the Endoplasmic Reticulum to the Nucleus Requires a Novel Bifunctional Protein Kinase/endoribonuclease (Ire1p) in Mammalian Cells.” *Genes & Development* 12 (12): 1812–24. doi:10.1101/gad.12.12.1812.

Todd-Corlett, Alicia, Ellene Jones, Conrad Seghers, and Mary-Jane Gething. 2007. “Lobe IB of the ATPase Domain of Kar2p/BiP Interacts with Ire1p to Negatively Regulate the Unfolded Protein Response in Saccharomyces

Cerevisiae.” *Journal of Molecular Biology* 367 (3): 770–87. doi:10.1016/j.jmb.2007.01.009.

Tomoyasu, Toshifumi, Teru Ogura, Takashi Tatsuta, and Bernd Bukau. 1998. “Levels of DnaK and DnaJ Provide Tight Control of Heat Shock Gene Expression and Protein Repair in Escherichia Coli.” *Molecular Microbiology* 30 (3). Blackwell Science Ltd: 567–81. doi:10.1046/j.1365-2958.1998.01090.x.

Urano, F, X Wang, A Bertolotti, Y Zhang, P Chung, H P Harding, D Ron, Matthew M. LaVail, and Peter Walter. 2000. “Coupling of Stress in the ER to Activation of JNK Protein Kinases by Transmembrane Protein Kinase IRE1.” *Science (New York, N.Y.)* 287 (5453). American Association for the Advancement of Science: 664–66. doi:10.1126/cience.287.5453.664.

van Anken, Eelco, David Pincus, Scott Coyle, Tomás Aragón, Christof Osman, Federica Lari, Silvia Gómez Puerta, Alexei V Korennykh, and Peter Walter. 2014. “Specificity in Endoplasmic Reticulum-Stress Signaling in Yeast Entails a Step-Wise Engagement of HAC1 mRNA to Clusters of the Stress Sensor Ire1.” *eLife* 3 (December). eLife Sciences Publications Limited: e05031. doi:10.7554/eLife.05031.

Volmer, Romain, Kattria van der Ploeg, and David Ron. 2013. “Membrane Lipid Saturation Activates Endoplasmic Reticulum Unfolded Protein Response Transducers through Their Transmembrane Domains.” *Proceedings of the National Academy of Sciences of the United States of America* 110 (12): 4628–33. doi:10.1073/pnas.1217611110.

Wall, D, M Zylicz, and C Georgopoulos. 1994. “The NH2-Terminal 108 Amino Acids of the Escherichia Coli DnaJ Protein Stimulate the ATPase Activity of DnaK and Are Sufficient for Lambda Replication.” *The Journal of Biological Chemistry* 269 (7): 5446–51.

Wang, Jie, Jessica Lee, David Liem, and Peipei Ping. 2017. “HSPA5 Gene Encoding Hsp70 Chaperone BiP in the Endoplasmic Reticulum.” *Gene* 618 (June): 14–23. doi:10.1016/j.gene.2017.03.005.

Wang, X Z, H P Harding, Y Zhang, E M Jolicoeur, M Kuroda, and D Ron. 1998. “Cloning of Mammalian Ire1 Reveals Diversity in the ER Stress

Responses.” *The EMBO Journal* 17 (19). EMBO Press: 5708–17. doi:10.1093/emboj/17.19.5708.

Wei, J, and L M Hendershot. 1995. “Characterization of the Nucleotide Binding Properties and ATPase Activity of Recombinant Hamster BiP Purified from Bacteria.” *The Journal of Biological Chemistry* 270 (44): 26670–76.

Wong, W L, M A Brostrom, G Kuznetsov, D Gmitter-Yellen, and C O Brostrom. 1993. “Inhibition of Protein Synthesis and Early Protein Processing by Thapsigargin in Cultured Cells.” *The Biochemical Journal* 289 (Pt 1) (January): 71–79.

Xing, Yi, Till Böcking, Matthias Wolf, Nikolaus Grigorieff, Tomas Kirchhausen, and Stephen C Harrison. 2010. “Structure of Clathrin Coat with Bound Hsc70 and Auxilin: Mechanism of Hsc70-Facilitated Disassembly.” *The EMBO Journal* 29 (3): 655–65. doi:10.1038/emboj.2009.383.

Yan, Wei, Christopher L Frank, Marcus J Korth, Bryce L Sopher, Isabel Novoa, David Ron, and Michael G Katze. 2002. “Control of PERK eIF2alpha Kinase Activity by the Endoplasmic Reticulum Stress-Induced Molecular Chaperone P58IPK.” *Proceedings of the National Academy of Sciences of the United States of America* 99 (25). National Academy of Sciences: 15920–25. doi:10.1073/pnas.252341799.

Yanagitani, Kota, Yusuke Imagawa, Takao Iwawaki, Akira Hosoda, Michiko Saito, Yukio Kimata, and Kenji Kohno. 2009. “Cotranslational Targeting of XBP1 Protein to the Membrane Promotes Cytoplasmic Splicing of Its Own mRNA.” *Molecular Cell* 34 (2). Elsevier Ltd: 191–200. doi:10.1016/j.molcel.2009.02.033.

Yanagitani, Kota, Yukio Kimata, Hiroshi Kadokura, and Kenji Kohno. 2011. “Translational Pausing Ensures Membrane Targeting and Cytoplasmic Splicing of XBP1u mRNA.” *Science* 331 (6017).

Yang, Liu, Zhen Xue, Yin He, Shengyi Sun, Hui Chen, and Ling Qi. 2010. “A Phos-Tag-Based Approach Reveals the Extent of Physiological Endoplasmic Reticulum Stress.” Edited by Neeraj Vij. *PLoS ONE* 5 (7): e11621. doi:10.1371/journal.pone.0011621.

Ye, J, R B Rawson, R Komuro, X Chen, U P Davé, R Prywes, M S Brown, and J L Goldstein. 2000. “ER Stress Induces Cleavage of Membrane-Bound ATF6 by the Same Proteases That Process SREBPs.” *Molecular Cell* 6 (6): 1355–64.

Ye, Libin, Suvrajit Maji, Narinder Sanghera, Piraveen Gopalasingam, Evgeniy Gorbunov, Sergey Tarasov, Oleg Epstein, and Judith Klein-Seetharaman. 2017. “Structure and Dynamics of the Insulin Receptor: Implications for Receptor Activation and Drug Discovery.” *Drug Discovery Today* 22 (7): 1092–1102. doi:10.1016/j.drudis.2017.04.011.

Yoshida, Hiderou, Toshie Matsui, Akira Yamamoto, Tetsuya Okada, and Kazutoshi Mori. 2001. “XBP1 mRNA Is Induced by ATF6 and Spliced by IRE1 in Response to ER Stress to Produce a Highly Active Transcription Factor.” *Cell* 107: 881–91.

Zhou, Jiahai, Chuan Yin Liu, Sung Hoon Back, Robert L Clark, Daniel Peisach, Zhaohui Xu, and Randal J Kaufman. 2006. “The Crystal Structure of Human IRE1 Luminal Domain Reveals a Conserved Dimerization Interface Required for Activation of the Unfolded Protein Response.” *Proceedings of the National Academy of Sciences of the United States of America* 103 (39): 14343–48. doi:10.1073/pnas.0606480103.

Zhu, X, X Zhao, W F Burkholder, A Gragerov, C M Ogata, M E Gottesman, and W A Hendrickson. 1996. “Structural Analysis of Substrate Binding by the Molecular Chaperone DnaK.” *Science (New York, N.Y.)* 272 (5268). NIH Public Access: 1606–14.

Appendix

Appendix table 1

ID	Primer name	Sequence	Description
5	mXBP1.14AS	GAATGCCCAAAAGGATATCAGACTC	For XBP1 Reverse transcription PCR assay
1097	IRE1_Q105C_knit_2as	ATGGGCTAGCACAGACTAATTCTGGG ATGGTAAAGGGAAGTTTC	Primer for Q105C repair template of Q105 region of CHO IRE1
1098	IRE1_Q105C_knit_3s	CAGAATTAGTCTGTGCTAGCCCATCC CGAAGTTCAGATGGAATCCTCTAC	Primer for Q105C repair template of Q105 region of CHO IRE1
1100	IRE1_Q105_region_1s	AGCCTCCATCTGCAGTGTGCTTCTCTG	Oligos for genotyping of CHO IRE1 Q105 region
1101	IRE1_Q105_region_2as	CACAACTTTCCCAGATTCCAGGATTC ACTGTC	Oligos for genotyping of CHO IRE1 Q105 region
1116	IRE1_Q105_region_3s	GCTAGAAATAGTGTGGAGTGATCAG	Oligos for generating repair template of CHO IRE1 Q105 region
1117	IRE1_Q105_region_4as	AACTATTCCCAGGTCACAGGTTATA	Oligos for generating repair template of CHO IRE1 Q105 region
1125	IRE1_Q105_region_1s [5'-6FAM]	AGCCTCCATCTGCAGTGTGCTTCTCTG	Oligo 1100 with 5'FAM for genotyping of CHO IRE1 Q105 region
1234	IRE1_11.1s_1s	CACCGTTCCTGCTGATTCGGAAAAA	Creating guide for targeting CHO IRE1 for screen I
1235	IRE1_11.1s_2as	AAACTTTTTCCGAATCAGCAGGAAC	Creating guide for targeting CHO IRE1 for screen I
1236	IRE1_11.1as_1s	CACCGATGCAGACAGAGGAGTTTCA	Creating guide for targeting CHO IRE1 for screen I
1237	IRE1_11.1as_2as	AAACTGAAACTCCTCTGTCTGCATC	Creating guide for targeting CHO IRE1 for screen I

1238	IRE1_11.2as_1s	CACCGGGGGAATCTCTCCAGCATCT	Creating guide for targeting CHO IRE1 for screen I
1239	IRE1_11.2as_2as	AAACAGATGCTGGAGAGATTCCCCC	Creating guide for targeting CHO IRE1 for screen I
1240	IRE1_11.3as_1s	CACCGAATCACATTTTCCCGATGTT	Creating guide for targeting CHO IRE1 for screen I
1241	IRE1_11.3as_2as	AAACAACATCGGGAAAATGTGATTC	Creating guide for targeting CHO IRE1 for screen I
1242	IRE1_12.1s_1s	CACCGTCCATACAAGGTTATCAACA	Creating guide for targeting CHO IRE1 for screen I
1243	IRE1_12.1s_2as	AAACTGTTGATAACCTTGTATGGAC	Creating guide for targeting CHO IRE1 for screen I
1244	IRE1_12.2s_1s	CACCGTCAGGCCGTGGAAGAGAAGC	Creating guide for targeting CHO IRE1 for screen I
1245	IRE1_12.2s_2as	AAACGCTTCTCTTCCACGGCCTGAC	Creating guide for targeting CHO IRE1 for screen I
1246	IRE1_12.3s_1s	CACCGCCATGCCCCCGCCAAGCCTG	Creating guide for targeting CHO IRE1 for screen I
1247	IRE1_12.3s_2as	AAACCAGGCTTGGCGGGGGCATGGC	Creating guide for targeting CHO IRE1 for screen I
1248	IRE1_12.1as_1s	CACCGACGGCCTGAGACACAGTGGA	Creating guide for targeting CHO IRE1 for screen I
1249	IRE1_12.1as_2as	AAACTCCACTGTGTCTCAGGCCGTC	Creating guide for targeting CHO IRE1 for screen I
1274	ERdj1_guide1_S	CACCGGGCCCCGGGCGCCGGCGCTG	CRISPR-Cas9 guide oligonucleotide ERdj1
1275	ERdj1_guide1_AS	AAACCAGCGCCGGCGCCCGGGGCCC	CRISPR-Cas9 guide oligonucleotide ERdj1
1276	ERdj1_guide2_S	CACCGGGCCGCTGTCGTCCTCCGTT	CRISPR-Cas9 guide oligonucleotide ERdj1
1277	ERdj1_guide2_AS	AAACAACGGAGGACGACAGCGGCCC	CRISPR-Cas9 guide oligonucleotide ERdj1
1278	ERdj2_guide1_S	CACCGTCCAAGTTTAATACTTCATA	CRISPR-Cas9 guide oligonucleotide ERdj2
1279	ERdj2_guide1_AS	AAACTATGAAGTATTAAACTTGGAC	CRISPR-Cas9 guide oligonucleotide ERdj2
1280	ERdj3_guide1_S	CACCGGAAATCTCGCCTGAGAGGAC	CRISPR-Cas9 guide oligonucleotide ERdj3
1281	ERdj3_guide1_AS	AAACGTCCTCTCAGGCGAGATTTCC	CRISPR-Cas9 guide oligonucleotide ERdj3

1282	ERdj3_guide2_S	CACCGGCCTCGGAGTGCCTCCGTAA	CRISPR-Cas9 guide oligonucleotide ERdj3
1283	ERdj3_guide2_AS	AAACTTACGGAGGCACTCCGAGGCC	CRISPR-Cas9 guide oligonucleotide ERdj3
1284	ERdj4_guide1_S	CACCGCTCAGAGCGACAAATCAAGA	CRISPR-Cas9 guide oligonucleotide ERdj4
1285	ERdj4_guide1_AS	AAACTCTTGATTTGTCGCTCTGAGC	CRISPR-Cas9 guide oligonucleotide ERdj4
1286	ERdj4_guide2_S	CACCGGATATCATAGTAGCTCTTTG	CRISPR-Cas9 guide oligonucleotide ERdj4
1287	ERdj4_guide2_AS	AAACCAAAGAGCTACTATGATATCC	CRISPR-Cas9 guide oligonucleotide ERdj4
1288	ERdj5_guide1_S	CACCGCTTCAGTGCTAATTTCTTAA	CRISPR-Cas9 guide oligonucleotide ERdj5
1289	ERdj5_guide1_AS	AAACTTAAGAAATTAGCACTGAAGC	CRISPR-Cas9 guide oligonucleotide ERdj5
1290	ERdj5_guide2_S	CACCGTTCTCTACTACTTGCAGTTT	CRISPR-Cas9 guide oligonucleotide ERdj5
1291	ERdj5_guide2_AS	AAACAAACTGCAAGTAGTAGAGAAC	CRISPR-Cas9 guide oligonucleotide ERdj5
1292	ERdj6_guide1_S	CACCGGTGACTGTTTCAGTAACCGC	CRISPR-Cas9 guide oligonucleotide ERdj6
1293	ERdj6_guide1_AS	AAACGCGGTTACTGAAACAGTCACC	CRISPR-Cas9 guide oligonucleotide ERdj6
1294	ERdj6_guide2_S	CACCGCTAAACCTTCCCGAATCTGC	CRISPR-Cas9 guide oligonucleotide ERdj6
1295	ERdj6_guide2_AS	AAACGCAGATTCGGGAAGGTTTAGC	CRISPR-Cas9 guide oligonucleotide ERdj6
1296	ERdj7_guide1_S	CACCGGAAAGATTATGACTACATGC	CRISPR-Cas9 guide oligonucleotide ERdj7
1297	ERdj7_guide1_AS	AAACGCATGTAGTCATAATCTTTCC	CRISPR-Cas9 guide oligonucleotide ERdj7
1298	ERdj7_guide2_S	CACCGACCACCCTAACATCCACTTT	CRISPR-Cas9 guide oligonucleotide ERdj7
1299	ERdj7_guide2_AS	AAACAAAGTGGATGTTAGGGTGGTC	CRISPR-Cas9 guide oligonucleotide ERdj7
1367	ERdj1_genomic_S	CCGGCGCGCTTACCTGC	Oligo for genotyping indels
1368	ERdj1_genomic_AS	CTCGGAACCCAGTGCGATGTG	Oligo for genotyping indels

1369	ERdj2_genomic_S	GCCATACAGTTGAATTTATTTATGTCATTTGTC	Oligo for genotyping indels
1370	ERdj2_genomic_AS	GTTAACAGTTCAAATTCTGATTTCTTTTGGAAATGTC	Oligo for genotyping indels
1371	ERdj3_genomic_S	AGTGGGGACTGTGAGAGAAGG	Oligo for genotyping indels
1372	ERdj3_genomic_AS	AATTTCTCCTGGGCTTGGGGATCG	Oligo for genotyping indels
1373	ERdj4_genomic_S	GTGCATAGCTTTTCGAATGCTGC	Oligo for genotyping indels
1374	ERdj4_genomic_AS	CTTCAGCATCAGGGCTCTTATTTTTG	Oligo for genotyping indels
1375	ERdj5_genomic_S	GTATCTTAATGTCACTTAAATAAGAACTTGC	Oligo for genotyping indels
1376	ERdj5_genomic_AS	CCAGATATTTAAAAGAGAAATTTTACCTACC	Oligo for genotyping indels
1377	ERdj6_genomic_S	CATTCAGGATTATGAAGCTGCTCAGG	Oligo for genotyping indels
1378	ERdj6_genomic_AS	ACGCTAAGGGCTCTCAGAATAACG	Oligo for genotyping indels
1379	ERdj7_genomic_S	TACGTGCCTTTAAGAGTATTGGGAAG	Oligo for genotyping indels
1380	ERdj7_genomic_AS	CACTGAAATGGCACATACACTGACC	Oligo for genotyping indels
1391	ERdj1_genomic_2_S	ATGTGGGCTCCCGGCTTCGGAC	Oligo for genotyping indels
1392	ERdj1_genomic_2_AS	TTACCTGCTGCACCCCGAGGAACTC	Oligo for genotyping indels
1393	ERdj2_genomic_S [5'-6FAM]	GCCATACAGTTGAATTTATTTATGTCATTTGTC	Oligo for genotyping indels (FAM)

1394	ERdj3_genomic_S [5'-6FAM]	AGTGGGGACTGTGAGAGAAGG	Oligo for genotyping indels (FAM)
1395	ERdj4_genomic_S [5'-6FAM]	GTGCATAGCTTTTCGAATGCTGC	Oligo for genotyping indels (FAM)
1396	ERdj5_genomic_S [5'-6FAM]	GTATCTTAATGTCACTTAAATAAG AACTTGC	Oligo for genotyping indels (FAM)
1397	ERdj6_genomic_S [5'-6FAM]	CATTCAGGATTATGAAGCTGCTCAGG	Oligo for genotyping indels (FAM)
1398	ERdj7_genomic_S [5'-6FAM]	TACGTGCCTTTAAGAGTATTGGGAAG	Oligo for genotyping indels (FAM)
1409	ERdj1_genomic_2_AS [5'-6FAM]	TTACCTGCTGCACCCCGAGGAACTC	Oligo for genotyping indels (FAM)
1470	hamXBP1.19S	GGCCTTGTAATTGAGAACCAGGAG	For XBP1 Reverse transcription PCR assay
1618	ERdj8_guide1_S	CACCGAGGCATATAAGAAGCTCGCC	CRISPR guide targeting Ch ERdj8 (Dnajc16)
1619	ERdj8_guide1_AS	AAACGGCGAGCTTCTTATATGCCTC	CRISPR guide targeting Ch ERdj8 (Dnajc16)
1650	ERdj8_genomic_1_S	gagagATGgaggtgaaaaagctgagcgtctc	genotyping ERdj8 KOs in CHO cells
1651	ERdj8_genomic_1_AS	ATCATAATTCAGGCTTCAGGC ACCTGCCTACTGC	genotyping ERdj8 KOs in CHO cells
1652	ERdj8_genomic_2_S	cagaaggaagagagATGgaggtgaaaaagctg	genotyping ERdj8 KOs in CHO cells
1653	ERdj8_genomic_2_AS	CAGGCTACTAGCTGAGCACCAATACTC	genotyping ERdj8 KOs in CHO cells
1675	ERdj8_genomic_2_AS[5'-6FAM]	[6FAM]CAGGCTACTAGCTGAGCAC CAATACTC	Oligo for genotyping indels (FAM)

2149	IRE1_10.1s_1s	CACCGGTGTCACCATTGAAGACAA	Creating guide for targeting CHO IRE1 for screen II
2150	IRE1_10.1s_2as	AAACTTGTCTTCAATGGTGACACC	Creating guide for targeting CHO IRE1 for screen II
2151	IRE1_10.2s_1s	CACCGAGTTTGACCCTGGACTCAAA	Creating guide for targeting CHO IRE1 for screen II
2152	IRE1_10.2s_2as	AAACTTTGAGTCCAGGGTCAAACTC	Creating guide for targeting CHO IRE1 for screen II
2153	IRE1_10.3s_1s	CACCGAGAGCAAGCTGAACTACTTG	Creating guide for targeting CHO IRE1 for screen II
2154	IRE1_10.3s_2as	AAACCAAGTAGTTCAGCTTGCTCTC	Creating guide for targeting CHO IRE1 for screen II
2155	IRE1_10.1as_1s	CACCGTGCTCTTCCCTTTGAGTCCA	Creating guide for targeting CHO IRE1 for screen II
2156	IRE1_10.1as_2as	AAACTGGACTCAAAGGGAAGAGCAC	Creating guide for targeting CHO IRE1 for screen II
2157	IRE1_10.2as_1s	CACCGAAACTTGAGGTCTGTGCTGG	Creating guide for targeting CHO IRE1 for screen II
2158	IRE1_10.2as_2as	AAACCCAGCACAGACCTCAAGTTTC	Creating guide for targeting CHO IRE1 for screen II
2159	IRE1_10.3as_1s	CACCGACACTCTCCTTTGTCTTCAA	Creating guide for targeting CHO IRE1 for screen II
2160	IRE1_10.3as_2as	AAACTTGAAGACAAAGGAGAGTGTC	Creating guide for targeting CHO IRE1 for screen II
2161	IRE1_10.4as_1s	CACCGATGGTGACACCATCTGTCTG	Creating guide for targeting CHO IRE1 for screen II
2162	IRE1_10.4as_2as	AAACCAGACAGATGGTGTCACCATC	Creating guide for targeting CHO IRE1 for screen II
2163	IRE1_10.5as_1s	CACCGTCTGGGGACCTTCCAGCAA	Creating guide for targeting CHO IRE1 for screen II
2164	IRE1_10.5as_2as	AAACTTGCTGGAAGGTCCCCAGAC	Creating guide for targeting CHO IRE1 for screen II
2165	IRE1_10.6as_1s	CACCGCAAAGGAAGAGTGCTTCCT	Creating guide for targeting CHO IRE1 for screen II
2166	IRE1_10.6as_2as	AAACAGGAAGCACTCTTCCTTTGC	Creating guide for targeting CHO IRE1 for screen II

Appendix table 2

ID	Plasmid name	Description
1047	PERK_GST_pCDNA3	mPERK 1-585 (LD + TM) fused to GST
1070	pFLAGM1_mP58dSP1_CMV1	FLAGM1 mP58 27_504 (ΔSP) in pFLAG_pCMV1
1314	pCEFL_mCherry_3XFLAG_C	pCEFL with 3XFLAG_C tagged from mCherry-tagged plasmid
1558	IRE1_Q105C_g1b_pSpCas9(BB)-2A-Puro	Cas9 targetted to CHO IRE1 exon 5 to introduce indel
1559	IRE1_Q105C_g2a_pSpCas9(BB)-2A-Puro	Cas9 targetted to CHO IRE1 exon 5 to introduce Q105C via HDR
1610	pSpCas9(BB)-2A-mCherry_V2	pSpCas9(BB)-2A vector to express mCherry together with guide RNA/Cas9
1624	CHO_IRE1_guide11.1s_pSpCas9(BB)-2A-Cherry	Cas9 and guide for targeting CHO IRE1 for screen I
1625	CHO_IRE1_guide11.1as_pSpCas9(BB)-2A-Cherry	Cas9 and guide for targeting CHO IRE1 for screen I
1626	CHO_IRE1_guide11.2as_pSpCas9(BB)-2A-Cherry	Cas9 and guide for targeting CHO IRE1 for screen I
1627	CHO_IRE1_guide11.3as_pSpCas9(BB)-2A-Cherry	Cas9 and guide for targeting CHO IRE1 for screen I
1628	CHO_IRE1_guide12.1s_pSpCas9(BB)-2A-Cherry	Cas9 and guide for targeting CHO IRE1 for screen I
1629	CHO_IRE1_guide12.2s_pSpCas9(BB)-2A-Cherry	Cas9 and guide for targeting CHO IRE1 for screen I
1630	CHO_IRE1_guide12.3s_pSpCas9(BB)-2A-Cherry	Cas9 and guide for targeting CHO IRE1 for screen I
1631	CHO_IRE1_guide12.1as_pSpCas9(BB)-2A-Cherry	Cas9 and guide for targeting CHO IRE1 for screen I
1682	ERdj1_g1_pSpCas9(BB)-2A-mCherry	mCherry-tagged CRISPR plasmid (UK1610) for hamster ERdj1
1683	ERdj1_g2_pSpCas9(BB)-2A-mCherry	mCherry-tagged CRISPR plasmid (UK1610) for hamster ERdj1
1684	ERdj2_g1_pSpCas9(BB)-2A-mCherry	mCherry-tagged CRISPR plasmid (UK1610) for hamster ERdj2

1685	ERdj3_g1_pSpCas9(BB)-2A-mCherry	mCherry-tagged CRISPR plasmid (UK1610) for hamster ERdj3
1686	ERdj3_g2_pSpCas9(BB)-2A-mCherry	mCherry-tagged CRISPR plasmid (UK1610) for hamster ERdj3
1687	ERdj4_g1_pSpCas9(BB)-2A-mCherry	mCherry-tagged CRISPR plasmid (UK1610) for hamster ERdj4
1688	ERdj4_g2_pSpCas9(BB)-2A-mCherry	mCherry-tagged CRISPR plasmid (UK1610) for hamster ERdj4
1689	ERdj5_g1_pSpCas9(BB)-2A-mCherry	mCherry-tagged CRISPR plasmid (UK1610) for hamster ERdj5
1690	ERdj5_g2_pSpCas9(BB)-2A-mCherry	mCherry-tagged CRISPR plasmid (UK1610) for hamster ERdj5
1691	ERdj6_g1_pSpCas9(BB)-2A-mCherry	mCherry-tagged CRISPR plasmid (UK1610) for hamster ERdj6
1692	ERdj6_g2_pSpCas9(BB)-2A-mCherry	mCherry-tagged CRISPR plasmid (UK1610) for hamster ERdj6
1693	ERdj7_g1_pSpCas9(BB)-2A-mCherry	mCherry-tagged CRISPR plasmid (UK1610) for hamster ERdj7
1694	ERdj7_g2_pSpCas9(BB)-2A-mCherry	mCherry-tagged CRISPR plasmid (UK1610) for hamster ERdj7
1703	hIRE1α_19-486_dC_GST_del3UTR _pCDNA3	GST-hIRE1α lacking luminal cysteines for mammalian expression
173	haBiP_27-654_pQE10	N-terminally His6-tagged hamster BiP
1739	pCEFL_mCherry_CHO_ERdj4_3XFLAG_C	3xFLAG-ERdj4 in mCherry vector for mammalian expression
1754	pCEFL_mCherry_CHO_QDL_ERdj4_3XFLAG_C	3xFLAG-QPD-ERdj4 in mCherry vector for mammalian expression
1765	hIRE1α_19-486_dC_dRVI_II_GST_del3UTR _pCDNA3	GST-Δ403-411-hIRE1α lacking luminal cysteines for mammalian expression
182	haBiP_27-654_V461F_pQE10	N-terminally His6-tagged hamster BiP V461F
1861	ERdj8_guide1_pSpCas(BB)-2A-mCherry_V2	mCherry-tagged CRISPR plasmid (UK1610) for hamster ERdj8
1862	hIRE1α_19-486_dC_Q105C_GST_del3UTR _pCDNA3	GST--Q105C-hIRE1α lacking luminal cysteines for mammalian expression
1881	EcBirA_WT_pGEX_TEV	Bacterial expression of fastidious E. coli BirA biotin ligase (R118 intact)

1915	pGEX_GST_TEV_hIRE1a_LDΔC_24-442_D443C	N-GST- cysteine free human Ire1LD 24-442 with a C-terminal cysteine
1920	huPPP1R15A_533_624_malE_pGEX_TEV_AviTag	N-tern AviTagged human GADD34 533–624
1968	CHO_IRE1_hIRE1-LD_reptemp4_pCR-Blunt2-TOPO	Repair template for WT hIRE1 LD reconstitution in CHO cells
2007	pGEX_GST_TEV_hIRE1a_LDΔC_24-443	N-terminally GST-tagged cysteine free human Ire1LD 24-442
2008	haBiP_27-405_NBD_pQE10	Bacterial expression of BiP NBD
2012	Smt3_cgERdJ4_24-222_pET-21a	N-terminally His6-Smt3-tagged chinese hamster ERdj4 24-222
2016	CHO_IRE1_hIRE1-LD(V437R)_reptemp4_pCR-Blunt2-TOPO	Repair template for V437R hIRE1 LD reconstitution in CHO cells
2017	CHO_IRE1_hIRE1-LD(L441R)_reptemp4_pCR-Blunt2-TOPO	Repair template forL441R hIRE1 LD reconstitution in CHO cells
2018	CHO_IRE1_hIRE1-LD_rVdel_pCR	Repair template for Δ403-411 hIRE1 LD reconstitution in CHO cells
2019	CHO_IRE1_hIRE1-LD_rVtoglyser_pCR	Repair template for hIRE1 LD with 403-441 hydrophobic residues mutated to Gly/Ser
2036	CHO_hIRE1-LD_predhel2_SerSer_pCR	Repair template for F400S, V403S, I404S, L406S hIRE1 LD reconstitution in CHO cells
2040	Smt3_QPD_cgERdJ4_24-222_pET-21a	N-terminally His6-Smt3-tagged chinese hamster ERdj4 24-222, H54Q
2041	Smt3_J4_domain_24-90_pET-21a	N-terminally His6-Smt3-tagged chinese hamster ERdj4 24-90
2045	pET22b_H7_Smt3_Ire1a_LDΔC_24_443 Q105C	N-terminally His6-Smt3-tagged cysteine free human Ire1LD 24-443, Q105C
2047	pET22b_H7_Smt3_Ire1a_LDΔC_24_443 S152C	Bacterial expression of Smt3-tagged cysteine-free Ire1a LDΔC S152C
2048	pET22b_H7_Smt3_Ire1a_LDΔC_24_443 R234C	N- His6-Smt3-tagged cysteine free human Ire1LD 24-443, R234C
2076	pET22b_H7_Smt3_Ire1a_LDΔC_24_443 S112C	N-terminally His6-Smt3-tagged cysteine free h Ire1LD 24-443, S112C

2080	pCMV1_SP_J4_mCherry_KDEL	mammalian expression CHO ERdj4 J domain alone mCherry + KDEL
2098	Smt3_cgERdJ4_24-222_AviTag_pET21a	N-His6-Smt3-ERdj4-Avi chinese hamster residues 24-222, H54Q
2108	Smt3_cgERdJ4_24-222_GS6_MalE_pET21a	N-His6-Smt3-ERdj4-MBP chinese hamster residues 24-222
2117	pET22b_H7_Smt3_Ire1a_LDΔC_24_390 R234C	N-His6-Smt3-tagged cysteine free human Ire1CLD 24-390, R234C
2118	pET22b_H7_Smt3_Ire1a_LDΔC_24_390 S112C	N-His6-Smt3-tagged cysteine free human Ire1CLD 24-390, S112C
2119	Smt3_cgERdJ4_24-222_QPD_GS6_MalE_pET21a	N-His6-Smt3-ERdj4-MBP chinese hamster residues 24-222 H54Q
2127	pCMV1_SP_ERdJ4_3xFLAG_mCherry_KDEL	mammalian expression CHO ERdj4 3xFLAG mCherry with KDEL
2132	pCMV1_SP_QPD_J4_mCherry_KDEL	mammalian expression CHO QPD J4 mCherry with KDEL
2247	CHO_IRE1_guide10.1s_pSpCas9(BB)-2A-Cherry	Cas9 and guide for targeting CHO IRE1 for screen II
2248	CHO_IRE1_guide10.2s_pSpCas9(BB)-2A-Cherry	Cas9 and guide for targeting CHO IRE1 for screen II
2249	CHO_IRE1_guide10.3s_pSpCas9(BB)-2A-Cherry	Cas9 and guide for targeting CHO IRE1 for screen II
2250	CHO_IRE1_guide10.1as_pSpCas9(BB)-2A-Cherry	Cas9 and guide for targeting CHO IRE1 for screen II
2251	CHO_IRE1_guide10.2as_pSpCas9(BB)-2A-Cherry	Cas9 and guide for targeting CHO IRE1 for screen II
2252	CHO_IRE1_guide10.3as_pSpCas9(BB)-2A-Cherry	Cas9 and guide for targeting CHO IRE1 for screen II
2253	CHO_IRE1_guide10.4as_pSpCas9(BB)-2A-Cherry	Cas9 and guide for targeting CHO IRE1 for screen II
2254	CHO_IRE1_guide10.5as_pSpCas9(BB)-2A-Cherry	Cas9 and guide for targeting CHO IRE1 for screen II
2255	CHO_IRE1_guide10.6as_pSpCas9(BB)-2A-Cherry	Cas9 and guide for targeting CHO IRE1 for screen II
838	haBiP_27-654_T229A_pQE10	N-terminally His6-tagged hamster BiP T229A
888	pFLAG_mCherry_KDEL_CMV1	mammalian expression of SP-FLAGM1-mCherry-KDEL (ER localized)

Appendix table 3

Gene	Clone	Allele	Amino acid sequence (number shows amino acid position at which insert/deletion occured)
ERDJ1	#15	1	…RIPQ13inRGM*
		2	…RIPQ13inSPAPGAAVVLRLAAAAVPAGGRGAGARLGERRPGVVRLGGRGAAQLLRVPRGAAGCFIC RHQKSIS*
	#16	1	…RRPG18indelLXRCGLCEPHTNVGGRRGGHIIGCCCCSCWRPWGRCAPGRAETWSCSTWWKRCSS TSTSSSGCSRMLHLQTSEKHIVSFH*
		2	…LSSS23inRLAAAAVPAGGRGAGARLGERRPGVVRLGGRGAAQLLRVPRGAAGCFICRHQKSIS*
ERDJ2	#9	1	...YNPY83inGSIKLGSWSNSSRN*
		2	...EYNP82delWILEQQ*
	#16	1	...YNPY83inGSIKLGSWSNSSRN*
		2	...QEYN81indelP*
ERDJ3	#8	1	...VPRS35delQETSPTASS*
		2	...VPRS35delAKGHQKGLQETSPTASS*
	#11	1	…RSAS37inDFELQESYCAAMNDSINLVFYIPSILDLGTKTRXLNTYKGHQKGLQETSPTASS*
		2	...VPRS35delAGN*
ERDJ4	#1	1	...ERQI42inTM*
		2	...ERQI42delRPFTN*

	#21	1	...LASK25inRATMIS*
ERDJ5	#4	1	…GVSK44inNCK*
		2	...YSLL40del*
	#11	1	…RQAF55indelITIIKWTFL*
		2	…RQAF55inKEISTEVTS*
ERDJ6	#3	1	...KAQR373inKNIMIEVSKKQKKYSMYSLISG*
		2	...EKAQ372inHLEFLAGHHRPAQHQEEPDRSPAVTETVTETRLL*
	#4	1	...QIRE366delGTETVTETRLL*
		2	…EKAQ372inRVTETVTETRLL*
ERDJ7	#22	1	…LAPK23inVMYWAQCQAGHLPSLTSIGGVLGI*
		2	…SHYY13indelQGDFGQCMCHFSVSVFQLVE*
	#25	1	…LAPK23inGATALRPPSAPEWMLGW*
		2	…RLAP22delSGC*
ERDJ8	#37	1	…YKKL52inSPGNGILTKIKTLELRTSSFRSARPMRYCPMRKRGQTMTTMAMPGRTRAIRSSSASTASAIS MTTSISRSPFSTSPSIRSAGTRLMRSTCCTFHTT*
		2	…ASQA43delGNGILTKIKTLELRTSSFRSARPMRYCPMRKRGQTMTTMAMPGRTRAIRSSSASTASAIS MTTSISRSPFSTSPSIRSAGTRLMRSTCCTFHTT*
	#41	1	...YKKL52insYGRAYHLAPVLQ*
		2	…IKKA48del*
IRE1	NC6	1	…KLPFT1100delSQN*

		2	…KLPFT1100delSQN*
IRE1	CV1	1	…KLPFTIPELVCASPSRSSDGILYM…
		2	…KLPFTIPELVCASPSRSSDGILYM…
	CV8	1	…KLPFTIPELVCASPSRSSDGILYM…
		2	…KLPFTIPELVCASPSRSSDGILYM…
IRE1	A2	cDNA	FEE|::|KDMATIILS
IRE1	B4	cDNA	FEEVINLVDQTSENAPTTVSRDVEE|::|KDMATIILS
IRE1	C13	cDNA	FEE|QLLR|KDMATIILS
IRE1	D23	cDNA	FEE|PCI|KDMATIILS

Appendix table 4

GCTAGAAATAGTGTGGAGTGATCAGTATAAGTCATCTCATTTGAACTTCTT
GCCCTATGGGTGTTGTCCCCACTCTAGAGGTATCAAAACTGAGCCTGGA
CAAGTCAAAGAATTTACCAAGACCAAAGCTTCCAGGAAGAGGTGTGATTT
CCCAAGGATACTCCCTCAGCTGTGATAGTATCTGTCCTGGAGCACAGGA
ATCCAGAGTGATTCCAGAAACATCTGGCAAAACTCTGGGCATTGTTCCCT
CTTGCTGTCATTTTCCTTTTTCTAAGGTTTAGTTTGAATGTAGGAGTGATA
GGAAAATCCAAATAGTTAATACCTCTGGCTCTGTTTATTAACACTACCAAG
AAATCTTTTATCCCTCAGAGAAAAGGTAATAGTATAGTAGAAGCCTAGCA
GCAAGTAGAGCAGGTATCTGCACAGTTTCAGGGCCCGTTCCAAAAATAAA
GTTCACCGAAACAAGCAGTTGTCAAAAGGGCCTGTCAGAAGTCAGCTGT
GGGCTCAGAAGAGGCAGTTGTATGATGAGATGTGTTGAAACGTTGGGAC
TTCTTGGAGTTTCTTTTCCGGGCACCTACCATAACTTCCTTTTTATAACCC
AAAGACTCTGTTTTCAGTAAAGAATTACTTACTGAAGAAAACATCAAAACT
CAGACCTTTGTTTGCCCTTGTAACCATTCTCCTTCTCTTGAACCTTGACTT
TCTTTTTTTTTTTTCCCAAGGCAGGGTTTCTCTGTAGCTTTGGAGCCTGTC
CTGGCACTCACTCTGGAGACCAGGCTGGCCTCGAACTCACAGAGATCCG
CCTGCCTCTGCCTCCCGAGTGCTGGGATTAAAGGCGTGCACCACCAACG
CCCAGCTTGAACCTTGACTTACTTCTAAGTTGCTTCTTTTCAGCATTAATG
GTCCTCCCATGGTAAAAGGCATTGTCTACCTGGCTTGGATTTATCTTTGG
CTGGGAGTTGAAGACAGATTTCTTTCTCCCTTACAATACCTAAGACTGTG
CAGCTTTTCACATTTGTGTAATTTTCTCAGAAAAGGCTTGTGGCACCCTCA
GGGAATACCGGGATGGGAGACCCGAGGGACCTGTGCATCCTATGTCAAA
TAAATGTGTTGGTGTACAGAGTTCAGAGGCTGGGGAGCCCAGAGGCTGT
TGGAAGTAGATGTGGAAACCTAGGATCTCCTCCGTAGGTTCCAACTAAAA
GCCTCCATCTGCAGTGTGCTTCTCTGTTTTTAGAACTGGGTAACAGAAGC
AGCATGCTTAGTAAAATTACAGCAATTTCACAAGACTTGGTTTACTTATTTT
TTTACTTTTTTTTTTTAAAGAAACTTCCCTTTACCATCCCAGAATTAGTCTG
TGCTAGCCCATCCCGAAGTTCAGATGGAATCCTCTACATGGGTAAGAGTT
CCCATTTTCAGCACCAAAAACTTGGCTCTTTTGACAGTGAATCCTGGAAT
CTGGGAAAGTTGTGATTAAGAGAGCAGGATATTGTCACCCTCTTTCAAAT
CTTTCTGAGAAAAGGTTTCCTTGCCTCAGTTGTGCTTTGGTGCTGCTGTT
CATGCCAGGATCATCTGGCCAATTAAGAAAGAGTTCTCTCTGAGGAAAAA

TTGACATCATTAATATGGTTACTCATTTAACAAGCTTTTAGCCATTTGCAAC
CTACCTAGCTGCAAATGGATAAAATTTAAAGTGAATACAGTAGTCTGAGC
CAAGGAAGGGAAGCCAGGCCCTGCCTATTAATTACAGAGCTTTCTTAGGA
TTTCCTGCTATCAGAATATTTGGTAGAAGCAGCACTTAACAGCTTGCCTA
GATAAGCTGTCTTCATACCTGTGGGGTCACAGCTTTCAAAGCATCAGCTC
ACCTGCTTTTCTTCAGCACATTGCTGCCAAAATGTCAATAAAAATGCATTG
GTTGCACAAAGAAGAGCTGTGTCCTGTGTTTATATAGCAGCTTTCTTTTTG
AGGAACTGAAAGTGCCTGTTGCCTATTCATGCCTCAGGAGCTCTATGTAC
ATTTTCAAGTCTCAAATGCAGGCCGGCTGGTTTTTAAGTTTTGCTAGGGA
CACCCAAGCTCCTGCTTCTTTGCACGAGCTTTTCAGAATGAGGAACTCCC
AACCAATATATTCGTAGGAAATGACCAGCAAACCTCTGGGCCATGCTCTG
GACCCATATGACCATCTTCTGTGTTATTGTTCTCTATCGGTCTTCCAGCAA
TCCATCATCTGTCATCAACTTAGGATATTTTGTTTCCACCATCTTTGTGTC
ATGTCTTAAGCTAGTTCACTGAGTATATTTATGAGCATGATAGTTACTCAA
TCCACCCATCATAGCTGTAGGTAGATTATACAGACTGCAGTGGTCCTTGA
AGTCACCAGGTGTATGTCTCATAGATGGAAGGTATTAATGGTCATAGTTA
TTTGGATATATTTTATTCTCTATATTTAGACCTTTTTAATTCTAAGACCTTAT
TGTTGAAAACAGTTAGGATCCACAAACAAGTTGGTCATGTGTGGAATCTG
GTGTATTACATCTGTTACAGCTAAGTATAGCTTTAGCAAATTCTGTTGCCC
TGTGACCTTCTCTGGCATCTCTGTATTCTACTTCCATAGGAACTTGAATGT
AGGAAACATCTATTAAAGTAGGAAGATATAAATGTCTAATAAATGTCCAGA
GGCGTGGCTTACAGAATAGAAATGCACACATTACAGTTGACTGTGTTGGC
CATCAAATATACCATACCATCCATACCGTAGACACATATGCTATATATTTT
CCTAAAAGTGTTTATGTGACTGTACTGTCTGTGTGTTTATATTTAATCAGC
TGACCAAGGCAAGAGGTATAACCTGTGACCTGGGAATAGTT

Appendix table 5

Figure	Original finding by:	Data for figure from:
2.02-2.03	M. Kamphuis	M. Kamphuis
2.23	N. Amin-Wetzel	H. Harding
3.05	N. Amin-Wetzel	R. Saunders
3.11-3.13	R. Saunders	R. Saunders
3.20-3.23	R. Saunders	R. Saunders
4.07	N. Kono	N. Amin-Wetzel